Doctoral Dissertation

Combined Wall and Trench Systems to Reduce Tsunami Impact on Coast

Kukulege Bhathisha Akalanka Silva

July 2020

Graduate School of Engineering,
Osaka University

COMBINED WALL AND TRENCH SYSTEMS TO REDUCE TSUNAMI IMPACT ON COAST

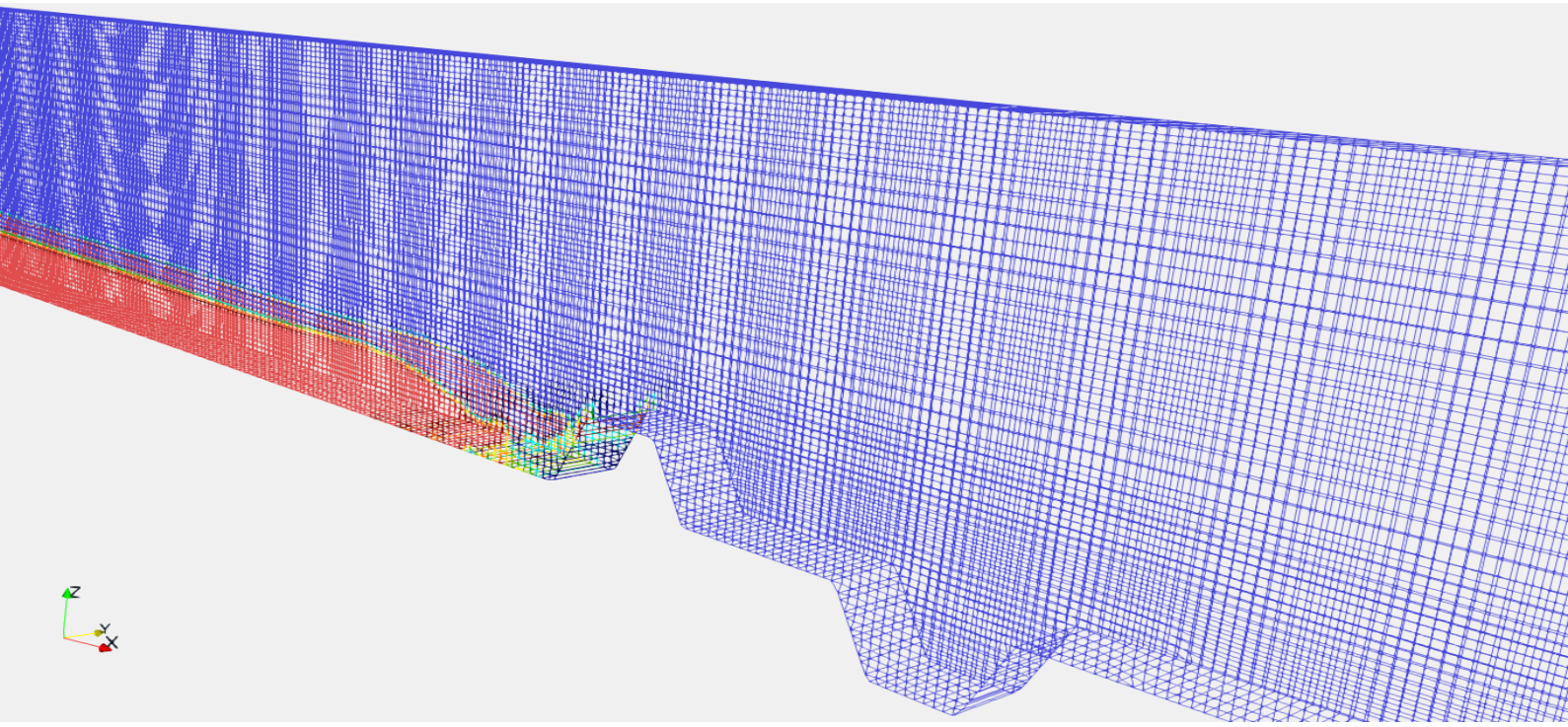

DOCTORAL DISSERTATION

KUKULEGE BHATHISHA AKALANKA SILVA

July, 2020

大阪大学

OSAKA UNIVERSITY

Doctor's Thesis

Combined Wall and Trench Systems to Reduce Tsunami Impact on Coast

By

Kukulege Bhathisha Akalanka Silva

In Partial Fulfillment of the Requirements for the Degree of

Doctor of Engineering

At

The International Program of Maritime and Urban Engineering

The Division of Global Architecture

The Department of Civil Engineering

Osaka University, Japan

On

1st of July, 2020

The Research is Supervised by

Associate Professor, Dr. Susumu Araki

Department of Civil Engineering, Osaka University

PREFACE

Firstly, I would like to thank Prof. Susumu Araki for his valuable guidance throughout last five years. Without his kind guidance and support, this dissertation would not have been completed.

Moreover, it is such a pleasure to work at the land development and management engineering laboratory headed by Prof. Shin-Ichi Aoki. Prof. Aoki's constructive comments lead me to achieve this goal in a more accurate way.

I would also like to thank the community and the makers of OpenFOAM and Delft 3D software suits for sharing their state-of-the art codes and guidance in open source which provided me a better platform to build on.

Further, I acknowledge Japan Ministry of Education, Culture, Sports, Science and Technology (MEXT) for funding my studies through Japanese Government (Monbukagakusho) scholarship for last five years. Without the scholarship, I may not have been able to follow the higher study courses at Osaka University.

At last but not least, I would like to express special thanks to my lovely wife and to my family for being with me and encouraging me at hard times. I would never finish this work without their support.

Akalanka Silva
Suita, Osaka, Japan
June 2020

ABSTRACT

Tsunami is a series of ocean waves that occur often due to subduction earthquakes. The gigantic waves send surges of water, sometimes reaching runup heights of over 30 meters on to land. These wave trains can cause widespread destruction within a very short time frame when they strike ashore. Once generated, tsunamis race across the sea at up to 800 kilometers per an hour. And their long wavelengths mean they lose very little energy along the way. When a tsunami strikes the coast, the damage it would cause is not only depend on wave energy but also on morphological features of the coastline. Disasters occurred in recent times left important evidences that proves above fact as some affected areas were totally destroyed while some showed very less damage.

Coastal dikes and sea walls are the most popular hard measures that are used as defense structures against tsunamis. Countries like Japan have strongly invested in building such structures along its tsunami vulnerable areas, especially since 2011 Great East Japan Tsunami, which has been identified as one of the largest natural disasters in recent history. Some of these structures can reach a height of 17 meters with a length of several kilometers along the East coast of Japan (Raby, 2015). However, there are increasing concerns of cons to their pros with these massive walls that are built within socially and environmentally sensitive areas.

Due to these concerns, researchers are keenly interested in finding alternative solutions to overcome the negative impacts of conventional tsunami defense structures. Applying submerged structures and also altering the design concepts of conventional onshore seawalls looks more practical than adapting into totally different types of mechanically operated defenses. In this study, a promising conceptual structure “a wall and trench system” is deeply investigated.

The first two chapters of this thesis is allocated to explain the related literature and to explain the theoretical aspects that are used to develop the study. Chapter 3 is allocated mainly for discussing the first part of the primary study. Submerged wall and trench systems are investigated in this first section to identify their usability as a defense measure against tsunamis. This chapter focuses on several arrangements of submerged wall and trench systems via a numerical model, which is calibrated by physical experiments of a tsunami-like wave transformation. A dam break event is used to model a tsunami-like wave interaction with

structures. Resulted wave properties are investigated to identify an optimum solution from the viewpoint of structure configuration. Our results clearly show that the submerged wall-trench systems at near-shore can suppress the impact of a tsunami-like waves on the shore.

Combined wall and trench systems at onshore are investigated and discussed in the fourth chapter to identify their usability as a defence measure against a tsunami-like waves. This part of the study focuses on several arrangements and geometries of combined wall and trench systems which are located at onshore. The structure system is assessed via a numerical model, which is calibrated by physical experiments of a tsunami-like wave transformation. A dam break event is used to model a tsunami-like wave interaction with structures. Resulted wave properties were investigated to identify the behavior of the structure system from the viewpoint of structure configuration. The results clearly show that the combined wall and trench systems at onshore can suppress the impact of a tsunami-like waves well than a conventional single seawall system.

TABLE OF CONTENTS

LIST OF FIGURES

LIST OF TABLES

CHAPTER 1

Chapter 1

INTRODUCTION

OUTLINE

This chapter consists of four main sections. Firstly, the background of a typical tsunami disaster is introduced. It is followed by three main topics which describe the focus points that would be addressed in this research study. Afterwards, objectives and research questions are described. At the end research approach is presented.

1.1 BACKGROUND

Tsunami is a water waveform (or series of waves) occur in the ocean in most cases that sends surges of water, sometimes reaching heights of over 30 meters on to land. This huge water mass of the wave front can cause widespread destruction when they strike ashore. 2004 Indian Ocean Tsunami and 2011 Great East Japan Tsunami can be given as most recent examples which caused massive damages on several nations (Figure 1.1 and Figure 1.2).

These awe-inspiring waves are typically caused by large, subduction earthquakes at tectonic plate boundaries. When the ocean floor at a plate boundary rises or falls suddenly due to an earthquake, it displaces the water above it and launches the rolling waves that will become a tsunami. Most tsunamis, about 80 percent, happen within the Pacific Ocean's "Ring of Fire," a geologically active area where tectonic shifts make earthquakes common (ITIC, 2019).

Once generated, tsunamis travel across the sea at up to 800 kilometers per hour - about as fast as a jet airplane. At that pace they can cross the entire expanse of the Pacific Ocean in less than a day. And their long wavelengths mean they lose very little energy along the way. When it reaches shallow propagation speed or celerity of the wave train will drop dramatically due shoaling and water will build up to several meters to convert the loosing kinematic energy into potential energy by keeping energy conservation as per ($H\sqrt[4]{h} = constant$), where H is wave height and h is water depth. Once approaching the shore, wave breaks or inundate as a surging front depending on the bed slope and other morphological features of the coast line. A tsunami can run up to several miles on a flat land until it dissipates the huge energy released

from the earthquake or the source. Thus, tsunami impact is considered as one of the most tremendous natural disasters.

Modern science still cannot predict the earthquakes and therefore the tsunamis. Whilst, tsunamis can track by various method of technologies once generated and thereby issuing early warnings, prior preparations can be arranged before waves strike the shore. However, the destruction of a mega earthquake generated tsunami cannot be fully faded every time.

Source: (*Daily News*, 2019)

Figure 1.1: Destruction at the coast line of Sri Lanka (2004 tsunami)

Source: (*Los Angeles Times*, 2019)

Figure 1.2: Destruction at North East coast of Japan (2011 tsunami)

Tsunamis are a major concern to the Pacific islands and Asian coastal nations because they may occur at any time, with little or no warning, and with destructive force. During the past decade, more people have died from tsunamis than from hurricanes, earthquakes, and floods combined (Wijesundara and Ranagalage, 2004).

The historical recurrence of tsunamis can not be estimated accurately due to its infrequent, unpredictable, and destructive nature. Therefore, the nearshore response of these destructive waves and the governing factors of destruction are not fully understood yet (Apotsos, Buckley, *et al.*, 2011). Therefore, adequate measures for tsunami response at nearshore cannot also be evaluated precisely. However, studies have been carried out to find out to understand tsunami generation, propagation and its response at nearshore since 1900s (Synolakis and Bernard, 2006). Nonlinear shallow water equations given in (Carrier and Greenspan, 1958) have generally been applied to solve tsunami transformation and propagation. Further numerous experimental studies have been done in two-dimensional wave flumes (Synolakis, 1987) and also with complex bathymetries in fully three-dimensional basins (Briggs *et al.*, 1995). In the recent past, the experimental studies have been done not only including tsunami propagation, but also including sediment transport under tsunami-like waves. (Tonkin *et al.*, 2003; Young *et al.*, 2009). Currently, the studies on tsunamis are being carried out not only with experimental studies, but also with numerical studies. Numerical models which are developed by various researchers and companies are available now to make this process feasible. For example, numerical codes like MOST, TUNAMI, Coulwave, Delft3D can simulate tsunami propagation and inundation using realistic wave forms and bathymetries in an acceptable accuracy (Apotsos, Gelfenbaum, *et al.*, 2011).

The impact of a tsunami on a coastline can be prevented for some extent via natural or man-made coastal protection barriers. Moreover, the destruction can be mitigated through community preparedness, timely warnings, and effective response. Man-made protection barriers are generally referred as hard counter measures and community preparedness activities are referred as soft measures. Both soft and hard counter measures have their own pros and cons in general. For example, hard measures are costly structures that cause direct impact on local society and local environment though it gives more protection not only for human lives but also for properties. On the other hand, soft measures can be organized with comparatively low cost but may not give protection for residential properties and also soft measures might need regular drills and well organized and well-functioning warning system with more accuracy and more reliability for effective performance.

To conclude, continuous investigation is necessary by both experimental and numerical approaches and also by real life observations to overcome the current limitations of both experimental and numerical approximations that we have today.

1.2 TSUNAMI DESTRUCTION AND COASTAL MORPHOLOGY

When a tsunami strikes, the impact results different outcomes to the coast which are not only related to tsunami wave properties but also to morphological features of the coastline itself. Disasters occurred in recent times left some important evidences that proves above fact as some affected areas were totally destroyed while some showed very less damage. For an example, Galle city which is the capital of southern Sri Lanka was totally destroyed and washed out by Indian Ocean Tsunami in 2004 while a nearby village known as Unawatuna showed less damage (Figure 1.3 and Figure 1.4). Moreover, Sendai coast line of Japan showed similar behavior (Figure 1.5). Sometimes, even though there are shore protection measures, tsunami wipes out the entire area with massive erosion. Arahama (Fukanuma) beach (Japan) is one of the best recent examples that showed massive erosion after 2011 tsunami.

Source: Google Earth

Figure 1.3: A satellite image of Galle City area of Sri Lanka (Before 2004 tsunami)

Source: Google Earth

Figure 1.4: A satellite image of Galle City area of Sri Lanka (After 2004 tsunami)

Source: (*NASA*, 2019)

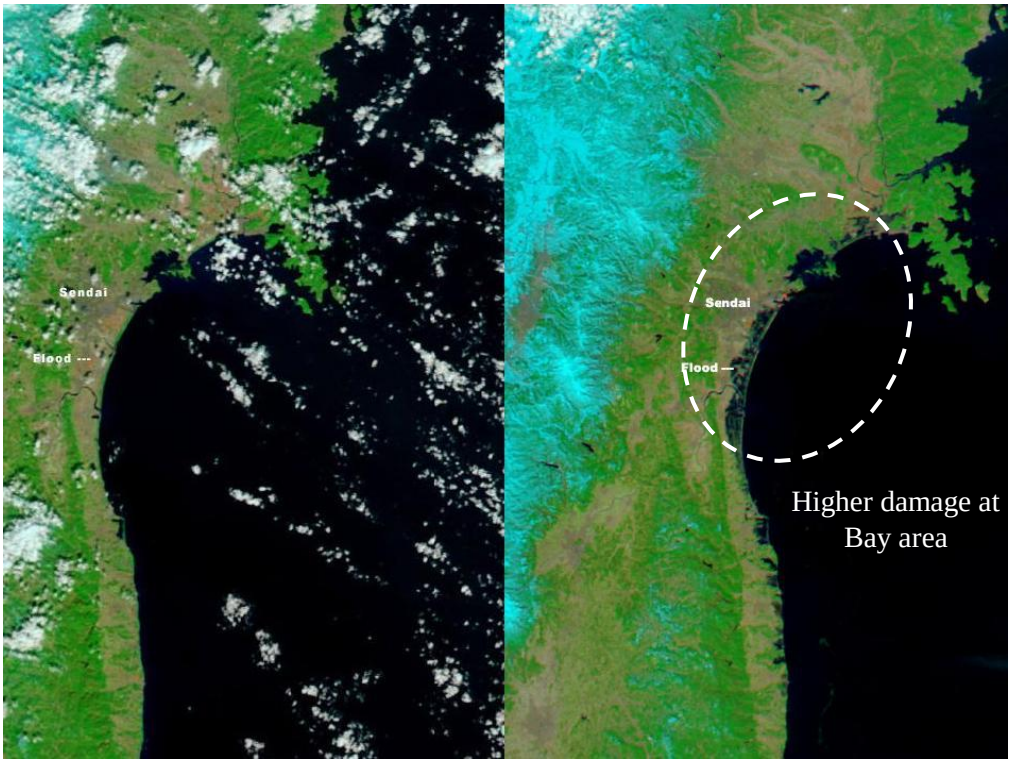

Figure 1.5: Satellite images showing before and after condition of Sendai area, Japan

Above evidences second the fact that beach morphology plays a significant role in a tsunami event. Therefore, the identification of the morphological features of areas which have

higher potential for destructive tsunami impact become very much important. Moreover, if a direct relation could be recognized as discussed above the findings will be very useful for planning and designing of hard tsunami disaster prevention measures.

The author carried out a study in 2017 to investigate on above observations (Silva and Araki, 2018). The primary objective of this study was to identify the common morphological features of coastal areas on which tsunamis would destructively impact. By doing that, the role of beach morphology in a tsunami event are to be defined for the use of future needs and further studies.

A numerical approach was used in this research mainly and in the conclusions, several important questions related to tsunami interaction with several coastal morphological features were answered as follows.

1. Which beach morphological features show higher tsunami damage on events occurred in the recent past?

Based on records and aftermath surveys of past events, it is known that flat lands with lower elevation with no protection showed higher damage on tsunamis. In addition to that, interesting observations are found from the results of this research. Higher energy from tsunami dissipated at partially closed bay areas making higher water level variation and higher current speeds. Moreover, bed shear stresses at bay areas showed higher values than that of pointed areas and headlands.

2. Does above identified beach morphological features have a common behavior when facing tsunamis regardless of location or time?

Yes! From the results of local models, a common relation was identified between 2004 and 2011 tsunami events. In both cases more tsunami dissipation observed at bay areas than that of pointed areas or headlands. In both cases, water level variations at partially closed bay areas showed comparatively higher oscillations sometimes reaching more than 10 meters. Meanwhile water level variations at pointed areas or near headlands showed comparatively smaller oscillations. Further, current velocities and induced bed shear stresses by striking tsunamis showed similar relation by reflecting higher variations at bay areas than that near pointed lands. However, the directional behavior of tsunami induced current speeds and bed shear stresses were varied depending on the location, surrounding bathymetry and topography and most importantly depending on the direction of the wave front.

3. Does above identified beach morphological features show the same behavior universally when those are remade without any identical local background?

Yes! From the results common model with an ideal bathymetry and ideal morphological features, the behavior discussed above was identified in a similar manner although there were

deviations existed in the dominant directions of current speeds and bed shear stresses. Thus, it could be concluded that the observed nature of tsunami energy dissipation at partially closed bay areas and in front of pointed areas or headlands is universal and not dependent on any identical local background.

4. What is the difference those morphological features show in a tsunami event that compared to the interaction with general wind waves?

As known, general wind waves concentrate at pointed beaches and spreads at bay areas due to refraction. And as wave breaking happens in most of the cases, higher energy dissipation is observed at pointed areas. Nevertheless, tsunami acts more like a budging surge or more of a water level change due to its much larger wave length. Thus, the wave rarely breaks when it attacks the shore. Due to this phenomenon more, portion of energy is reflected when it strikes pointed headlands with comparatively steep slope. On the other hand, the wave surges without any disturbance into shore at bay areas showing very little reflection.

1.3 TSUNAMI INTERACTION WITH SUBMERGED STRUCTURES

As it is mentioned under Section 1.1, various defense structures are currently being used to protect coastlines from probable tsunami attacks. Although, most of these structures are constructed on land, submerged structures can also provide some protection against a tsunami-like wave attack. Most researchers are interested on submerged protection structures due to the negative outcomes which are combined with massive onshore sea walls like environmental and social impacts.

A structure is considered as submerged, when the crest level is lower than the still water level. Due to several reasons like lower construction cost, aesthetics and non-disturbance nature to water circulation, submerged structures have many advantages over sun-areal structures (Kobayashi and Wurjanto, 1989). The *B/L* and *R/H* rations are important from the view point of the effectiveness of a submerged structure. Where *B* is crest width, *L* is wave length, *R* is the distance between water level and breakwater crest and *H* is wave height.

Increasing *B/L* will reduce the transmission and thus increase the effectiveness of the structure. As the wave length of a tsunami is quite large, the transmission reduction that could be achieved by a submerged structure is limited. When *L* is large, he ratio *B/L* becomes small, which results high transmission (Plas, 2007). Numerous experimental, numerical and analytical

studies have investigated the wave transmission over a submerged structure. The studies done by Kobayashi and Wurjanto (1989) and Huang and Dong (2001) can be given as examples for experimental studies.

A numerical study to simulate the interaction between a solitary wave and a submerged porous breakwater was carried out by Huang, Chang and Hwung (2003) via solving Navier-Stokes type model equations for porous flows. The results of the model were also verified by experimental data. He concluded that if the structure is wide enough compared to the wave length of the wave, the porosity of the structure had a negative impact on wave transmission coefficient. If the structure is too small, porosity of the structure had no impact on wave transmission.

An experimental study to investigate the breaking wave height of multi- directional random waves passing over an impermeable submerged breakwater was carried out by Hur, Kawashima and Iwata (2003). Through this study an empirical formula to estimate the breaking limit of multi-directional random waves was developed. Transmission characteristics of a submerged breakwater were also investigated by Rambabu and Mani (2005) via a numerical study where the effect of depth of submergence, crest width, initial wave conditions and material properties on the transmission characteristics of the submerged breakwaters were determined.

Wave transformation over a submerged permeable breakwater on a porous slope seabed was investigated by Tsai, Chen and Lee (2006). Through that investigation time-depend mild-slope equation for waves propagating over two layers of porous medium was developed, and the numerical outcome was validated by experimental data. The reflection and transmission of long waves from a trapezoidal breakwater and a series of trapezoidal breakwaters was also investigated by Chang and Liou (2007). A new method for calculating the 2D wave setup behind a submerged breakwater was proposed by (Calabrese, Vicinanza and Buccino, 2008). This method was also validated by experimental data.

With this background, Irtem, Seyfioglu and Kabdasli (2011) has carried out an experimental study to investigate the effects of submerged breakwaters on tsunami run-up height. In this study, he concluded that the permeable submerged breakwater is more effective than impermeable breakwater at reducing runup height. Wave passes through the permeable breakwater rather than jumping over it and through that some portion of wave energy is

dissipated. He has also concluded that the crest width of submerged breakwater does not substantially affect run-up height.

This background comes in handy as a new type of submerged protection structure is introduced and investigated in this thesis under chapter 3.

1.4 TSUNAMI INTERACTION WITH ONSHORE PROTECTION STRUCTURES

Onshore protection structures are the most common type of hard measures which are built to withstand tsunami disasters. Countries like Japan, which have the most tsunami vulnerability, often use onshore structures (coastal dikes, seawalls, etc.) built along in coastal areas.

The repetitive tsunami events experienced at the Pacific coast of Japan were studied by Raby et al. (2015). Presences of seawalls was questioned in a way as the definitive protection was actually observed only with seawalls height than 5m. When seawalls are smaller than that, the damage happened was higher due to the exaggerated development of the protected area thinking that the seawall would provide full protection. In this study, the authors suggested multiline defense systems and elevated topography as most effective defense measures.

(Source: Raby et al., 2015)

Figure 1.6. Damage to Yamamoto sea dikes observed during the 2011 tsunami disaster: (a) exposed sand core on the lee side; (b) evidence of sand core having been washed out; (c) exposed section through the sea dike; and (d) remnants of the dike into the distance, lying in pools of seawater to the lee side of the structure having not subsequently drained away.

If a tsunami overtops the onshore defense structures or if the structures fail ahead of the wave attack, an unexpected damage occurs at the lee side of the protection measures. This happened during the 2011 Great East Japan Earthquake and Tsunami disaster. Most of the tsunami prevention structures were overtopped by the massive wave and most of them failed. (Figures 1.6 and 1.7)

(Source: Raby et al., 2015)

Figure 1.7. Seawall damage observed during the 2011 tsunami disaster: (a) damage to seawall and quay at Minamisanriku; (b) close-up of sea wall block at Minamisanriku showing no inter linkages; (c) recovery work on the seawall at MiyakoBay; and (d) remaining seawall buttress at Tarō.

1.5 WALL AND TRENCH SYSTEMS

As explained in Sections 1.3 and 1.4, a tsunami wave attack cannot be always turned down by conventional hard measures. Therefore, researchers have been always keen to find new type of tsunami defense mechanisms which not only theoretically, but also practically can provide better protection to coastal areas.

In this study, a new type of protection structure system is proposed by the author. The structure system is conceptually designed by combining a wall with an associated trench. The

behavior of the structure was numerically investigated both in submerged and onshore conditions. Physical experiments were also carried out to calibrate the numerical investigations.

The first part of the study investigates the proposed structure system in (impermeable) submerged conditions and is elaborated in Chapter 3. The second part of the study investigates the proposed structure system in onshore conditions and is discussed in Chapter 4. Chapter 2 consist of the theoretical background that is needed for Chapter 3 and Chapter 4. At the end, Chapter 5 gives the conclusions and recommendations that the author came across by carrying out the study.

CHAPTER 2

Chapter 2

THEORITICAL BACKGROUND

OUTLINE

Chapter 2 consists of five main sections. Firstly, the mathematical background of classical formulation of tsunami propagation is elaborated which is important for numerically recreating tsunami wave models. Next, the important aspects of the shallow water Boussinesq model which is used in Chapter 3 is explained. Afterwards, the Computational Fluid Dynamics (CFD) model that is used in Chapter 4 is introduced and explained.

2.1 TSUNAMI MODELLING

2.1.1 List of Symbols for Section 2.1

$\Delta u_i\ (\xi_1, \xi_2, \xi_3)$ - Dislocation field

$\sqrt{G_{\eta\eta}}$ - Coefficient used to transform curvilinear to rectangular coordinates

$\sqrt{G_{\xi\xi}}$ - Coefficient used to transform curvilinear to rectangular coordinates

D - Depth below some horizontal plane of reference (datum)

g - Acceleration due to gravity

H - Total water depth $(H = D + \varsigma)$

m, n, k - Grid coordinates

t - Time

U - Depth-averaged velocity in ξ direction

u - Flow velocity in the x or ξ direction

$u_i(x_1, x_2, x_3)$ - Displacement field

V - Depth-averaged velocity in y or η direction

v - Fluid velocity in y or η direction

$v^{\sim}$ - Total velocity due to flow and Stokes drift in y or η direction

x, y, z - Cartesian coordinates

ς - Water level above some horizontal plane of reference (datum)

λ, μ - Lame's constants,

ξ, η - Horizontal, curvilinear coordinates

σ - Scaled vertical co-ordinate; $\sigma = (z - \varsigma)/(d + \varsigma)$

ω - Angular frequency waves

2.1.2 Classical Formulation of Tsunami Propagation

The propagation of water waves can be explained by the governing equations of fluid motion. As tsunami propagation can be treated as a special case of water wave propagation, it can also be described by considering governing equations of fluid motion while giving special attention to several important parameters which directly impact the propagation of tsunami-like waves.

An interesting explanation on governing equations for fluid motion from the perspective of tsunami propagation can be found in Dutykh's publication (Dutykh, 2008). In this chapter, Sections 2.1.2 to 2.1.4 are prepared by closely following the equations and explanations of Dutykh work (Dutykh, 2008).

Let's start by defining the continuity and momentum equations which govern the fluid motion in 3D space (x, y, z) over time (t).

The horizontal coordinates are denoted by *x* and *y*, and the vertical coordinate by *z*. The horizontal gradient is denoted by

$$\nabla := \left(\frac{\partial}{\partial x}, \frac{\partial}{\partial y}\right)$$

The horizontal velocity is denoted by

$$\boldsymbol{u}(x, y, z, t) = (u, v)$$

and the vertical velocity by

$$\boldsymbol{w}(x, y, z, t).$$

By considering water as an inviscid and an incompressible fluid, conservation of mass can be expressed as follows for three-dimensional flow.

$$\nabla . \boldsymbol{u} + \frac{\partial w}{\partial z} = 0 \tag{2.1}$$

and the conservation of momentum can be expressed as

$$\rho \frac{Du}{Dt} = -\nabla p \quad , \quad \rho \frac{Dw}{Dt} = -\rho g - \frac{\partial p}{\partial z} \tag{2.2}$$

where Df/Dt is the material derivative defined as,

$$\frac{Df}{Dt} = \frac{\partial f}{\partial t} + u . \nabla f \quad , \quad u = (u, w) = (u, v, w) \tag{2.3}$$

In equation (2.2), ρ is the density of water (assumed to be constant throughout the fluid domain), g is the acceleration due to gravity and $p(x, y, z, t)$ the pressure field.

When the flow is assumed as irrotational, the scalar function of velocity potential $\phi(x, y, z, t)$ can be defined and $\boldsymbol{u}$ and $\boldsymbol{w}$ can be expressed by using velocity potential.

$$\boldsymbol{u} = \nabla \phi \quad , \quad w = \frac{\partial \phi}{\partial z} \tag{2.4}$$

By substituting velocity potential into the continuity equation, equation (2.1) becomes equation (2.5) which is identified as the Laplace's equation.

$$\nabla^2 \phi + \frac{\partial^2 \phi}{\partial z^2} = 0 \tag{2.5}$$

By substituting velocity potential into the momentum conservation, equation (2.2) can be integrated into equation (2.6) which is identified as the Bernoulli's equation.

$$\frac{\partial \phi}{\partial t} + \frac{1}{2}|\nabla \phi|^2 + \frac{1}{2}\left(\frac{\partial \phi}{\partial z}\right)^2 + gz + \frac{p - p_o}{\rho} = 0 \tag{2.6}$$

The reference pressure (commonly, atmospheric pressure) is denoted by p_o. The effects of surface tension can be neglected for tsunami propagation.

If a surface wave bounded by the free surface (represented by $f(x, y, z, t) = \eta(x, y, t) - z = 0$) and a solid bottom boundary (represented by $z = -h(x, y)$) under gravitational attraction is considered, the Laplace's equation (2.5) in time domain (t) can be solved by applying kinematic and dynamic boundary conditions.

Kinematic boundary condition is stated as $Df/Dt = 0$. When $Df/Dt = 0$, the material derivative of f vanishes and leads to

$$\eta_t + \nabla \phi \cdot \nabla \eta - \phi_z = 0 \ \ at \ \ z = \eta(x, y, t) \tag{2.7}$$

Secondly, Dynamic boundary condition is applied. In dynamic condition, the normal stresses are in the balance at the free surface. In Bernoulli's equation (2.6), the normal stress at the free surface is given by the difference of pressure. At $z = \eta$, the equation leads to

$$\phi_t + \frac{1}{2}|\nabla \phi|^2 + \frac{1}{2}\phi_z^2 + g\eta = 0 \text{ at } \ z = \eta(x, y, z) \tag{2.8}$$

The boundary condition at the bottom can be written as

$$\nabla \phi \cdot \nabla h + \phi_z = 0 \text{ at } \ z = -h(x, y) \tag{2.9}$$

If initial conditions are given at $t = 0$, the equations (2.5), (2.7), (2.8) and (2.9) can be solved for water surface elevation $\eta(x, y, t)$ and the velocity potential $\phi(x, y, z, t)$. Thereafter, the momentum equation can be used to solve for pressure p when surface elevation $\eta(x, y, t)$ and the velocity potential $\phi(x, y, z, t)$ are found by the initial solving the initial value problem of the continuity equation.

By giving various assumptions, the full water wave equations can be simplified. Shallow water approximations and Boussinesq approximations can be given as most common and widely used assumptions which are closely related to tsunami wave propagation. Linear shallow water equations are the simplest. If we want to consider non-linearity without dispersion, non-linear the full water wave equations can be simplified to non-linear shallow-water equations. If we want to consider both non-linerity and dispersion, the full water wave equations are reduced to Boussinesq equations.

In this study, non-linear Boussinesq equations were used to model the tsunami flow under Chapter 03.

Shallow water assumptions can be only applied to the full water wave equation only if the water depth is much smaller than the wavelength. For tsunami waves, this condition can be assumed as true due to much larger wave length of the wave (hundreds of kilometers) compared to the depth of the ocean floor (few kilometers).

Here, we can discuss two dimensionless parameters to understand the concept.

$$\alpha = \frac{a}{d} \ll 1 \ , \qquad \beta = \frac{d^2}{l^2} \ll 1 \tag{2.10}$$

where d is a typical water depth, a a typical wave amplitude and l a typical wavelength.

If we consider Indian Ocean Tsunami (2004) for example, the conditions of (2.10) are found out to be satisfied by the observed satellite altimetry data. The wave amplitude was roughly measured as 60 cm while the ocean depth ranges up to 4 km. The wave length was experienced around 160 and 240 km which gives following ranges for α and β.

$$1.5 \times 10^{-4} < \alpha < 6 \times 10^{-4}, \qquad 2.2 \times 10^{-5} < \beta < 6.25 \times 10^{-4} \tag{2.11}$$

The water wave equations can also be written in non-dimensional form to incorporate α and β, so that we can later eliminate non-significant parts of the equation by assuming the smallness of these parameters. The non-dimensional independent variables of the water wave equation can be written as follows.

$$x = l\tilde{x}, \qquad y = l\tilde{y}, \qquad z = d\tilde{z}, \qquad t = l\tilde{t}/c_o \tag{2.12}$$

where $c_o = \sqrt{gd}$, the celerity of propagation of tsunamis (deep water propagation of waves) in the open ocean ranging from 356 km/h for a 1 km water depth to 712 km/h for a 4 km water depth. The non-dimensional dependent variables are

$$\eta = a\tilde{\eta}, \qquad h = d\tilde{h}, \qquad \phi = gal\tilde{\phi}/c_o \tag{2.13}$$

By substituting all the defined dimensionless variables in water wave equations and by eliminating tidal effect, following set of equations can be written.

$$\beta\nabla^2\phi + \phi_{zz} = 0 \tag{2.14}$$

$$\beta\nabla\phi \cdot \nabla h + \phi_z = 0 \ \ at \ \ z = -h(x,y) \tag{2.15}$$

$$\beta\eta_t + \alpha\beta\nabla\phi \cdot \nabla\eta = \phi_c \ \ at \ \ z = \alpha\eta(x,y,t) \tag{2.16}$$

$$\beta\phi_t + \frac{1}{2}\alpha\beta|\nabla\phi|^2 + \frac{1}{2}\alpha\phi_z^2 + \beta\eta = 0 \ \ at \ z = \alpha\eta(x,y,t) \tag{2.17}$$

2.1.3 Shallow-Water Equations

The water column can be treated as shallow, when β is small. Also, the equations become linear, when α is assumed to be zero. When β is small, the expression of ϕ can be simplified.

$$\phi = \phi_0 + \beta\phi_1 + \beta^2\phi_2 + \cdots$$

By substituting the expression into water wave equations for boundary conditions, the ϕ_0 term in the continuity equation for the vertical coordinate *z* can be written as:

$$\phi_{0zz} = 0 \tag{2.18}$$

For horizontal coordinates, the first term of ϕ can be written as $\phi_{0x} = u(x,y,t)$ and $\phi_{0y} = v(x,y,t)$. If we assume a constant water depth (*h = 1)*, the solution of the continuity

equation with kinematic boundary condition gives following expressions for second and third terms of ϕ_1 and ϕ_2:

$$\phi_1(x,y,z,t) = -\frac{1}{2}(1+z)^2(u_x + u_y) \tag{2.19}$$

$$\phi_2(x,y,z,t) = \frac{1}{24}(1+z)^4\left[(\nabla^2 u)_x + (\nabla^2 v)_y\right] \tag{2.20}$$

When equation (2.19) is substituted into the dynamic boundary condition (2.17) and kinematic boundary condition (2.16) at $z = 0$, by keeping the terms of order $\alpha\beta$ and β^2 we can obtain:

$$\beta\phi_{0t} - \frac{1}{2}\beta^2\left(u_{tx} + u_{ty}\right) + \beta\eta + \frac{1}{2}\alpha\beta(u^2 + v^2) = 0 \tag{2.21}$$

$$\beta\left[\eta_t + \alpha\left(u\eta_x + u\eta_y\right) + (1+\alpha\eta)\left(u_x + u_y\right)\right] = \frac{1}{6}\beta^2\left[(\nabla^2 u)_x + (\nabla^2 v)_y\right] \tag{2.22}$$

Then we differentiate equation (2.21) with respect to x and with respect to y to obtain equations (2.23) and (2.24).

$$u_t + \alpha(uu_x + vv_x) + \eta_x - \frac{1}{2}\beta\left(u_{txx} + u_{txy}\right) = 0 \tag{2.23}$$

$$v_t + \alpha\left(uu_y + vv_y\right) + \eta_y - \frac{1}{2}\beta\left(u_{txy} + u_{tyy}\right) = 0 \tag{2.24}$$

The equation of kinematic condition (2.22) can be rewritten as

$$\eta_t + [u(1+\alpha\eta)]_x + [v(1+\alpha\eta)]_y = \frac{1}{6}\beta^2\left[(\nabla^2 u)_x + (\nabla^2 v)_y\right] \tag{2.25}$$

Now we can drop the terms of β by giving the condition that β is small and equations (2.26) – (2.28) are obtained. These set of equations are so called, linear shallow water equations.

$$u_t + \alpha\left(uu_x + vu_y\right) + \eta_x = 0 \tag{2.26}$$

$$v_t + \alpha(uv_x + vv_y) + \eta_y = 0 \tag{2.27}$$

$$\eta_t + [u(1 + \alpha\eta)]_x + [v(1 + \alpha\eta)]_y = 0 \tag{2.28}$$

Note that we assumed a constant water depth to obtain equations (2.19) and (2.20). Now, we can rewrite, equations (2.26) - (2.28) by applying an arbitrary water depth $(h + \eta)$ with dimensional variables. These set of equations can be referred as non-linear shallow water equations.

$$u_t + uu_x + vu_y + g\eta_x = 0 \tag{2.29}$$

$$v_t + uv_x + vv_y + g\eta_y = 0 \tag{2.30}$$

$$\eta_t + [u(h + \eta)]_x + [v(h + \eta)]_y = 0 \tag{2.31}$$

2.1.4 Boussinesq Equations

We need another condition to explain the Boussinesq equations other than α and β for which, another dimention-less parameter (S) is introduced in addition to α and β and assume $(S \approx 1)$ (Bona, Chen and Saut, 2002). S is referred as Stokes number or sometimes as Ursell number.

$$S = \frac{\alpha}{\beta} \tag{2.32}$$

From the observations that are mentioned mentioned under shallow water equations, the range of S for Indian Ocean tsunami is

$$0.24 < S < 46 \tag{2.33}$$

Therefore, the condition $S \approx 1$ is satisfied by the Indian Ocean tsunami for some extent. The water depth is assumed to be constant here as well for the derivation. The potential and the

derivatives of the velocity potential are denoted by $\Phi(x,y,t) = \Phi(x,y,\eta,t)$ and $\Phi_*(x,y,t) = \Phi_*(x,y,\eta,t)$. Where the star stands for *x*, *y*, *z* or *t*. The vertical velocity at the free surface is denoted by $W(x,y,t) = \phi_z(x,y,\eta,t)$. Then, the dynamic boundary conditions on the free surface can be written from equations (2.7) and (2.8).

$$\eta_t + \nabla\Phi \cdot \nabla\eta - W(1 + \nabla\eta \cdot \nabla\eta) = 0 \tag{2.34}$$

$$\Phi_t + g\eta + \frac{1}{2}|\nabla\Phi|^2 - \frac{1}{2}W^2(1 + \nabla\eta \cdot \nabla\eta) = 0 \tag{2.35}$$

In addition, the continuity equation and the kinematic boundary condition on the bottom must be satisfied. The velocity potential is given as a formal expansion for Boussinesq-type models (2.36), which leads to the dispersive effect.

$$\phi(x,y,z,t) = \sum_{n=0}^{\infty} \phi^{(n)}(x,y,t) z^n \tag{2.36}$$

Here the expansion is about $z = 0$, which is the location of the free surface at rest. ϕ_0 denote the velocity potential at $z = 0$, u_o the horizontal velocity at $z = 0$, and w_0 the vertical velocity at $z = 0$. By looking at the equation (2.36), note that ϕ_0 and w_0 are nothing else than $\phi^{(0)}$ and $\phi^{(1)}$. Now, the velocity potential ϕ can be expressed in terms of ϕ_0 and w_0 only. For the whole water column ($-h \le z \le \eta$) the velocity field can be written by using ϕ_0 and w_0 as follows.

$$u(x,y,z,t) = \cos(z\nabla)u_o + \sin(z\nabla)w_o \tag{2.37}$$

$$w(x,y,z,t) = \cos(z\nabla)w_o + \sin(z\nabla)u_o \tag{2.38}$$

The Taylor series operators of $\cos(z\nabla)$ and $\sin(z\nabla)$ are expressed as, (Madsen, Bingham and Schäffer, 2003)

$$\cos(z\nabla) = \sum_{n=0}^{\infty} (-1)^n \frac{2^{2n}}{(2n)!} \nabla^{2n}, \qquad \sin(z\nabla) = \sum_{n=0}^{\infty} (-1)^n \frac{2^{2n+1}}{(2n+1)!} \nabla^{2n+1} \tag{2.39}$$

Not that, equations (2.39) give just a notation to ∇. It should be understand in conjunction with equations (2.37) and (2.38).

Thereafter, we can substitute the representation (2.37) and (2.38) into the kinematic bottom boundary condition and use successive approximations to obtain an explicit recursive expression for w_o in terms of u_o to infinite order in $h\nabla$. We also can generalize the expansions to an arbitrary *z* level, instead of the *z = 0* level. For that, Taylor series for the cosine and sine operators can be truncated, Pad´e approximants can be used in operators at $z = -h$ and/or at z = 0.

Let's consider writing the Boussinesq equations in non-dimentional form by using dimensionless variables used under shallow water equations. Here we only consider one horizontal dimension (*x*). we still assume *h* is constant and the tidal effect is ignored. By substituting the expression for ϕ into the free-surface boundary conditions evaluated at *z = 1 + αη(x, t)* leads to two equations in η and ϕ_o with terms of various order in α and β. The expressions written only by keeping the most linear terms of α and β, and and by giving the condition $S \approx 1$, following expressions can be derived.

$$u_t + uu_x + g\eta_x - \frac{1}{2}h^2 u_{txx} = 0 \tag{2.40}$$

$$\eta_t + [u(h+\eta)]_x - \frac{1}{6}h^3 u_{txx} = 0 \tag{2.41}$$

When the velocity (*u*) is replaced by the depth averaged velocity as shown below, the expressions are referred to as the classical Boussinesq equations.

$$\frac{1}{h}\int_{-h}^{\eta} u dz$$

They read

$$u_t + uu_x + gn_x - \frac{1}{3}h^2 u_{txx} = 0 \tag{2.42}$$

$$\eta_t + [u(h+\eta)]_x = 0 \tag{2.43}$$

2.2 IMPORTANT ASPECTS OF DELFT3D-FLOW MODULE

The numerical simulations which are described in this chapter are carried out with the use of Delft3D-FLOWmodule. Delft3D is the integrated flow and transport modelling system of Deltares for the aquatic environment (Deltares, 2018). The hydrodynamic module Delft3D-FLOW simulates two-dimensional (2DH, depth-averaged) or three-dimensional (3D) unsteady flow.

Delft3D-FLOW solves the Navier Stokes equations for an incompressible fluid, under the shallow water and the Boussinesq assumptions (Deltares, 2018). Therefore, it can be used to simulate tsunami propagation. This Section 2.2 closely follows the details that are given in the user's guide of Delft3D (Deltares, 2018).

2.2.1 Grid system used in Delft3D-FLOW

Delft3D-FLOW uses finite differences finite difference method to solve the equations numerically. The horizontal grid coordinates can be defined in two ways as cartesian or orthogonal. The vertical grid coordinates can also be defined in two ways known as σ and z. Curvilinear discretization is applied in the σ grid and cartesian discretization is applied in the z grid. As the author only simulated the tsunami flow in depth averaged form in Chapter 03, the details of vertical discretization are not discussed here.

2.2.2 Open Boundary Conditions

Open boundaries are introduced to the model domain so that they will reproduce a similar impact of natural flow at the edges of the model domain. By introducing open boundaries, we can reduce the size of the computational area by only focusing the interested domain. There are several types of open boundary definitions in the Delft3D-FLOW module. Open boundaries can be defined by using physical measurements like water level elevations and current velocities. When we consider an open water area, the most common problem arising at the open boundaries is the reflection of waves. To overcome this problem, various open boundary conditions have been derived by researchers. For example, Verboom and Slob

(1984) derived a so-called zero and first order weakly reflecting boundary condition based on the work of Engquist and Majda (1979) (Deltares, 2018). Assuming zero flow along the boundary, the zero-order boundary condition may also be obtained using the so-called Riemann invariants for the linearized 1D equation normal to the open boundary:

$$R = U \mp \sqrt{gH} \tag{2.44}$$

The two Riemann invariants are two waves moving in opposite direction with propagation speed *R*. The sign is dependent on the direction of propagation. At the open boundary, the incoming wave should be specified (Deltares, 2018). We restrict ourselves to the positive sign (left boundary). The linearized Riemann invariant is given by:

$$U + 2\sqrt{gH} = U + 2\sqrt{g(d+\zeta)} \approx U + 2\sqrt{gd} + \zeta\sqrt{\frac{g}{d}}, \quad \frac{|\zeta|}{d} \ll 1 \tag{2.45}$$

The author used, Riemann boundary conditions for the simulations of the study that was briefly explained in Section 1.2 of Chapter 01. However, for the main study that is given in detail in Chapter 03, defining open boundary conditions was not necessary, as the domain of the wave flume only had fully reflective closed boundaries.

2.2.3 Time Integration of Shallow Water Equations

An explicit time integration of the shallow water equations on a rectangular grid is subject to a time step condition based on the Courant number for wave propagation (Deltares, 2018):

$$CFL_{wave} = 2\Delta t\sqrt{gH}\sqrt{\frac{1}{\Delta x^2} + \frac{1}{\Delta y^2}} < 1 \tag{2.46}$$

where Δt is the time step, g is the acceleration of gravity, H is the total water depth and $\Delta x = G_{\xi\xi}$ and $\Delta y = G_{\eta\eta}$ are the smallest grid spaces in ξ- and η-direction of the physical space.

When we use explicit time integration, it requires quite small-time step to simulate wave propagation. Instabilities may occur if the time step is large. Therefore, implicit methods are usually considered and found to be more applicable from the view point of robustness.

Leendertse (1967); Leendertse and Gritton (1971); Leendertse and Liu (1975) introduced an Alternating Direction Implicit (ADI) method for the shallow water equations. The ADI method splits one-time step into two stages (Deltares, 2018). Each stage consists of half a time step. In both stages, all the terms of the model equations are solved in a consistent way with at least second order accuracy in space (Deltares, 2018).

2.2.4 Spatial Discretization of Shallow Water Equations

2.2.4.a Horizontal Advection Terms

Four schemes are available in Delft3D-FLOW to discretize the horizontal advection terms:

- WAQUA-scheme
- Cyclic method
- Flooding-scheme
- Multi directional upwind (Z-model only)

The author used the second method (Cyclic) to perform simulations that are discussed in detain under Chapter 03. Thus, explanations on the other methods are not stated here.

Stage 1:

$$\left|\frac{v}{\sqrt{G_{\eta\eta}}}\frac{\partial u}{\partial \eta}\right|_{mnk} = \frac{\tilde{v}^{\varepsilon\eta}_{m,n,k}}{\left(\sqrt{G_{\eta\eta}}\right)_{m,n}}\left(\frac{3u_{m,n+1,k} - u_{m,n-1,k}}{2\Delta\eta}\right), \quad \tilde{v}^{\varepsilon\eta}_{m,n,k} \geq 0 \qquad (2.47)$$

And stage 2:

$$\left|\frac{v}{\sqrt{G_{\eta\eta}}}\frac{\partial u}{\partial \eta}\right|_{mnk} = \frac{\tilde{v}^{\varepsilon\eta}_{m,n,k}}{\left(\sqrt{G_{\eta\eta}}\right)_{m,n}}\left(\frac{3u_{m,n+1,k} - 4u_{m,n-1,k} + u_{m,n-2,k}}{2\Delta\eta}\right), \quad \tilde{v}^{\varepsilon\eta}_{m,n,k} \geq 0$$

$$\left|\frac{v}{\sqrt{G_{\eta\eta}}}\frac{\partial u}{\partial \eta}\right|_{mnk} = \frac{\tilde{v}^{\varepsilon\eta}_{m,n,k}}{\left(\sqrt{G_{\eta\eta}}\right)_{m,n}}\left(\frac{-3u_{m,n+1,k} + 4u_{m,n-1,k} - u_{m,n-2,k}}{2\Delta\eta}\right), \quad \tilde{v}^{\varepsilon\eta}_{m,n,k} < 0 \qquad (2.48)$$

The Cyclic method is based on the dissipative reduced phase error scheme Eqs. (2.47) and (2.48) for both the normal advection term $u\ \partial u\ \partial\xi$ and the cross-advection term $v\ \partial u\ \partial\eta$ (Stelling and Leendertse, 1992) (Deltares, 2018).

2.2.4.b Vertical Advection Term

To discretize the vertical advection term, a second order central difference is used (Deltares, 2018) and given in the following equation:

$$\left[\frac{\omega}{H}\frac{\partial u}{\partial \sigma}\right]_{m,n,k} = \tilde{\omega}^{\varepsilon\sigma}_{m,n,k}\left[\frac{u_{m,n,k-1} - u_{m,n,k+1}}{\frac{1}{2}h_{m,n,k-1} + h_{m,n,k} + \frac{1}{2}h_{m,n,k+1}}\right] \tag{2.49}$$

where $h_{m,n,k}$ denotes the thickness of the computational layer within index k defined by $h_{m,n,k} = \Delta\sigma k H_{m,n}$ and H the total water depth or $h_{m,n,k} = \Delta z_{m,n,k}$ in the z-model.

2.2.4.c. Viscosity Terms

The approximation of the vertical viscosity terms is based on central differences (Deltares, 2018). The vertical viscosity term in the u-equations is discretized as:

$$\left[\frac{1}{H^2}\frac{\partial}{\partial\sigma}\left(\nu V\frac{\partial u}{\partial\sigma}\right)\right]_{m,n,k} = \frac{[\nu V]_{m,n,k-1}}{h_{m,n,k}}\left(\frac{u_{m,n,k-1} - u_{m,n,k}}{\frac{1}{2}\left(h_{m,n,k-1} + h_{m,n,k}\right)}\right) - \frac{[\nu V]_{m,n,k}}{h_{m,n,k}}\left(\frac{u_{m,n,k} - u_{m,n,k+1}}{\frac{1}{2}\left(h_{m,n,k} + h_{m,n,k+1}\right)}\right) \tag{2.50}$$

The vertical eddy viscosity is computed at the layer interface, with $h_{m,n,k} = \Delta\sigma H_{m,n,k}$ or $h_{m,n,k} = \Delta z_{m,n,k}$ in the z-model (Deltares, 2018).

2.3 USE OF RANS SOLVERS IN TSUNAMI MODELLING

As explained under the previous Section 2.1.4, time domain shallow water Boussinesq models are generally used by researchers to model tsunami propagation. However, it would be more accurate if we can solve least averaged fluid motion equations (Navier Stokes Equations) rather than solving shallow water Boussinesq equations. Shen, Ng and Zheng (2004) used the Reynolds-Averaged Navier-Stokes equations (RANS) and Engsig-Karup *et al.* (2006) applied the Galerkin finite-element method for solution of the high-order Boussinesq-type equations.

In 2013, Gadelho, Lavrov and Soares (2013) used the OpenFOAM InterFOAM solver to successfully calibrate a 2D numerical wave flume to evaluate the effect of obstacles on the wave propagation. The main disadvantage of a RANS solver over a Boussinesq solver is its massive computational cost. However, it is a matter of time that the use of RANS solvers can be applied to large scale applications like coastal modelling with the rapid development of the computers. Nevertheless, we can use a RANS solver like "interFOAM" for small scale simulations like tsunami wave tank with an average computational power which is available today.

2.4 IMPORTANT ASPECTS OF OPENFOAM – INTERFOAM SOLVER

"OpenFOAM^{TM}" is a collection of open sources codes, primarily built for solving continuum mechanics problems including computational fluid dynamics (CFD). The company of OpenCFD based in United Kingdom developed the code mainly in C++ language. Original development started in the late 1980s at Imperial College, London, motivated by a desire to find a more powerful and flexible general simulation platform at the time of Fortran. Since then it has evolved by exploiting the latest advanced features of the C++ language, having been actively re-written several times over. The collection of codes has been released to public in open source in 2004.

The interFOAM solver of OpenFOAM^{TM} Toolbox is a multiphase solver able to reproduce the characteristics of multiphase flow.

2.5 MATEMATICAL FORMULATION OF THE INTERFOAM SOLVER

In this section, the mathematical formulation and equation discretization of interFoam solver are explored to better understand the formulation. The author followed the PhD thesis of Lopes (2013) to understand the background of OpenFOAM, interFOAM solver. Lopes (2013) has given a clear and simplified explanation to the formulation in InterFoam solver by following the original work of Jasak (1996), Ubbink (1997) and Rusche (2003).

2.5.1 Continuity and Momentum Equations

As mentioned under Section 2.1.2, fluid motion can be explained by a set of partial differential equations, so called governing equations of fluid motion. These equations can be written in the differential form for a 3D system as follows.

Conservation of mass:

$$\frac{\partial \rho}{\partial t} + \nabla \cdot (\rho u) = 0 \tag{2.51}$$

Conservation of momentum:

$$\frac{\partial \rho u}{\partial t} + \nabla \cdot (\rho u u) = \rho g + \nabla \cdot \sigma \tag{2.52}$$

Conservation of energy:

$$\frac{\partial \rho e}{\partial t} + \nabla \cdot (\rho e u) = \rho g u + \nabla \cdot (\sigma u) - \nabla \cdot q + \rho Q \tag{2.53}$$

where ρ is the fluid density, u is the three-dimensional velocity field, σ is the shear stress tensor, e is the total specific energy, Q is the volume energy source, q is the heat flux and g is the gravity acceleration vector.

As the number of unknown variables is larger than known variable, assumptions and relations are needed in order to solve the set of equations. Consequently, it is necessary to include a set of constitutive relations which can be consulted in Jasak's (1996) thesis as stated by Lopes (2013). By considering the fluid as Newtonian, incompressible (ρ constant) and isothermal, the system of equations (2.51), (2.52) and (2.53) can be written in the simplified form:

$$\nabla \cdot u = 0 \tag{2.54}$$

$$\frac{\partial u}{\partial t} + \nabla \cdot (u u) = g - \nabla p + \nabla \cdot (v \nabla u) \tag{2.55}$$

where v is the kinematic viscosity and p is kinematic pressure.

The final form of the continuity and momentum equations are stated by multiplying the momentum equation by the density of fluid.

$$\nabla \cdot u = 0 \tag{2.56}$$

$$\frac{\partial \rho u}{\partial t} + \nabla \cdot (\rho u u) = -\nabla P + \nabla \cdot \tau + \rho g + F \tag{2.57}$$

where P is the pressure ($P = p * \rho$), τ is the viscosity stress tensor and F represents the source of the momentum in regard to the surface tension (Rusche, 2003):

$$F = \int_{S(t)} \sigma \kappa' n' \delta(x - x') dS \tag{2.58}$$

where σ is the surface tension coefficient, κ' is the curvature and n' is the normal vector of the interface. The viscous stress term can be reformulated to obtain more efficiency. The final form of this term is as follows (μ – dynamic viscosity of the fluid):

$$\nabla \cdot \tau = \nabla \cdot (\mu [\nabla u + (\nabla u)^T]) = \nabla \cdot (\mu \nabla u) + (\nabla u) \cdot \nabla \mu \tag{2.59}$$

By removing the hydrostatic pressure ($pg \cdot x$) from the pressure P, the modified pressure p^* is adopted in interFoam. The gradient of the p^* is defined as:

$$\nabla p^* = \nabla P - \nabla(\rho g \cdot x) = \nabla P - \rho g - g \cdot x \nabla \rho \tag{2.60}$$

2.5.2 Indicator Function of the Volume of Fluid Method (VOF)

The VOF method presented by Hirt and Nichols (2018) is applied in the interFoam solver. It uses the indicator α to capture the interface between two fluids (Lopes, 2013).

$$\alpha(x,y,z,t) = \begin{cases} 1 & \text{for a place}(x,y,z,t)\text{occupied by the fluid 1} \\ 0 < \alpha < 1 & \text{for a place}(x,y,z,t)\text{in the interface} \\ 0 & \text{for a place}(x,y,z,t)\text{occupied by the fluid 2} \end{cases} \quad (2.61)$$

The time dependent transport function of α is stated as an advection function:

$$\frac{\partial \alpha}{\partial t} + \nabla \cdot (\alpha u) = 0 \quad (2.62)$$

In the vicinity of the interface between two fluids (fluid 1 and fluid 2), mixing is possible and therefore, the local fluid properties (ρ and μ) is expressed as weighted function by incorporating the indicator α.

$$\rho = \alpha\rho_1 + (1-\alpha)\rho_2 \quad (2.63)$$

$$\mu = \alpha\mu_1 + (1-\alpha)\mu_2 \quad (2.64)$$

Fluid velocity u is also treated as a combination of velocities of two fluids u_1 and u_2.

$$\overline{u} = \alpha u_1 + (1-\alpha)u_2 \quad (2.65)$$

To reduce the significant errors of physical fluid properties, specially when using high density fluids, an additional term is introduced (artificial compression term) to the phase fraction function (Jasak and Weller 2002).

$$\frac{\partial \alpha}{\partial t} + \nabla \cdot (\alpha\overline{u}) + \nabla \cdot [u_r \alpha(1-\alpha)] = 0 \quad (2.66)$$

Where $u_r = u_1 - u_2$ the vector of relative velocity between the two fluids, also called as compression velocity (Berberović *et al.*, 2009) and $\overline{u}$ is the mean velocity, calculated by equation (2.65).

2.5.3 Surface Tension Force

In the vicinity of the interface of two fluids, surface tension force can act significantly. Therefore, the source term of the momentum equation should be rearranged as an indicator function. The Continuum surface Force (CSF) model developed by Brackbill, Kothe and Zemach (1992) is applied in interFoam, converting the F term into a volume force function of the surface tension. There, the surface curvature (κ) is formulated from local gradients in the surface normal (n) at the interface, which is a function of the phase fraction ($n = \nabla\alpha$) (Tang and Wrobel, 2005):

$$\kappa = \nabla \cdot \hat{n} = \nabla \cdot \frac{n}{|n|} = \nabla \cdot \left(\frac{\nabla\alpha}{|\nabla\alpha|}\right) \tag{2.67}$$

The volumetric surface tension force (**F**) is written in terms of the surface tension, and subsequently, to the jump pressure across the interface.

$$\mathbf{F} = \sigma\kappa \frac{\rho}{0.5(\rho_1 + \rho_2)} \nabla\alpha \approx \sigma\kappa\nabla\alpha \tag{2.68}$$

By considering the volumetric form of surface tension (2.68), the viscous stress term (2.59) and the modified pressure (2.60), the final form of the momentum equation can be written as:

$$\frac{\partial \rho \mathrm{u}}{\partial t} + \nabla \cdot (\rho \mathrm{uu}) - \nabla \cdot (\mu \nabla \mathrm{u}) = -\nabla p * + (\nabla \mathrm{u}) \cdot \nabla\mu - \mathrm{g} \cdot \mathrm{x}\nabla\rho + \mathrm{ac}\,\nabla\alpha \tag{2.69}$$

In conclusion, the interFoam solver solves continuity equation (2.51), the modified indicator function (2.66) and the momentum equation (2.69). These equations are solved together with the constitutive relations for density and dynamic viscosity given by (2.63) and (2.64).

2.5.4 Turbulence Modelling

Reynolds Averaged Navier Stokes Equations (RANS) are solved in the interFoam solver, meaning that we should use a turbulence model to calculate Reynolds stresses (last term) in equation (2.71). The general form of Navier Stokes Equations and the RANS are given in equations (2.70) and (2.71) respectively.

.

$$\frac{D}{Dt}\begin{pmatrix} u \\ v \\ w \end{pmatrix} = \frac{\partial}{\partial t}\begin{pmatrix} u \\ v \\ w \end{pmatrix} + (u \cdot \nabla)\begin{pmatrix} u \\ v \\ w \end{pmatrix} = \frac{-\nabla P}{\rho} + g + \nu\nabla^2\begin{pmatrix} u \\ v \\ w \end{pmatrix} \tag{2.70}$$

$$\frac{D}{Dt}\begin{pmatrix} \overline{\bar{u}} \\ \bar{v} \\ \overline{w} \end{pmatrix} = \frac{\partial}{\partial t}\begin{pmatrix} \bar{u} \\ \bar{v} \\ \overline{w} \end{pmatrix} + (u \cdot \nabla)\begin{pmatrix} \bar{u} \\ \bar{v} \\ \overline{w} \end{pmatrix} \tag{2.71}$$

$$= \frac{-\nabla P}{\rho} + g + \nu\nabla^2\begin{pmatrix} \bar{u} \\ \bar{v} \\ \overline{w} \end{pmatrix} + \nabla\begin{pmatrix} |-u'u' & -u'v' & -u'w'| \\ |-v'u' & -v'v' & -vw'| \\ |-w'u' & -w'v' & -w'w'| \end{pmatrix}$$

An additional number of transport equations are needed to calculate Reynolds stresses in the equation (2.71). For that, several methods have been developed and are generally identified as turbulence models. Zero-equation model (Mixing-length), one-equation model, two-equations model (*k-ε, k-ω*, SST *k-ω*) and seven-equations (RSM - Reynolds Stress Model) can be stated as most common turbulence models.

The *k-ε* turbulence model is proposed by (Launder and Spalding, 1974) accounts from turbulent kinetic energy *k* and turbulent dissipation rate *ε*. To integrate wall turbulence functions at higher Reynolds number, the *k-ε* model is needed. The model is later improved by Yakhot *et al.* (1992) by removing small scales of motion from the governing equations. The simulations which are discussed in Chapter 4 uses the *k-ε* model. The initial conditions for *k-ε* should be given when solving the RANS equations.

2.5.5 Finite Volume Method (FVM)

As mentioned under Section 2.1.2, full fluid motion equations canot be solved analytically. Therefore, numerical methods are applied under a computational mesh. The finite

Volume Method (FVM) is used in interFoam to solve Reynolds Averaged Navier-Stokes Equations. This process can be extensively found in the bibliography Jasak (1996), Ubbink (1997), Rusche (2003), Versteeg and Malalasekera (2005). The FVM of solution is subdivided in two components: space and time domains (Rusche, 2003) as stated in Lopes (2013). Figure 2.5 is considered for discretization and temporal integration that are discussed below.

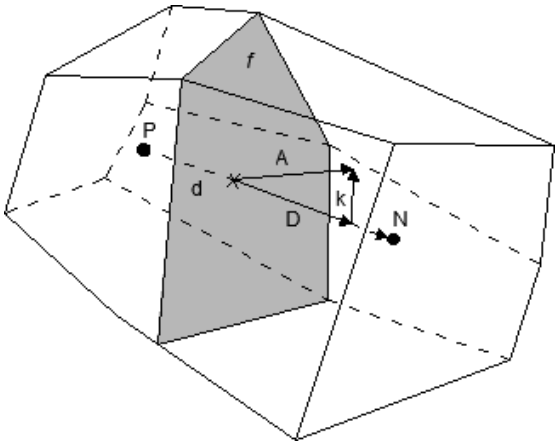

Figure 2.1 – Control Volume the solution domain. *P* and *N* are the centroid of two neighboring cells, *d* is the vector between *P* and *N* and *A* the vector normal to the face f common to both cells; adapted from Ubbink (1997)., (Lopes, 2013)

The face *f* is common for the computational cell with centroid of *P* and the neighboring cell with centroid of *N*. is the area vector, which always points outwards from the computational cell. Vectors, *d* and *D* connects the centroids to satisfy the conditions proposed by Jasak (1996): (Lopes, 2013)

$$A = D + k \tag{2.72}$$

$$D = \frac{d|A|^2}{d - A} \tag{2,73}$$

2.5.6 Discretization of the General Transport Equation

The finite volume discretization of the general transport equation using a general scalar Φ can be represented as follows.

$$\frac{\partial \rho \Phi}{\partial t} + \nabla \cdot (\rho u \Phi) - \nabla \cdot (\rho \Gamma_{\Phi} \nabla \Phi) = S_{\Phi}(\Phi) \tag{2.74}$$

where ρ is the density, u the velocity field and Γ the diffusivity. Equation (2.75) can be derived by discretizing (2.74) over a time interval t, $t+\Delta t$ and over the volume V_P (cell with the centroid point P), and can be written in volume integral form

$$\int_{t}^{t+\Delta t} [\frac{\partial}{\partial t} \int_{V_p} \rho \phi dV + \int_{Vp} \nabla \cdot (\rho \mathbf{u} \phi) dV - \int_{Vp} \nabla \cdot (\rho \Gamma_{\phi} \nabla \phi) dV] \, dt = \int_{t}^{t+\Delta t} [\int_{V_p} S_{\phi}(\phi) dV] \, dt \tag{2.75}$$

2.5.7 Gradient Terms

Gradient terms (advection and diffusion terms) are written by using surface integrals of cell faces. Gauss theorem is used for this transformation. The discretization of any tensor field ϕ can be given as.

$$\int_{V_p} \nabla \phi dV = \oint_{\partial V_p} \phi dS = \sum_{p} (\int_{f} \phi dS) \approx \sum_{p} A_f \phi_f \tag{2.76}$$

where A is the outward normal surface area vector of the faces in the control cell, and ϕ_f is the value of the variable in the face.

2.5.8 Interpolation Schemes

Central differencing (CD) and the upwind differencing (UD) are commonly applied in interFoam solver to interpolate any fluid field ϕ between adjacent control volumes. CD assumes a linear variation of ϕ while, UD assumes takes the direction of the flow into account The author used both schemes for different fluid fields in the simulations described under Chapter 4. The description of the used interpolation schemes are given in table 4.1. Equations

(2.77) and (2.78) gives the expressions for CD and UD respectively, where F is the flux across the control volume.

$$\phi_f = f_x\phi_p + (1 - f_x)\phi_N \tag{2.77}$$

$$\phi_f = \begin{cases} \phi_p \text{for} F \geq 0 \\ \phi_N \text{for} F < 0 \end{cases} \tag{2.78}$$

2.5.9 Temporal Derivative

The Euler implicit scheme can be stated as an example for the discretization of time derivative of the first term of equation (2.74). It has an accuracy of the 1st order.

$$\int_{V_p} \frac{\partial \rho\phi}{\partial t} dV \approx V_p \frac{\rho^n\phi^n - \rho^0\phi^0}{\Delta t} \tag{2.79}$$

where u^0 is the known value of u from the previous time step and u^n is the unknown value of u at the current time step $t_n = n\Delta t$.

Backward differencing scheme can be given as an example for a scheme that have the 2nd order accuracy.

$$\int_{V_p} \frac{\partial \rho\phi}{\partial t} \mathrm{dV} \approx \mathrm{V_p} \frac{3(\rho^{\mathrm{n}}\phi^{\mathrm{n}}) - 4(\rho^0\phi^0) + (\rho^{00}\phi^{00})}{2\Delta t} \tag{2.80}$$

where u^{00} is the value of u from a time step previous to the last.

2.5.10 Convection Term

The convection term of the momentum equation is written by substituting equation (2.76)

$$\int_{V_p} \nabla \cdot (\rho \mathbf{u} \phi) dV = \sum_f \mathbf{A}_f \cdot (\rho \mathbf{u} \phi)_f = \sum_f \mathbf{A}_f \cdot (\rho \mathbf{u})_f \phi_f = \sum_f F_f \phi_f \qquad (2.81)$$

where F_f represents the face mass flux through the face based on a known velocity field and ϕ_f is determined through one interpolation scheme.

2.5.11 Diffusion Term

The discretization of the diffusion term of the momentum equation is done in a similar way.

$$\int_{V_p} \nabla \cdot (\Gamma \nabla \phi) dV = \sum_f \Gamma_f A_l \cdot (\nabla \phi)_t \qquad (2.82)$$

where the diffusivity Γ at the face Γ_f is calculated using either by CD or UD.

2.5.12 Source Term

Source terms of the momentum equation are discretized in a more simple way considering linearization following the work of Patankar (1980). (Lopes, 2013).

$$S_\Phi(\phi) = Su + Sp\Phi \qquad (2.83)$$

where Su and Sp can also depend on ϕ. The volume integral of the source term can be written as:

$$\int_{V_p} S_\phi(\phi) dV = SuV_p + Sp\phi_p V_p \qquad (2.84)$$

2.5.13 Discretization of the Spatial Terms of Momentum Equation

The method that was used to discretize the general transport equation can be used to

discretize the spatial terms of the momentum equation and can be presented as follows by discretizing over the control volume with a time step of Δt.

$$\int_t^{t+\Delta t} [\frac{\partial}{\partial t}\int_{V_p} \rho u dV + \int_{V_p} \nabla \cdot (\rho u u) dV - \int_{V_p} \nabla \cdot (\mu \nabla u) dV]\, dt \tag{2.85}$$
$$= \int_t^{t+\Delta t} [\int_{V_p} (-\nabla p * + (\nabla u) \cdot \nabla \mu + g \cdot x \nabla \rho + \sigma \kappa \nabla \alpha) dV]\, dt$$

The final form of the momentum equation after the term's discretization is stated as:

$$\int_t^{\Delta t} [V_p \frac{\rho^n u^n - \rho^0 u^0}{\Delta t} + \sum_f F_f u_f - \sum_f \mu_f A_f \cdot (\nabla u)_f]\, dt \tag{2.86}$$
$$= \int_t^{\Delta t} [Su V_p + Sp \phi_p V_p]\, dt$$

2.5.14 Discretization of the Phase Fraction (α) transport Equation

The transport equation of phase fraction α is described under Section 2.5.2, equation (2.62). The discretization of this equation over a control volume at a time step Δt can be assumed as follows.

$$\int_t^{t+\Delta t} [\int_V \frac{\partial \alpha}{\partial t} dV] dt \quad + \int_t^{t+\Delta t} [\int_V \nabla \cdot (\alpha u) dV]\, dt + \int_t^{t+\Delta t} [\int_V \nabla \cdot [\mathbf{u}_r \alpha (1-\alpha)] dV]\, dt \tag{2.87}$$
$$= 0$$

If the variation of α is assumed as linear, the first term of the equation can be simplified to:

$$\int_V \frac{\partial \alpha}{\partial t} dV = \frac{\partial \alpha_p}{\partial t} V_p \tag{2.88}$$

Gauss theorem is used to discretize the second term. In the discretization of the artificial

compression term (third term) with $\mathbf{u}_r$, the velocity at the cells is determined from the gradient of phase fraction:

$$u_{r,f} = n_f min[C_\alpha \frac{|\Phi|}{|A_f|}, max(\frac{|\phi|}{|A_f|})] \tag{2.89}$$

where Φ is the face volume flux and n_f is the face unit normal flux, calculated in the interface region based on the phase fraction gradient at cell faces:

$$n_f = \frac{(\nabla\alpha)_f}{\lceil(\nabla\alpha)_f + \delta_n|} A_f \tag{2.90}$$

where δ_n is the stabilization parameter, which considers the non-uniformity of the grid. This parameter usually takes the value of 10^{-5}.

2.5.15 Temporal Discretization

By considering the spatial terms ϕ, the equation (2.78) can be simplified as follows. The description is given in the OpenFOAM manual (OpenFOAM, 2020).

$$\int_t^{t+\Delta t} [\frac{\partial}{\partial t}\int_{V_p} \rho\phi dV + \int_{V_p} \mathcal{A}\,\phi dV]\, dt = 0 \tag{2.91}$$

where $\mathcal{A}$ is a spatial operator.

The first term of the equation (2.91) can then be discretized by using Euler's implicit method given in equation (2.79).

$$\int_t^{t+\Delta t} [\frac{\partial}{\partial t}\int_{V_p} \rho\phi dV]\, dt = \int_t^{t+\Delta t} [\frac{(\rho_P\phi_p V_p)^n - (\rho p\phi_p V_p)^0}{\Delta t}]\, dt \tag{2.92}$$

$$= \rho_p \frac{(\phi_p)^n - (\phi p)^0}{\Delta t} V_p$$

The second term of the equation (2.91) can be discretized in OpenFOAM either by Euler implicit, Euler explicit or Crank Nicholson methods. Euler implicit and Euler explicit methods are the 1st order methods accurate in time while Crank Nicholson method is the 2nd order method which is also accurate in time.

However, as the second method is an explicit method, it uses old time step values of ϕ rather than current time step values. Therefore, instabilities could occur if Courant number criteria is not achieved as follows. For stable calculations, Co should not exceed one.

$$Co = \frac{u_f \cdot d}{|d|^2 \Delta t} \tag{2.93}$$

The Crank Nicholson method uses the trapezoidal rule to discretize the spatial terms. It uses old values of ϕ and there by the boundedness of the solution is not guaranteed (Jasak, 1996). The method is unconditionally stable (Hirsch, 1991).

$$\int_t^{t+\Delta t} \mathcal{A}\,\phi dt = \frac{1}{2}\mathcal{A}(\phi^n + \phi^0) \tag{2.94}$$

While keeping the density and viscosity constant, Crank Nicolson scheme (2.94) can be applied to the momentum equation and gives equation (2.95)

$$\begin{aligned} &\mathrm{V_p}\frac{\rho \mathrm{u^n}}{\Delta \mathrm{t}} + \frac{1}{2}\left[\sum_f \mathrm{F}_f \mathrm{u}_f^{\mathrm{n}} - \sum_f \mu_f \mathrm{A}_f \cdot (\nabla \mathrm{u})_f^{\mathrm{n}} - \mathrm{SpVp}\phi_{\mathrm{p}}^{\mathrm{n}}\right] \\ &= \mathrm{V_p}\frac{\rho \mathrm{u}^0}{\Delta \mathrm{t}} - \frac{1}{2}\left[\sum_f \mathrm{F}_f \mathrm{u}_f^0 - \sum_f \mu_f \mathrm{A}_f \cdot (\nabla \mathrm{u})_f^0 - \mathrm{SpVp}\,\phi_{\mathrm{p}}^0\right] + \mathrm{SuVp} \end{aligned} \tag{2.95}$$

2.5.16 Boundary and Initial Conditions

Initial conditions and boundary conditions for the dependent variables are needed in order to solve the problem. Boundary conditions in OpenFOAM can be applied mainly by two

ways.

01. Fixed value (Dirichlet)
02. Fixed gradient (Neumann)

The author only used fixed value boundary conditions for this study as the tsunami wave flume is bounded by fixed walls. The values of initial conditions of required parameters are given under Chapter 04. Table 2.1 shows a summery of boundary conditions that are available in OpernFOAM.

Table 2.1 – Numerical boundary conditions available in OpenFOAM (Retrieved from Rusche, 2003) as stated in Lopes (2013).

Variable	No-Slip Wall	Inlet	Outlet	Symmetry Plane
u	Fixed Value	Fixed Value	Zero Gradient	Mirror Image
α	Zero Gradient	Fixed Value	Zero Gradient	Mirror Image
p	Zero Gradient	Zero Gradient	Fixed Value	Zero Gradient
k	Fixed Value	Fixed Value	Zero Gradient	Zero Gradient
ε	Fixed Value	Fixed Value	Zero Gradient	Zero Gradient

2.5.17 Calculating Pressure Forces

The pressure forces acting on a structure can be calculated in OpenFOAM by inversely integrating the calculated pressure over a surface area vector of the structure. Equation (2.96) gives the pressure force integration procedure.

$$F_p = \sum_i \rho_i s_{f,i}(p_i - p_{ref}) \tag{2.96}$$

Where F_p in the pressure force, ρ is the density of fluid, $s_{f,i}$ is the surface area vector, and p is the pressure.

CHAPTER 3

Chapter 3

TSUNAMI INTERACTION WITH SUBMERGED WALL AND TRENCH SYSTEMS

OUTLINE

This chapter is allocated mainly for discussing the first part of the primary study. Submerged wall and trench systems are investigated in this first section to identify their usability as a defense measure against tsunamis. This chapter focuses on several arrangements of submerged wall and trench systems via a numerical model, which is calibrated by physical experiments of a tsunami-like wave transformation. A dam break event is used to model a tsunami-like wave interaction with structures. Resulted wave properties are investigated to identify an optimum solution from the viewpoint of structure configuration. Our results clearly show that the submerged wall-trench systems at near-shore can suppress the impact of a tsunami-like waves on the shore.

This chapter consists of four main sections. Firstly, a brief introduction is given on the background with previous studies, which is followed by the focus and objectives. Then, the methodology and the procedure are explained in detail. At the end results are presented which are related to this chapter with a detailed discussion.

3.1 INTRODUCTION

As briefly described in Chapter 1, a tsunami is a water waveform (or series of waves) that occurs in the ocean (in most cases) that sends a surge of water, sometimes reaching runup heights of over 30 meters on to land. This kinetic energy within the wave front can cause widespread destruction when they land onshore. The most common tsunami generation mechanism is an abrupt vertical displacement of a large area within the epi-central region (or its vicinity) associated with a strong submarine earthquake. However, massive submarine

landslides and the fall of large soil masses from steep slopes cannot be excluded in generating tsunamis.

The amplitude of a typical tsunami wave in the open ocean is rather small (normally from 1 to 30 centimeters) (Goring and Raichlen, 1992). Its length can reach hundreds of kilometers, which is much greater than the depth of the ocean. As this wave approaches the shore, with decreasing celerity, its amplitude increases dramatically, which can lead to the destruction of various facilities in the coastal zone leading to flooding.

Coastal dikes and sea walls are the most popular defense structures against tsunamis, which are commonly used across the world. Countries like Japan have strongly invested in building such structures along its tsunami vulnerable areas, especially since 2011 Great East Japan Tsunami, which has been identified as one of the largest natural disasters in recent history. Some of these structures can reach a height of 17 meters with a length of several kilometers along the East coast of Japan (Raby *et al.*, 2015). There are however increasing concerns of cons to their pros with these massive walls that are built within socially and environmentally sensitive areas.

Tsunami interaction with defense structures like seawalls was observed in largely during recent disaster events like the 2011 Great East Japan Tsunami. During these events, the failure of strong hard measures gave another perspective to the field of tsunami defense. Even with a world-class disaster warning system, the massive destruction of 2011 Great East Japan Tsunami, could not be mitigated successfully. It demonstrated that current popular protective structures, such as seawalls, dikes, and breakwaters, cannot be the only countermeasures to protect coastal communities from serious natural disasters (Kimura, 2016).

Therefore, alternative methods and applications are required to find solutions for these problems. Some researchers have paid their attention on submerged structures. Although the submerged structures are less effective from the view point of wave transmission as explained under Chapter 1, their low cost and environmentally friendly nature can be taken in to account. As a result, extensive research on hazard mitigation using submerged structures has been conducted (Ha *et al.*, 2014). The numerical investigations of Huang, Chang and Hwung (2003) and Ha *et al.* (2014) concluded that submerged structures can mitigate a tsunami-like wave for some extent. Also the solitary wave interaction with submerged bumps was investigated by

Chugunov, Fomin and Shankar (2014). In this study, authors concluded that the amplitude of the incident wave exponentially decays when the number of submerged bumps is increased.

Fridman *et al.* (2010) performed an experimental study, which showed that double submerged barriers are more efficient than single barriers of the same size in reducing the tsunami wave run-up. He also observed that a minimum run-up existed for a particular distance between two submerged barriers.

3.2 FOCUS AND OBJECTIVES

The majority of studies on submerged structures have been carried out in an attempt to understand the evolution of an incident wave during propagation over a submerged crest, while examining the reduction of wave transmission and wave run-up at the shore line. In most of these studies, researchers have only considered vertical type walls or wall systems against a tsunami-like waves. However, the manner in which a submerged wall and trench type system can influence the runoff of a tsunami-like wave on a beach has rarely been studied.

In spite of that, Dao, Adithyawan and Tanaka (2013) carried out a series of numerical experiments to investigate the sensitivity and effects of ashore-parallel canal to reduce a tsunami's energy. Their results showed that a canal parallel to the shoreline has a significant effect in reducing tsunami energy and plays an important role in the mitigation of tsunami impacts. Although his study focused on a cannel on land, it showed some promising outcomes of a wall trench system that would significantly be effective in reducing current speeds of a tsunami-like wave.

In this first part of the study, focus is placed more on a submerged wall and trench system near the shore, which would act as a tsunami defense structure. A set of numerical simulations were performed through a calibrated model that predicts the run-up heights of a tsunami-like wave on a sloping beach in accordance to the dimensions of a submerged wall and trench systems. Finally, variations in the run-up processes for different cases were investigated.

3.3 METHODOLOGY

3.3.1 Experimental Setup

Firstly, an experiment was setup in a 2D flume (wave tank) to physically simulate a dam break event. The purpose of the experiment was to fine tune the numerical setup which is explained in the next stage.

The schematic diagram of the experiment is shown in Figure 3.1. The dimensions of the 2D wave flume are 44m, 0.7m, 0.9m (length, width, depth). The difference of water level between reservoir and the experimental tank is initially maintained to be 0.13m (13 cm). The basin length of 44 m is comprised of two slopes: 1/40 slope and 1/100 slope.

Model scale is the most important factor, when performing hydraulic experiments. The main parameters governing the selection of the model scale are:

- Flume dimensions
- Length and depth of the sea bed profile
- Overall width of the structure section
- Final crest level of the structure section
- Wave heights to be tested

Scaling down of the prototype to model has to be done by considering geometric, kinematic and dynamic similarities according to Froude's similarity and showed as follows.

Length Scale $= 1: \lambda$

Time and Velocity scales $= 1:\sqrt{\lambda}$

Forces, Volume and Mass Class $= 1: \lambda^3$

Taking into consideration geometric, kinematic and dynamic similarities, a scale ratio of 0.0125 (1:80) is assumed to represent reality. The initial conditions were decided from a series of trial and error experiment cases to generate a tsunami-like wave having a height of about 7 m (in real scale) at near shore. Current speeds were also measured and considered when deciding the initial conditions. The selected initial conditions or the water column of 13cm at

the reservoir end, generated a maximum current speed of about 6.25 m/s (in real scale) when reaching the shore.

Historical records of the 2004 Indian Ocean Tsunami and the 2011 Great East Japan Tsunami were taken into consideration when deciding the initial conditions for the experimental set up.

Observed water level data is published online for the 2011 Great East Japan Tsunami by the Nationwide Ocean Wave Information Network for Ports and Harbours (NOWPHAS). In the case of the 2004 Indian Ocean Tsunami, Grilli *et al.* (2007) published observed tide gauge data. These were both considered for this study. Although these data recordings have significant deviation due to dependences on the location, measuring depth and the event itself, it was decided to follow a 7m tsunami wave height at near shore. This provided a realistic representation of an average tsunami wave height in the modelling environment.

Once the initial water condition was consistent at the reservoir end, the gate was raised manually to generate a dam break waveform. The transforming waveform was measured by several water level gauges at different locations (A, B, C and D) along the wave tank. Also, the current speeds of the upcoming wave were measured at several locations (B, C and D) near the shore. An electromagnetic current meter was used to measure current speeds. The location of each gauge is also given in Figure 1.

Readings of the water level gauges and current meters were used to calibrate the numerical model in the next stage.

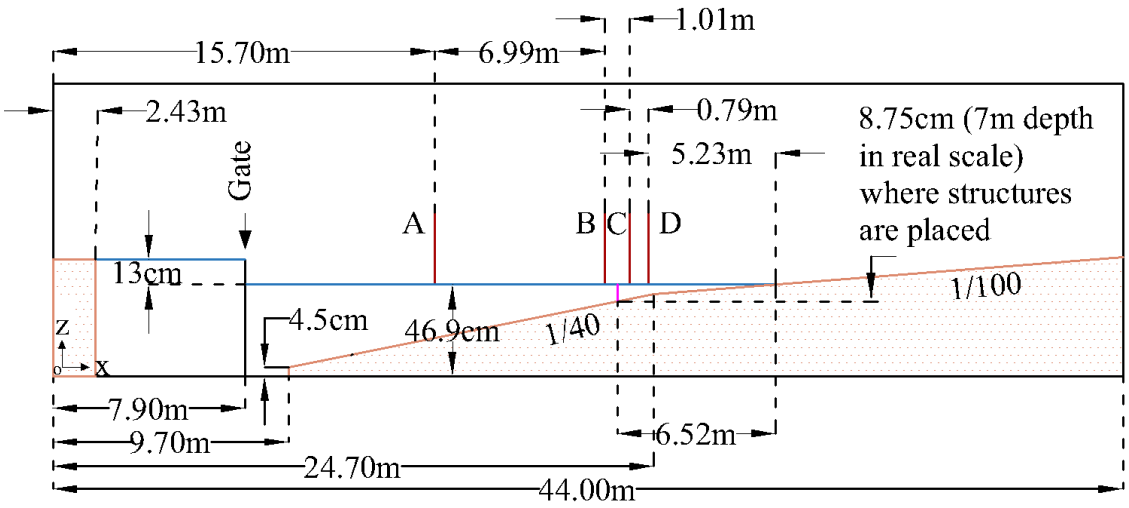

Figure 3.1. Dimensions of the wave tank and details of the experimental setup

3.3.2 Numerical Setup

A characteristic feature of a tsunami-like wave is the smallness of the parameter h_0/λ_0, where h_0 is characteristic value of the depth of the ocean and λ_0 is a typical wavelength. The presence of this small parameter allows us to use the shallow water equations (Stoker, 1957) to model a tsunami-like wave dynamics. In this first part of the study, a tsunami-like wave propagation was simulated via Delft3D-FLOW module by applying water surface deformation resulting from a dam break event for the initial conditions. Delft3D-FLOW is an open source, multi-dimensional hydrodynamic simulation program in which several dimensional modes are available. The 2D (depth averaged) mode is applied for the current study. The flow module is based on shallow water equations. (Eqs. 3.1~3.5).

A detailed description of the numerical model is given under Chapter 2 (Section 2.2)

$$\frac{\partial h}{\partial t} + \frac{\partial}{\partial x}(hu) + \frac{\partial}{\partial y}(hv) = 0 \tag{3.1}$$

$$\frac{\partial}{\partial t}(hu) + \frac{\partial}{\partial x}\left(hu^2 + \frac{1}{2}gh^2\right) + \frac{\partial}{\partial y}(huv) = -gh\frac{\partial b}{\partial x} - \tau_x \tag{3.2}$$

$$\frac{\partial}{\partial t}(hv) + \frac{\partial}{\partial y}\left(hv^2 + \frac{1}{2}gh^2\right) + \frac{\partial}{\partial x}(huv) = -gh\frac{\partial b}{\partial y} - \tau_y \tag{3.3}$$

Where *t* is time, *h(x,y,t)* is the total water depth. *b(x,y)* is the bottom elevation function describing natural bathymetry. *u(x,y,t)* and *v(x,y,t)* are the two components of depth averaged velocities in the *x* and *y* directions and *g* denotes the acceleration due to gravity. The components of the bottom friction term are:

$$\tau_x = \frac{gn^2}{h^{7/3}} hu\sqrt{(hu)^2 + (hv)^2} \tag{3.4}$$

$$\tau_y = \frac{gn^2}{h^{7/3}} hv\sqrt{(hu)^2 + (hv)^2} \tag{3.5}$$

Where *n* is Manning coefficient, representing the roughness of the bottom.

The numerical model was set up to simulate the same dam break event. The domain is constructed in 2D depth averaged environment, with a resolution of (Δx = 2cm, Δy = 5cm). This resolution is defined under the Courant number (CFL) criteria that is given in equation (3.6). Depth contours were introduced into the grid by defining the same depth levels from the experiment. The domain is then introduced into Delft3D-FLOW module by applying a set of initial conditions (13cm water column at the reservoir end) to calculate the evolution of the wave generated by the dam break event. Defining open boundary conditions was not necessary, as the domain of the wave flume only had fully reflective closed boundaries.

$$CFL_{wave} = 2\Delta t\sqrt{gh}\sqrt{\frac{1}{\Delta x^2}+\frac{1}{\Delta y^2}} < 1 \qquad (3.6)$$

Time step interval (Δt) is selected as 0.0001 minutes ($6x10^{-3}$ seconds), which was derived through several trial and error simulation. As it would not only satisfy the Courant number criteria (Deltares, 2018) but would also generate minimum numerical instabilities. Fully reflective boundaries (Deltares, 2018) were assumed at the sidewalls to allow for similar reflection as in the experiments. A constant value of 0.012 was used as Manning's roughness coefficient at the bottom of the domain. This value represents a closer roughness for a smoothed concrete bottom. A partial slip condition of 0.2m length is applied to generate friction from the sidewalls of the domain. Gravitational attraction and water density were taken as 9.81 m/s^2 and 1000 kg/m^3. A constant value of 0.0025 m^2/s was applied as horizontal eddy viscosity in background viscosity/diffusivity. Flooding scheme (Deltares, 2018) was used as the time integration scheme for the advection terms of equations. Water level variations and current velocities were extracted at the same gauge locations as the experiment and compared with recordings from the experiment. Plots of comparison are given under results and discussion.

3.3.3 Simulations with Submerged Structures

Submerged structures are then introduced (Figures 3.2 and 3.3) to the numerical domain by altering the bottom profile. Several types of submerged structures were assessed including a single vertical wall, double vertical walls and wall-trench systems in different orientations.

The results of Fridman *et al.* (2010) and Ha *et al.* (2014) were both considered when deciding the height and width of the structures. (Indexes: *b*: barrier height, *h*: water depth, *a*: barrier width, *d*: spacing between barriers) In the study of (Ha *et al.*, 2014), it is clearly suggested that a *b/h* ratio of 0.7 be used, which lead to a significant increment of a tsunami-like wave dissipation, particularly for higher a/h ratios.

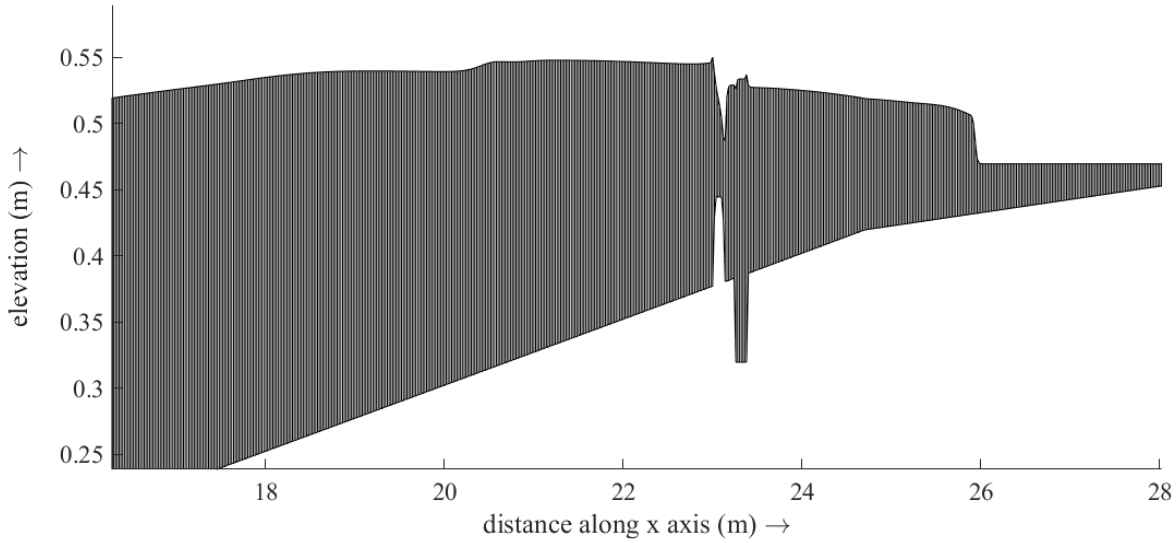

Figure 3.2. Tsunami bore passing through the submerged wall and trench system in the depth averaged domain (not into scale)

Table 3.1. Description of simulation cases with details of submerged structures (in real scale)

Case no.	Description	Wall height (m)	Wall width (m)	Trench depth (m)	Trench width (m)	Spacing (m)
1	Without Structures	-	-	-	-	-
2	Single wall	5	10	-	-	-
3	Double wall	5	10	-	-	10
4	Wall-trench	5	10	5	10	0
5	Wall-trench	5	10	5	10	10
6	Wall-trench	5	10	5	10	5
7	Wall-trench	5	10	5	5	0
8	Wall-trench	5	10	5	15	0
9	Wall-trench	5	10	5	20	0

10	Wall-trench	5	5	5	10	0
11	Wall-trench	5	15	5	10	0
12	Wall-trench	5	20	5	10	0
13	Wall-trench	5	10	2.5	10	0
14	Wall-trench	5	10	7.5	10	0

Table 3.2. Description of simulation cases with details of submerged structures (in model scale)

Case no.	Description	Wall height (mm)	Wall width (mm)	Trench depth (mm)	Trench width (mm)	Spacing (mm)
1	Without Structures	-	-	-	-	-
2	Single wall	62.5	125	-	-	-
3	Double wall	62.5	125	-	-	125
4	Wall-trench	62.5	125	62.5	125	0
5	Wall-trench	62.5	125	62.5	125	125
6	Wall-trench	62.5	125	62.5	125	62.5
7	Wall-trench	62.5	125	62.5	62.5	0
8	Wall-trench	62.5	125	62.5	187.5	0
9	Wall-trench	62.5	125	62.5	250	0
10	Wall-trench	62.5	62.5	62.5	125	0
11	Wall-trench	62.5	187.5	62.5	125	0
12	Wall-trench	62.5	250	62.5	125	0
13	Wall-trench	62.5	125	31.25	125	0
14	Wall-trench	62.5	125	93.75	125	0

Furthermore, the experimental study of Fridman *et al.* (2010) examined *b/d* ratio for a double wall design, with results showing a significant run-up reduction of a tsunami-like wave at the shore; starting from *b/d*~2. When considering these findings, it was decided to use a *b/h* ratio of 0.7 and *b/d* ratio of 2 when incorporating structures into the domain. The structures are constructed at a depth of 7m underwater with a height of 5m. The depth of the trench of the wall-trench system is also set to 5m in real scale. The orientations and real scale dimensions of each submerged structure system is listed in Table 1. The same information for the model scale is given in Table 2.

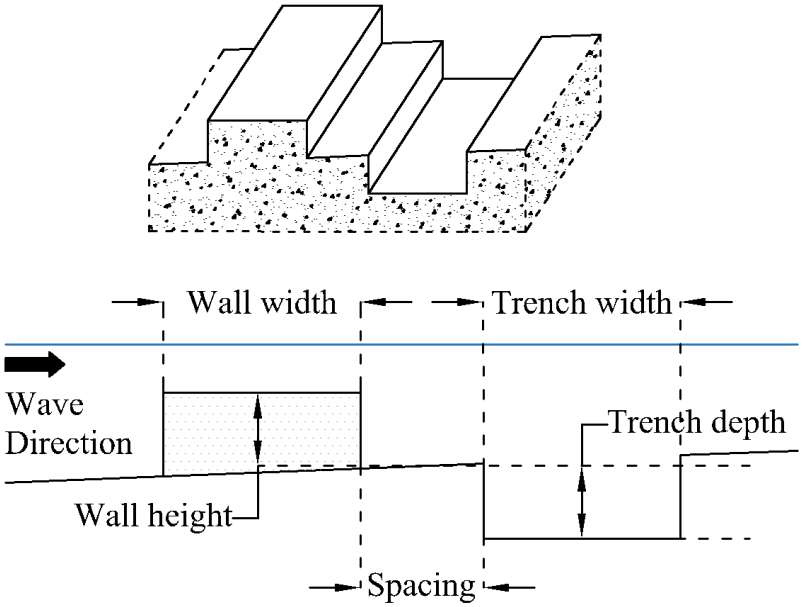

Figure 3.3. Geometry of the wall and trench system

3.4 RESULTS AND DISCUSSION

3.4.1 Comparison of Wave Transformation

Figures 3.4.a, 3.4.b and 3.4.c illustrate the comparison between measured and simulated water level variations at each gauge location. Elevation is measured from the bottom of the wave tank (Figure 3.1).

From the above figures, it can be proposed that the numerical model is capable of reproducing the water level variations, which are generated by the striking wave. However, the model cannot calculate the turbulence that occurs once the wave breaks at near shore. As the wave-induced turbulence after the breaking point (observed between A and B) was not considered in the numerical model, current velocities that were reproduced by the model have some limitations.

Nevertheless, Figures 3.5.a, 3.5.b, and 3.5.c shows the comparison of measured and simulated current velocity variations at each gauge location along the x-axis. When examining

all three figures, it is clear that the shape of the current velocity variations is not well reproduced by the numerical model. However, the difference between the measured and simulated maximum current velocity matches marginally with a deviation of about 10%.

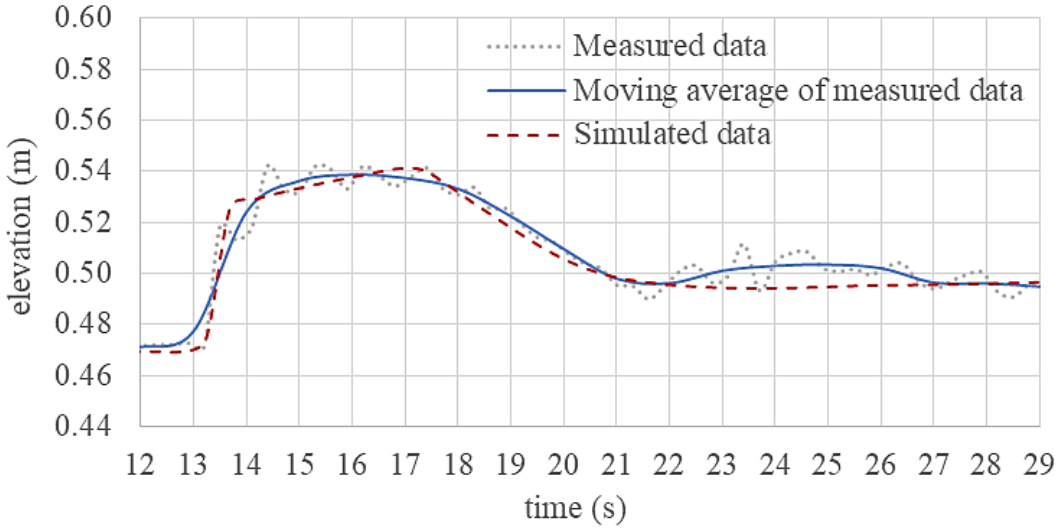

Figure 3.4.a. Comparison of water level variations at location B

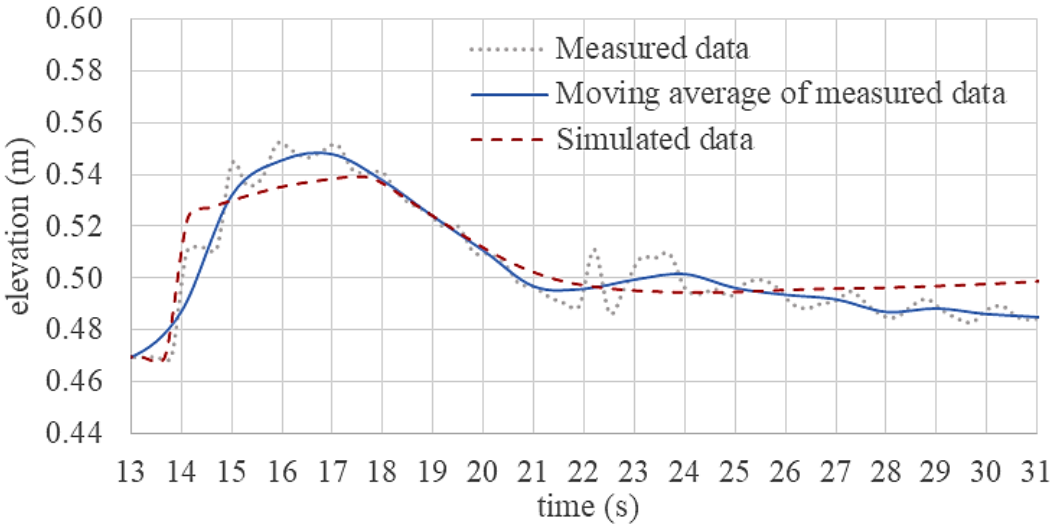

Figure 3.4.b. Comparison of water level variations at location C

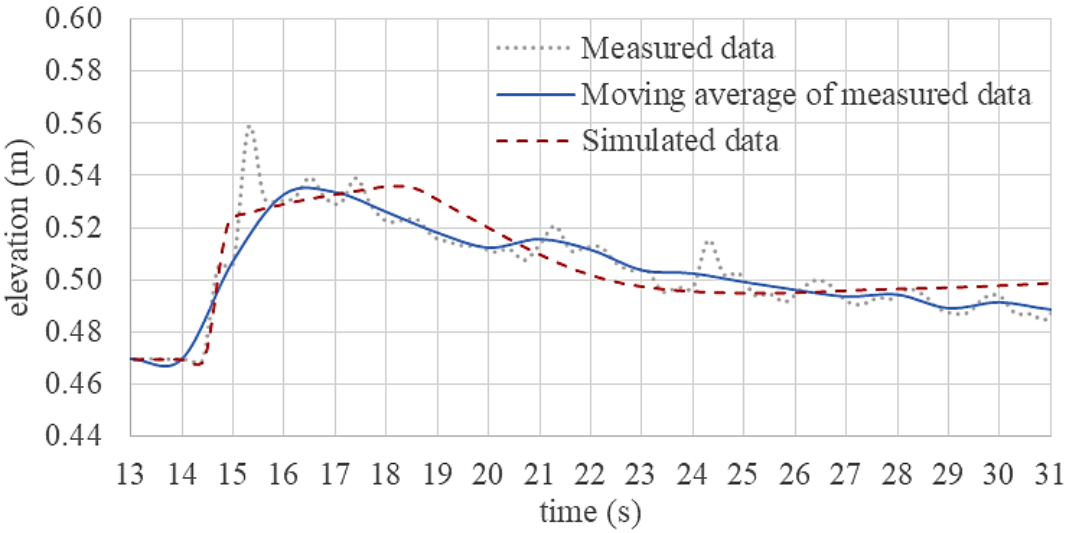

Figure 3.4.c. Comparison of water level variations at location D

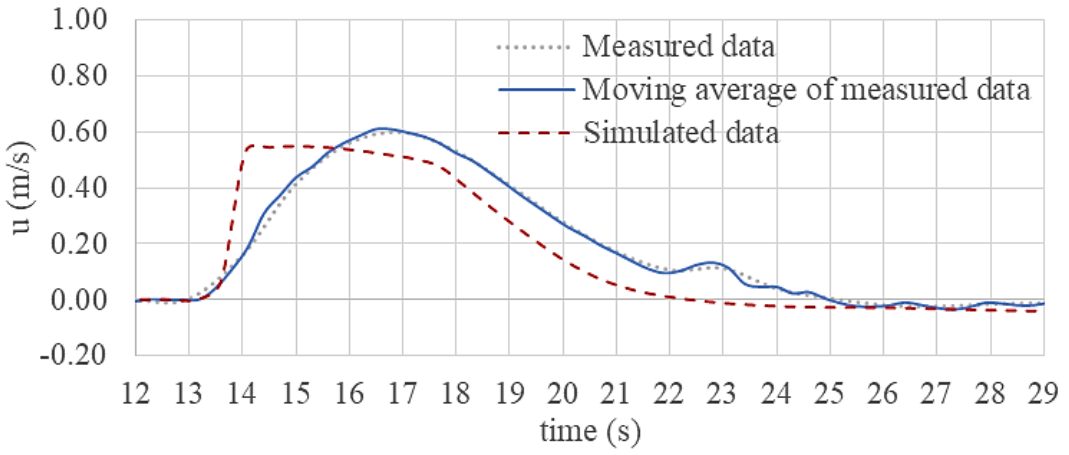

Figure 3.5.a. Comparison of current velocity (x-component) at location B

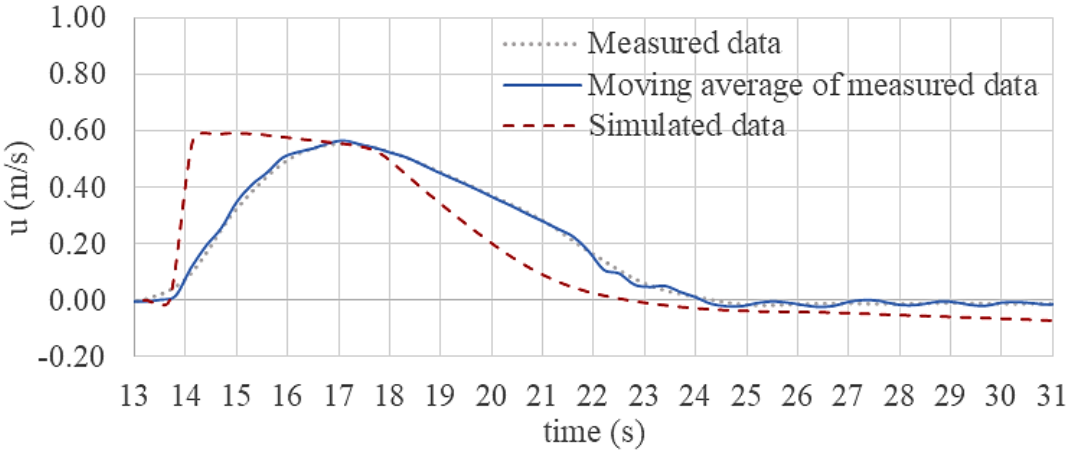

Figure 3.5.b. Comparison of current velocity (x-component) at location C

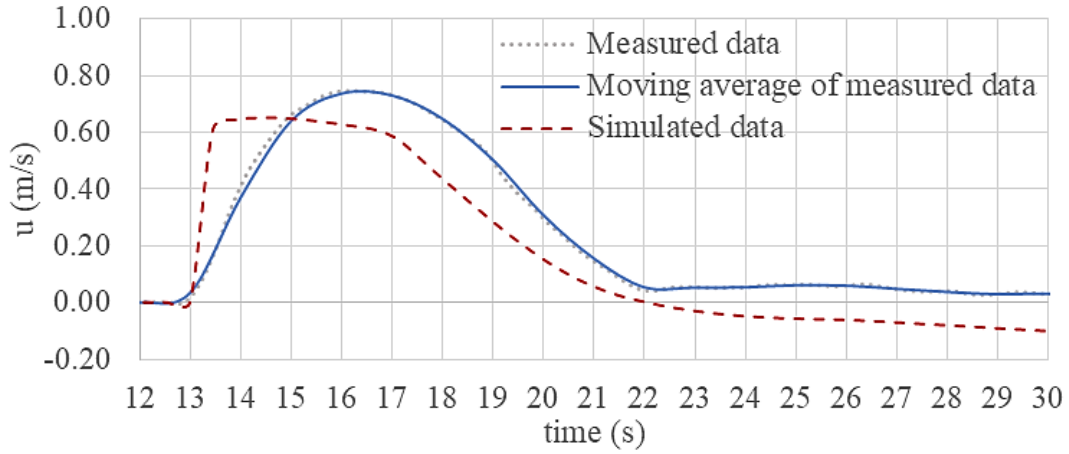

Figure 3.5.c. Comparison of current velocity (x-component) at location D

3.4.2 Assessment of Each Submerged Structure

The water level variations and current velocity variations at gauge locations are given in the following figures. Figures 3.6.a and 3.6.b represent the variations of above parameters at location A. A comparative examination is made with the first four simulation cases that are described in Table 1 and Table 2.

Case 1 is a simulation without submerged structures. Case 2 is a simulation with a single submerged wall. Case 3 is a simulation with double submerged walls with a spacing of 10m

and Case 4 is a simulation with a wall and trench system (Figure 2.9) having 0m spacing in between the wall and trench.

The first peak in Figure 3.6.a. between 0 and 10 seconds reflects the upcoming wave. Then, a portion of the wave energy is reflected by the submerged structures, resulting in a reflected wave in the opposite direction. This is identified by the second peak of Figure 3.6.a. and by the dip between 10 and 20 seconds of Figure 3.6.b. The reflected wave from the structure travels backward and reflects again from the back wall of the wave tank. Thus, the third peak of Figure 3.6.a. and the second peak of Figure 3.6.b. are generated.

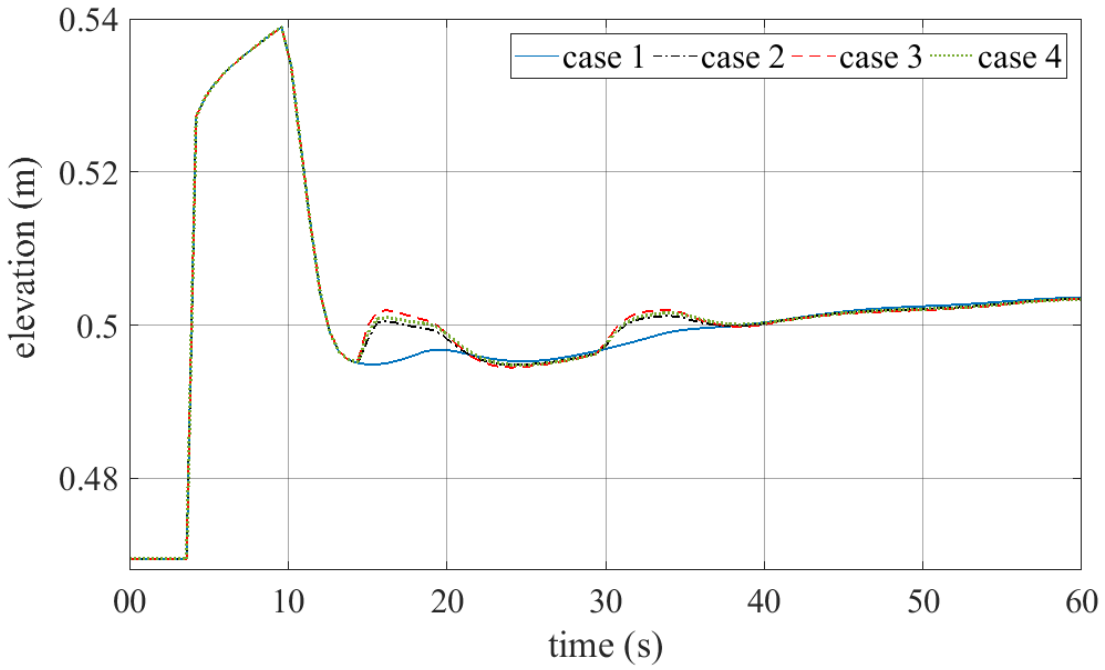

Figure 3.6.a. Comparison of water level variations at location A

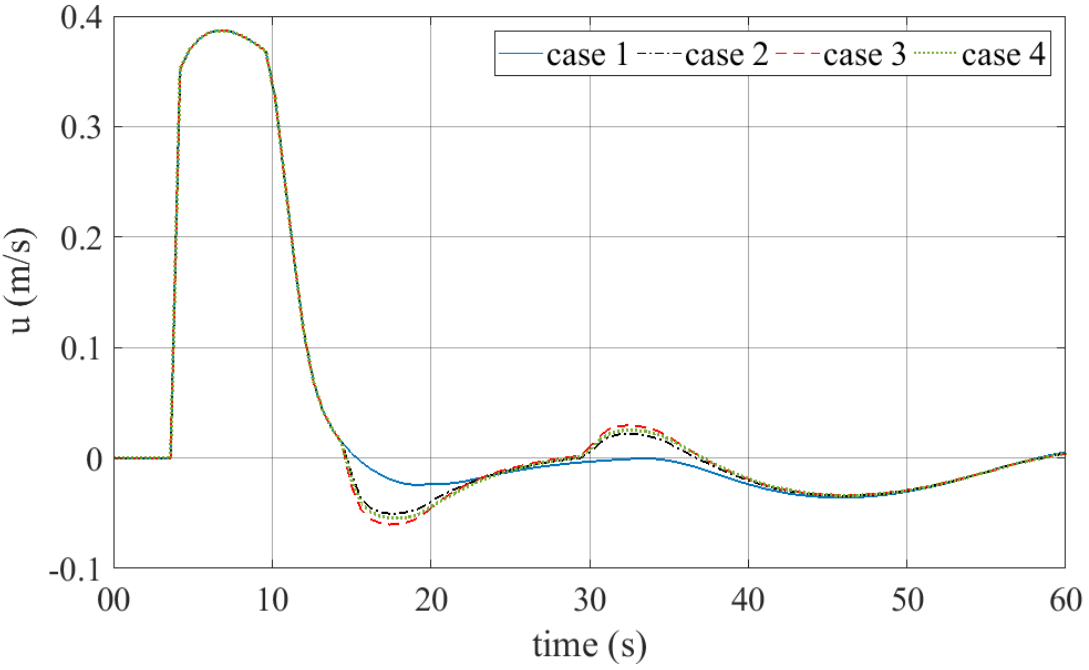

Figure 3.6.b. Comparison of current velocity (x-component) variations at location A

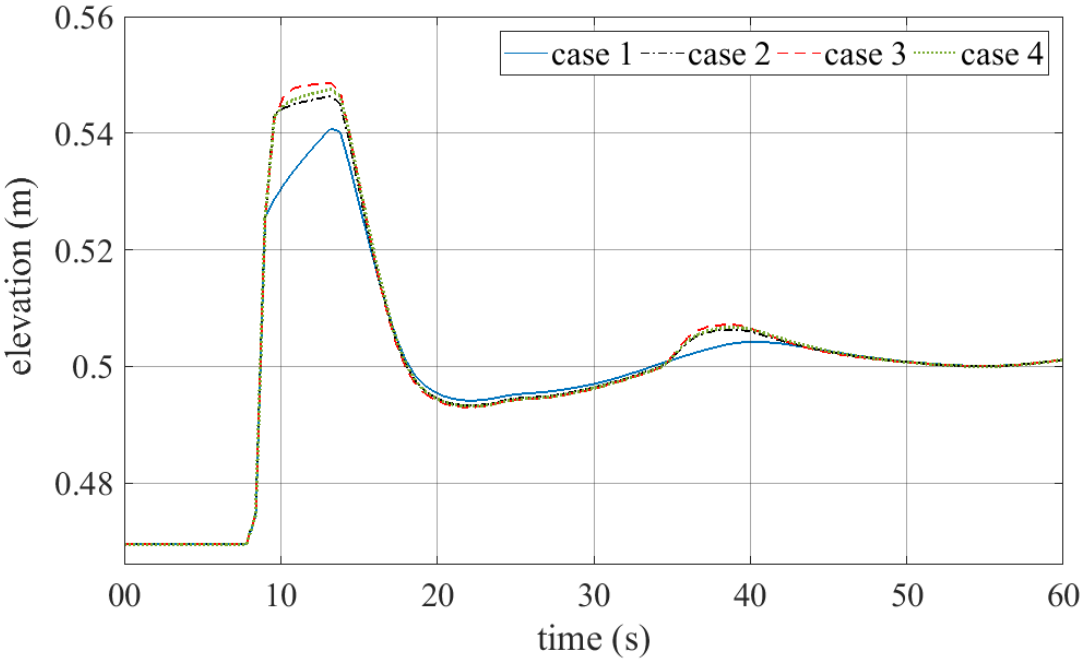

Figure 3.7.a. Comparison of water level variations at location B

Water levels are build up at location B (in front of the structure) in simulations with submerged structures compared to the simulation without structure (Figure 3.7.a.). Current

velocity variations at the same location (Figure 3.7.b.) also indicate a sudden drop once the upcoming wave interacts with the underwater structures.

Figure 3.8.a. and Figure 3.9.a. give the water level variation at the lee side of the structure where location C is located closer to the structure and location D is located nearer to the shore. Both of these figures show a suppressed upcoming wave being reflected from the submerged structures simulations compared to the simulation without submerged structures.

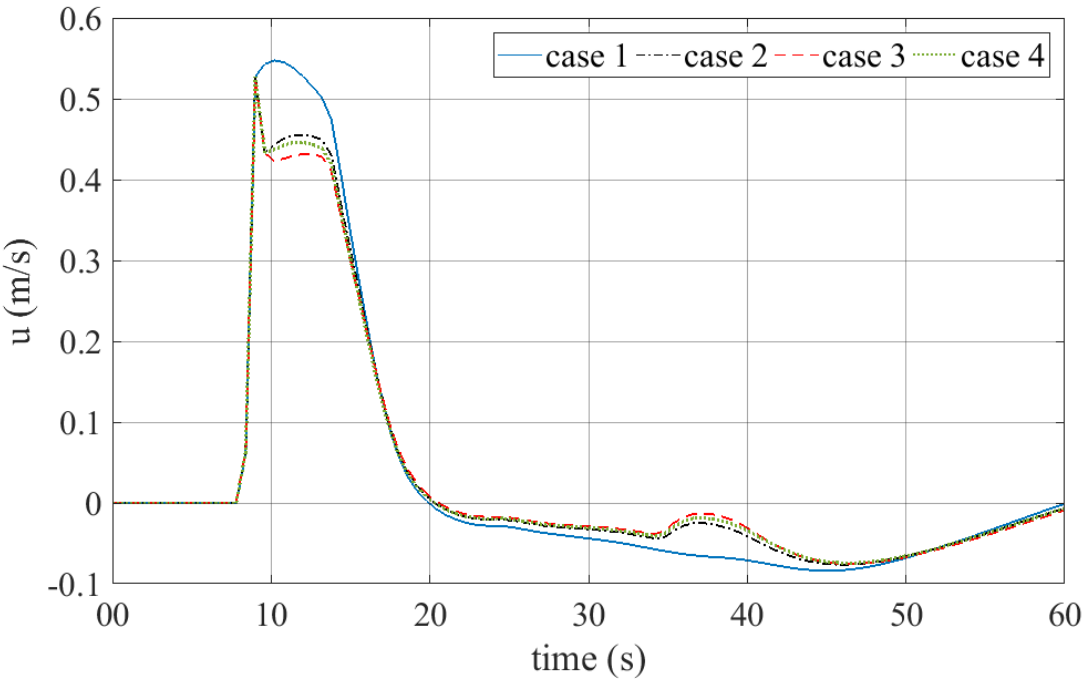

Figure 3.7.b. Comparison of current velocity (x-component) variations at location B

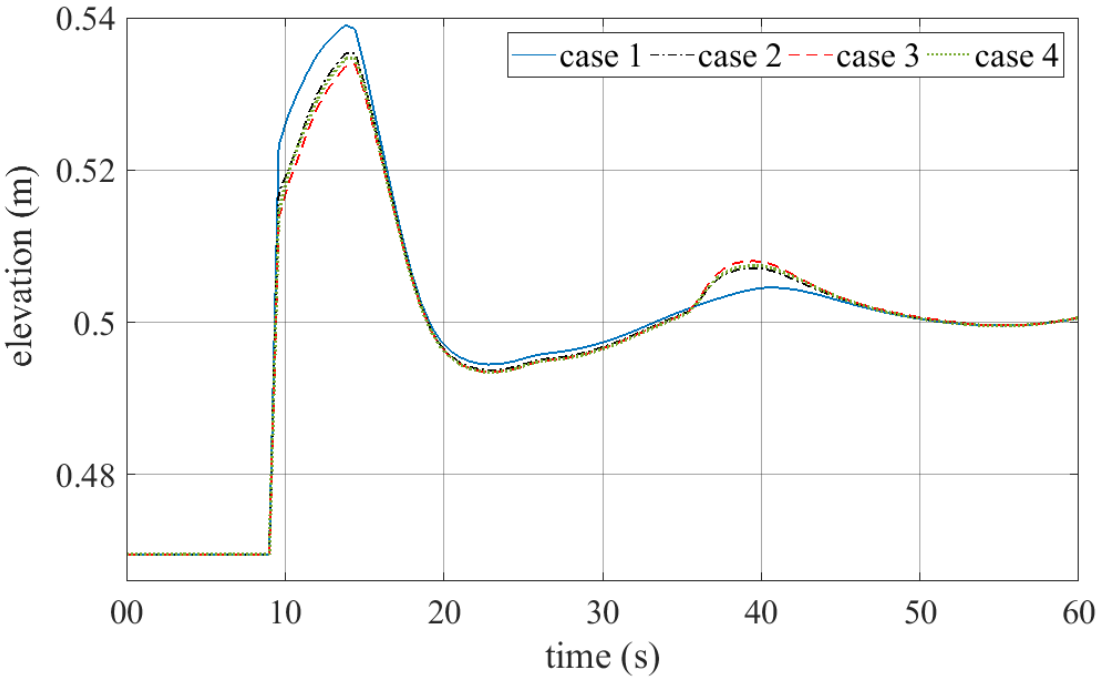

Figure 3.8.a. Comparison of water level variations at C

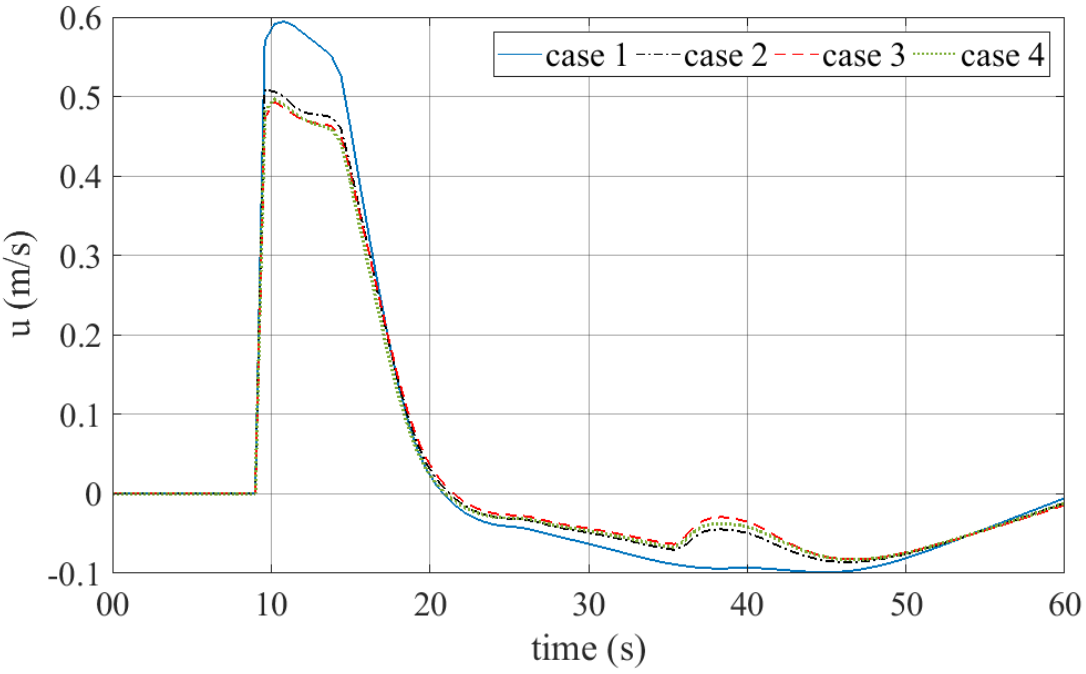

Figure 3.8.b. Comparison of current velocity (x-component) variations at location C

In addition, the second wave that is reflected by the back wall of the wave tank is also visible in both figures; the second peak indicates this. Figure 3.8.b. and Figure 3.9.b. give the current velocity variation at locations C and D consecutively.

These two figures also reflect the behavior that is previously discussed. These figures (Figure 3.5.a. to Figure 3.9.b.) clearly prove that the submerged structures suppress the wave heights at the lee side. It was found that a double wall system acted as the most effective submerged structure to suppress an upcoming wave. The wall and trench system reduced the striking wave better than a single submerged wall.

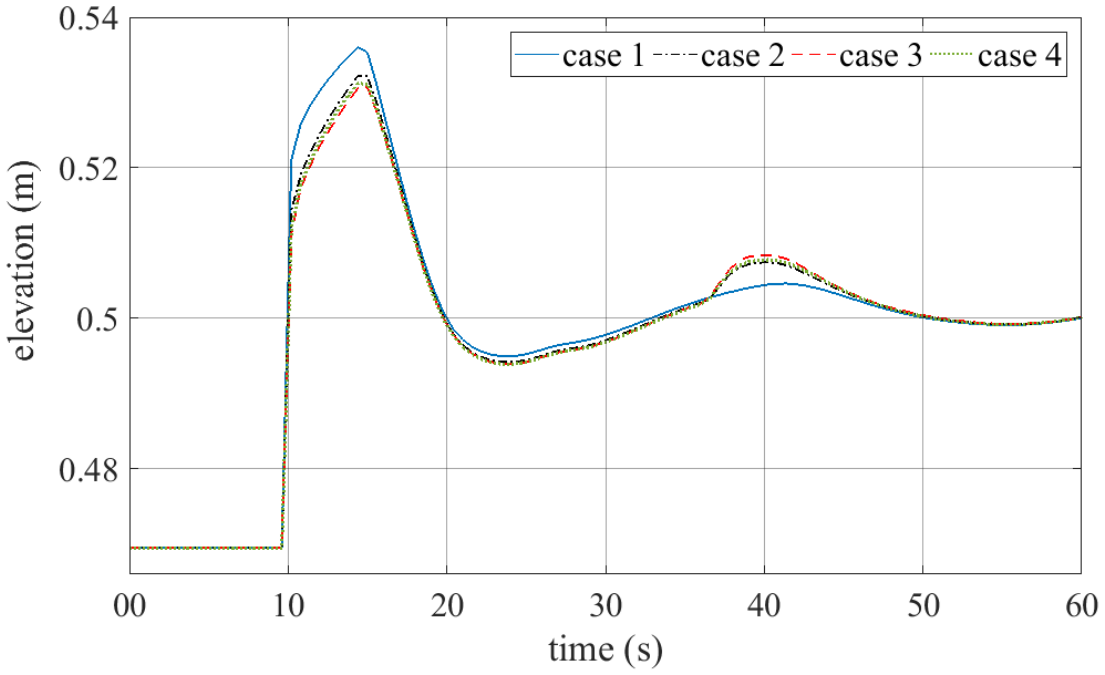

Figure 3.9.a. Comparison of water level variations at location D

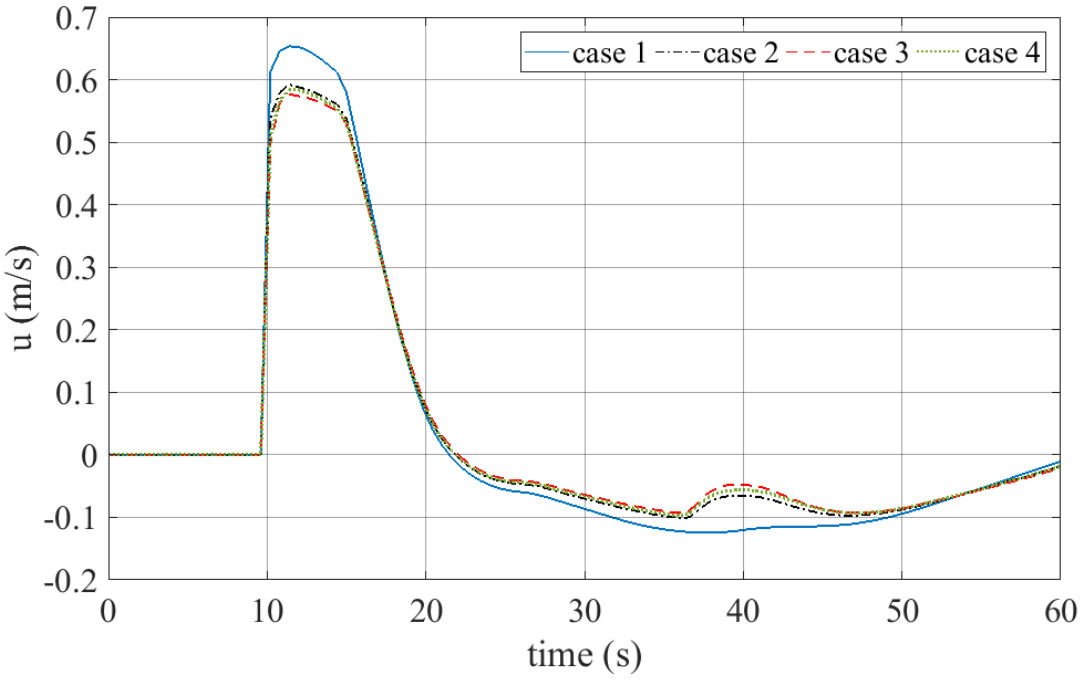

Figure 3.9.b. Comparison of current velocity (x-component) variations at location D

Figure 3.10. plots the calculated maximum water level along the x-axis for each simulation case. The wave run-up heights for a 1:100 beach slope can also be identified when the water level lines cross the ground level line. The wave height suppression, which occurs due to the submerged structures, results in a vital reduction in wave run-up at the shore. The average run-up reduction is about 1m in real scale. Furthermore, there is an average reduction of about 50m in wave travel length, inland. The double submerged barriers gave the most effective suppression to the wave while the wall-trench system was more effective than the single submerged wall.

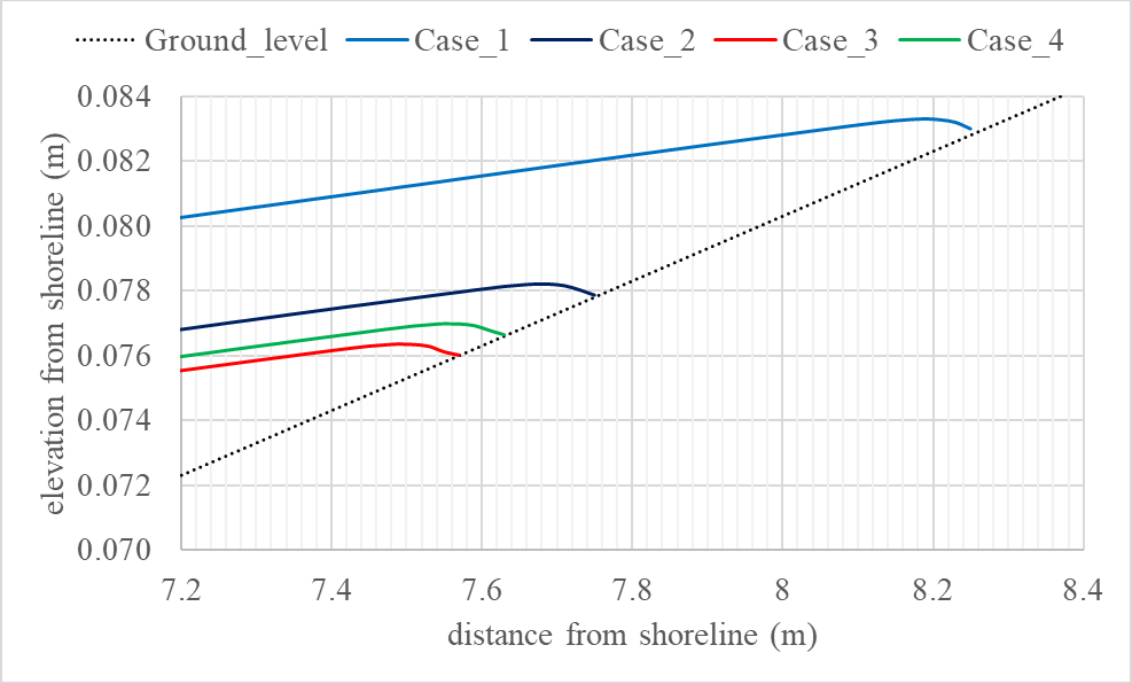

Figure 3.10. Comparison of run-up height for different structure system

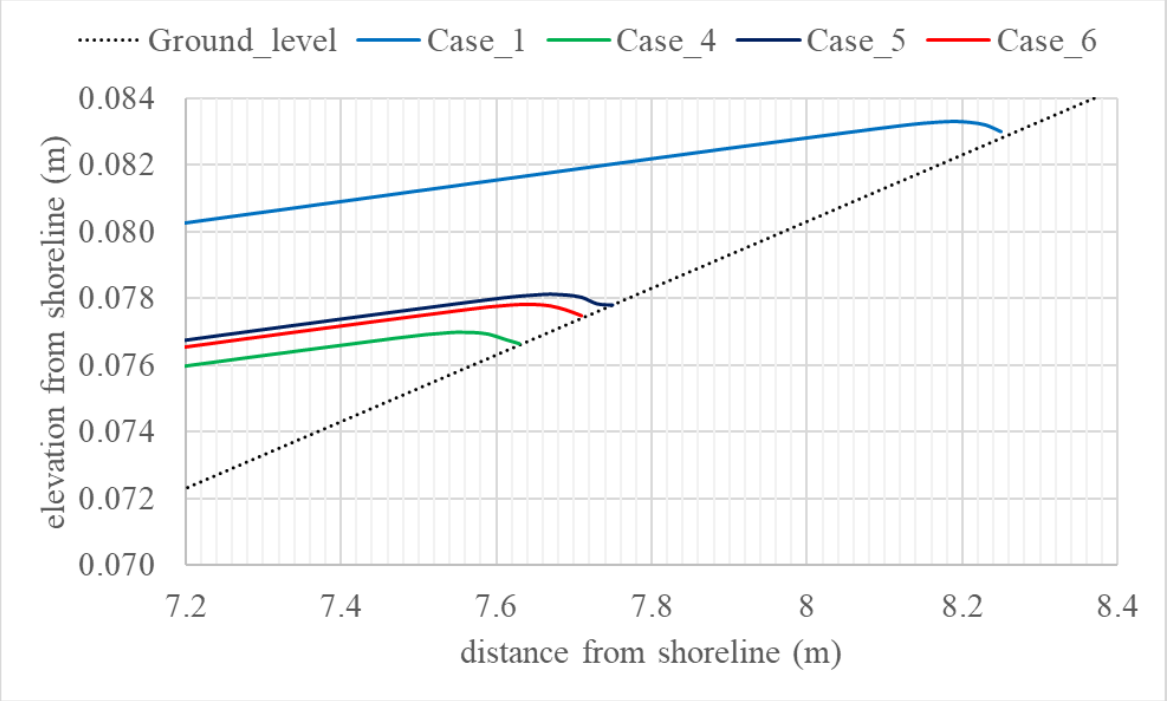

Figure 3.11. Comparison of run-up heights of each simulation case with different spacing between wall and trench.

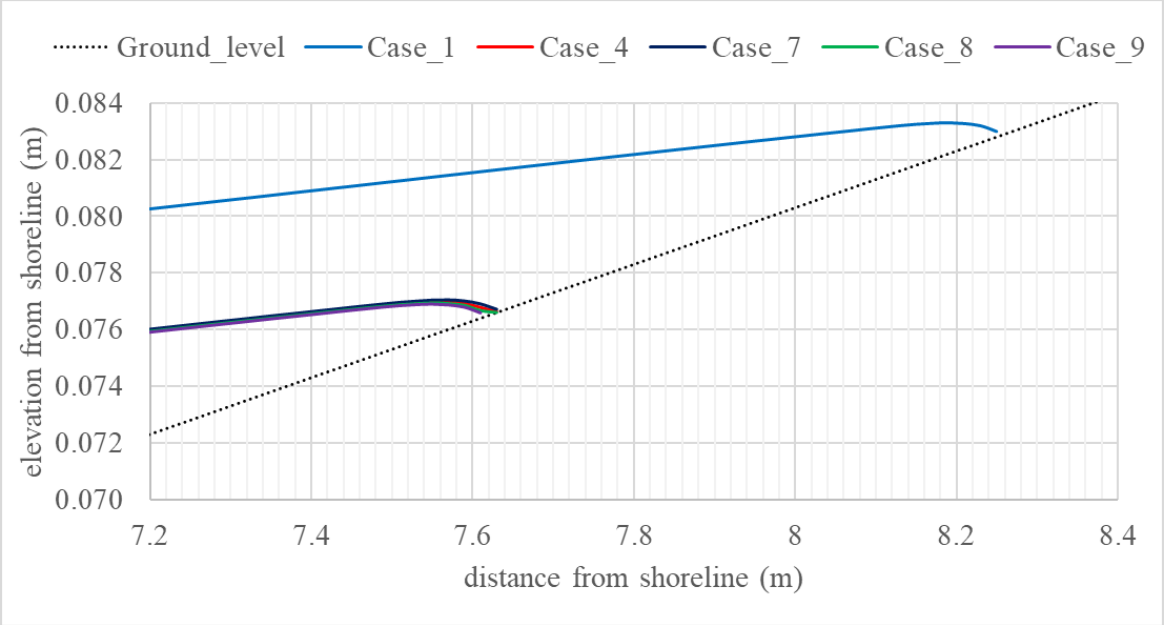

Figure 3.12. Comparison of run-up heights of each simulation case with different trench widths.

As explained in the introduction, double submerged structures have been investigated thoroughly by a number of researchers. On the other hand, rarely investigated are wall-trench systems, which have shown to have promising behaviors that are similar to a double barrier system. Therefore, it has been decided that this study will focus only on wall-trench system from here on.

Figure 3.11 was plotted from simulations with submerged wall and trench systems (Table 3.2) with variable spacing in between the wall and the trench. It gives the maximum water level along the x-axis for each simulation case (similar to Figure 3.10.).

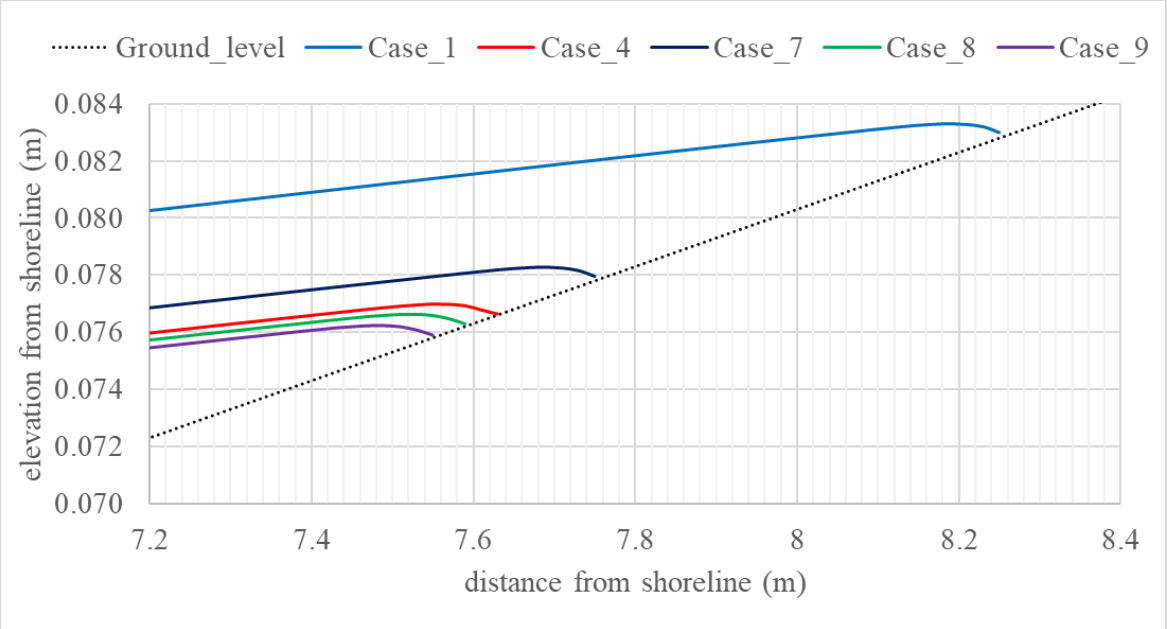

Figure 3.13. Comparison of run-up heights of each simulation case with different wall widths.

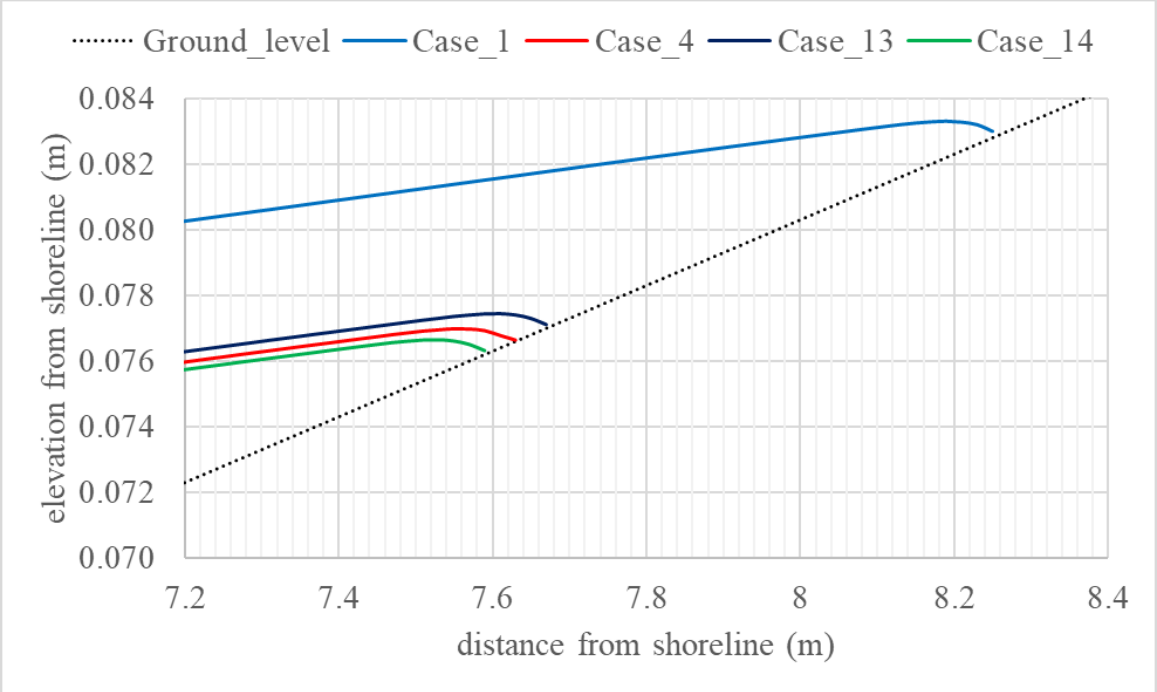

Figure 3.14. Comparison of run-up heights of each simulation case with different trench depths.

By looking at the run-up reduction, it is clear that the wall and trench system with a 0m spacing produced the most effective suppression of the upcoming wave. Figure 3.12. is plotted from simulations with submerged wall and trench systems by changing the width of the trench. It shows the calculated maximum water level along the x-axis for each simulation case. The run-up reduction proves that the wall and trench system with a wider trench width can suppress an upcoming wave compared to the systems with narrower trench widths.

However, the impact of trench width on the run-up reduction is apparently not very significant. The widths of the walls were then changed for several simulation cases, while maintaining a fixed geometry for the trench, which is plotted in Figure 3.13. giving the maximum water level along the x-axis for each simulation case (similar to Figure 3.12.).

By looking at the run-up reduction, it is clear that a wider wall will produce the most effective suppression for an upcoming wave. Lastly, the depth of the trench was also considered as a variable, which was plotted in Figure 3.14. giving the maximum water level along the x-axis for each simulation case (similar to Figure 3.13.). The run-up reduction reflects that the deeper the trench resulted in a higher suppression of the striking wave.

3.5 SUMMARY

A submerged wall and trench combination is assessed in this chapter to find out its usability as a tsunami defense measure. The geometrical parameters of the structure system, such as wall width, wall height, trench width, trench height and the spacing between wall and trench were evaluated by numerical simulations. Experimental results were used to calibrate the numerical model mainly for water level variations. The impact of the structure system resulted in reduced water level variations and current velocities at the land side. Although the reduction is not very significant, it could be suggested that the structure system can mitigate an upcoming tsunami wave better than a single submerged wall. Conclusions of the results of these numerical and experimental tests are explained in detail under Section 5.1 of Chapter 5.

CHAPTER 4

Chapter 4

TSUNAMI INTERACTION WITH ONSHORE WALL AND TRENCH SYSTEMS

OUTLINE

Combined wall and trench systems at onshore are investigated in this chapter to identify their usability as a defence measure against a tsunami-like waves. This part of the study focuses on several arrangements and geometries of combined wall and trench systems which are located at onshore. The structure system is assessed via a numerical model, which is calibrated by physical experiments of a tsunami-like wave transformation. A dam break event is used to model a tsunami-like wave interaction with structures. Resulted wave properties were investigated to identify the behavior of the structure system from the viewpoint of structure configuration. The results clearly show that the combined wall and trench systems at onshore can suppress the impact of a tsunami-like waves well than a single sea wall system.

This chapter consists of four main sections. Firstly, a brief introduction is given on the background with previous studies, which is followed by the focus and objectives. Then, the methodology and the procedure are explained in detail. At the end results are presented which are related to this chapter with a detailed discussion.

4.1 INTRODUCTION

As it is explained in detail under Chapter 3 (Section 3.1) researchers are interested in finding alternatives to conventional tsunami protection structures due to their significant side effects.

The investigation of Hsiao and Lin (2010) on Tsunami-like solitary waves impinging and overtopping an impermeable seawall is one example that can be given as a pre-2011

tsunami disaster study where he focused on describing three typical cases of tsunami wave interacting with seawall: a turbulent bore rushes inland and subsequently impacts and overtops the seawall (Type 1); a wave directly collapses on the seawall and then generates overtopping flow (Type 2); and, a wave straightforwardly overtops the seawall crown and collapses behind the seawall (Type 3). There he gave an insight into tsunami wave overtopping a seawall descriptively. Further, the study of Esteban *et al.* (2017) on overtopping of coastal structures by tsunami waves discusses insight into tsunami overtopping on different types of seawalls.

The Buckingham Canal in Andhra Pradesh in India was a significant mitigating factor, saving the lives of numerous fishermen, particularly in coastal areas around Chennai (Rao *et al.*, 2005), during the 2004 Indian Ocean Tsunami. This information leaded to the discussion that canals can be an effective countermeasure to protect coastal areas from tsunami strike.

Furthermore, during 2011 Great East Japan Tsunami, Tokida and Tanimoto (2012) showed that the water pool made by the flood stream of a tsunami, called a dug pool, can be effective in reducing the tsunami flow velocity. In spite of that, Dao, Adithyawan and Tanaka, (2013) carried out a series of numerical experiments to investigate the sensitivity and effects of ashore-parallel canal to reduce a tsunami's energy. His results showed that a canal parallel to the shoreline has a significant effect in reducing tsunami energy and plays an important role in the mitigation of tsunami impacts. Although the study of (Dao, Adithyawan and Tanaka, 2013) focused on a cannel on land, it showed some promising outcomes of a wall trench system that would significantly be effective in reducing current speeds of a tsunami-like wave.

Rahman, Schaab and Nakaza, (2017) carried out an experimental and numerical study to investigate the tsunami mitigation by canals where he concluded a positive reduction of tsunami waves by incorporating a narrow canal which is located perpendicular to the wave direction.

In most of these cases, researchers have only considered vertical type seawalls or trenches/canals against a tsunami-like waves. Silva and Araki, (2019) conducted a study the behavior of a submerged wall and trench system at near shore where it was discussed how the structure configuration and geometry affects an upcoming tsunami wave. However, the manner in which a combined wall and trench system can influence the runoff of a tsunami-like wave at onshore has rarely been studied.

As mentioned under Section 3.1 in Chapter 3, from the lessons learnt through the 2011 Great East Japan Tsunami, it could be stated that significant destruction in coastal areas is possible even with strong protection structures.

4.2 FOCUS AND OBJECTIVES

Within this background, the need of enhancing the effectiveness of conventional seawalls have raised. Number of researchers have focused on improving costal defense against tsunami by applying different type of structures and solutions in addition to sea walls and sea dikes.

For this chapter, focus is placed more on a combined wall and trench system at onshore, which would act as a tsunami defense structure. A set of numerical simulations following physical experiments were performed through a computational fluid dynamics (CFD) model that predicts the run-up heights of a tsunami-like wave on a sloping beach in accordance to the dimensions of a submerged wall and trench systems. Finally, variations in the run-up processes for different geometries of the structure system were investigated.

4.3 METHODOLOGY

4.3.1 Experimental Setup

The experimental set-up is similar to the set-up described under Chapter 3. However, the locations of water level gauges current meter was changed by considering the location change of the structure. The location of each gauge is also given in Figure 4.1. Readings of the water level gauges and current meters were used to calibrate the numerical model in the next stage. A different type of current meter was used in these experiments as we could not capture current velocities in the experiments that are described under Chapter 3.

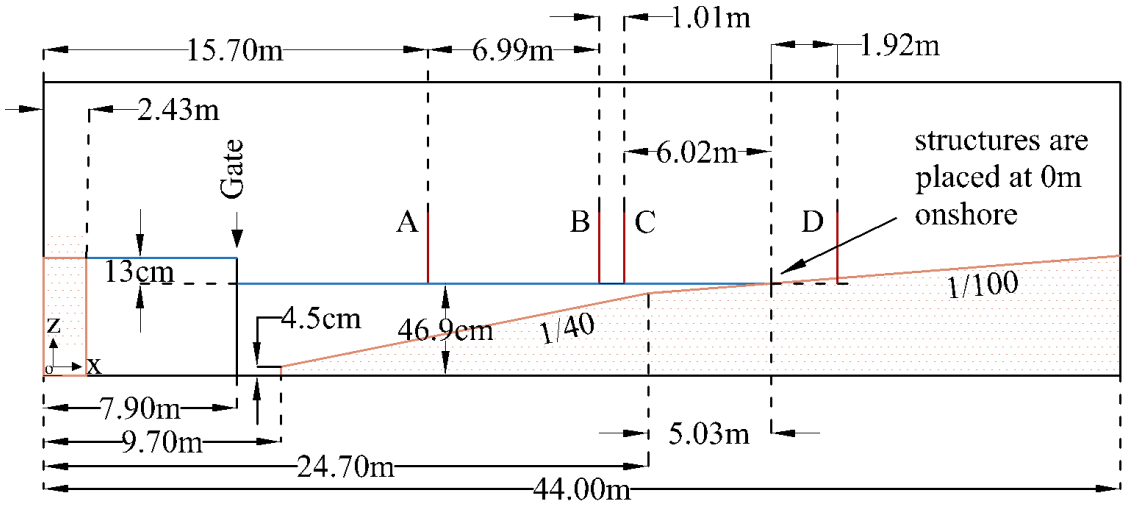

Figure 4.1. Dimensions of the wave tank and details of the experimental setup

4.3.2 Numerical Setup

The open source CFD code pack, OpenFOAM® was used to set up the experiments numerically. OpenFOAM® features a three-dimensional, two-phase (Reynolds Averaged Navier Stokes) RANS solver called "interFoam", which was presented in detail in Higuera et al (2013). The dynamics is solved for both water and air in all the cases presented in this chapter, which is an advantage, as it is a more complete approach. Water is simulated with density ρ=1000 kg/m^3 and kinematic viscosity ν=10^{-6} Pa/s, while air has density ρ=1 kg/m^3 and kinematic viscosity ν=1.48 10^{-6} Pa/s.

The governing equations include continuity and momentum equations, respectively given in equations (4.1) and (4.2):

$$\frac{\partial u_i}{\partial x_i} = 0 \tag{4.1}$$

$$\frac{\partial \rho u_i}{\rho t} + u_j \frac{\partial \rho u_i}{\partial x_j} = -\frac{\partial p^*}{\rho x_i} - g_j x_i \frac{\partial \rho}{\rho x_i} + \frac{\partial}{\rho x_j}\left(2\mu S_{ij}\right) + \sigma_T K \frac{\partial \alpha}{\rho x_i} \tag{4.2}$$

Where x_i are the Cartesian coordinates, u_i are the mean components of the velocities, p^* is the pressure minus the hydrostatic potential $\rho g_j x_i$, ρ is the fluid density (which takes the constant value α_{water} in the water and jumps at the interface to the constant value α_{air} in the air phase), , g_j is the gravitational acceleration, $\mu = \rho\upsilon$ is the dynamic molecular viscosity (υ being the kinematic viscosity), and S_{ij} is the mean strain rate tensor given by

$$S_{ij} = \frac{1}{2}\left(\frac{\partial u_i}{\partial x_j} + \frac{\partial u_j}{\partial x_i}\right) \tag{4.3}$$

The effect of surface tension σ_T is accounted in the last term in equation (2). where α is the indicator field introduced in volume of fluid method, which takes value 0 in air and 1 in water and K is the local surface curvature. α can be defined in terms of the density as

$$\alpha = \frac{\rho - \rho_{air}}{\rho_{water} - \rho_{air}} \tag{4.4}$$

Similar to density, any fluid property, Φ, can be expressed in terms of α

$$\Phi = \alpha\Phi_{water} + (1 - \alpha)\Phi_{air} \tag{4.5}$$

To calculate the evolution of α the continuity equation can be applied as follows.

$$\frac{\partial \alpha}{\partial t} + \frac{\partial \alpha u_i}{\partial x_j} = 0 \tag{4.6}$$

"Multidimensional Universal Limiter with Explicit Solution" (MULES) limiter, which is a numerical interface compression method with limited phase fluxes is applied to keep the

sharp interface between two fluids (air and water). The compression is calculated by adding another term (4.7) to equation (4.6)

$$\frac{\partial \alpha}{\partial t} + \frac{\partial \alpha u_i}{\partial x_j} + \frac{\partial}{\partial x_j}\left(\alpha(1-\alpha)u_j^r\right) = 0 \qquad (4.7)$$

Where u_j^r is modelled as a relative velocity used to compress the interface. More information on the numerical implementation, can be found in Deshpande's (2012) evaluation of interFoam solver.

A detailed description of the numerical model is given under Chapter 2 (Section 2.4)

The numerical model was set up to simulate the same dam break event. The domain is constructed in a 3D environment. Depth contours were introduced into the grid by defining the same depth levels from the experiment. The domain is then introduced into interFoam module by applying a set of initial conditions (13cm water column at the reservoir end) to calculate the evolution of the wave generated by the dam break event. The complete flume is replicated in 3D at the initial stage and then performed 3D to 2D conversion by extruding cells of the Y direction. The longest length of the flume corresponds to the X axis, and it is meshed varying the cell discretization, which allows for better resolution in critical zones as near the structures, while providing adequate resolution for other zones where dynamics are less restrictive. Maximum resolution in *X* and *Y* directions were maintained as 1 cm. Higher resolution is applied at near shore area by decomposing the domain. This disposition totals ~0.4 million cells. The inbuilt meshing tool, snappyHexMesh was used further smoothing and rearranging cells. Turbulence is modelled using $k-\varepsilon$ turbulence model. Initial values for k and ε were given as 0.0023 m^2/s^2 and 0.0548 m^2/s^3 respectively. The other important interFoam parameters that we applied in simulations are given in Table 4.1. Tsunami propagation with the computational domain is shown in Figure 4.3.

Table 4.1. interFoam parameters

controlDict	Scheme/Value
adjustTimeStep	true
maxCo	0.5
maxAlphaCo	0.5
fvSchemes	Scheme/Value
ddt	Euler
grad	Gauss linear
div(rhoPhi,U)	Gauss linearUpwind grad(U)
div(phirb, alpha)	Gauss linear
div(phirb, alpha)	Gauss linear
div(phi,k)	Gauss upwind
div(phi,epsilon)	Gauss upwind
laplacian	Gauss linear corrected
interplolation	linear
snGrad	corrected
fvSolution	Scheme/Value
alpha.water.* (solver, tol, relTol)	smoothSolver, 1e-8, 0
pcorr(solver, prec, tol, relTol)	PCG, DIC, 1e-8, 0
p_rgh(solver, prec, tol, relTol)	PCG, DIC, 1e-8, 0
U|K|epsilon	smoothSolver, 1e-8, 0

Water level variations and current velocities were extracted from simulation results at the same gauge locations as the experiment and compared with recordings from the experiment. Plots of comparison are given under results and discussion.

4.3.3 Simulations with Onshore Structures

The onshore structures were then introduced to the numerical domain by altering the bottom profile. Several types of structures were assessed including a single vertical seawall and

wall-trench systems with different geometries. The orientations and real scale dimensions of each structure system are listed in Table 4.2. The same information for the model scale are given in Table 4.3. Schematic diagram of the wall and trench system is given in Fig 4.2.

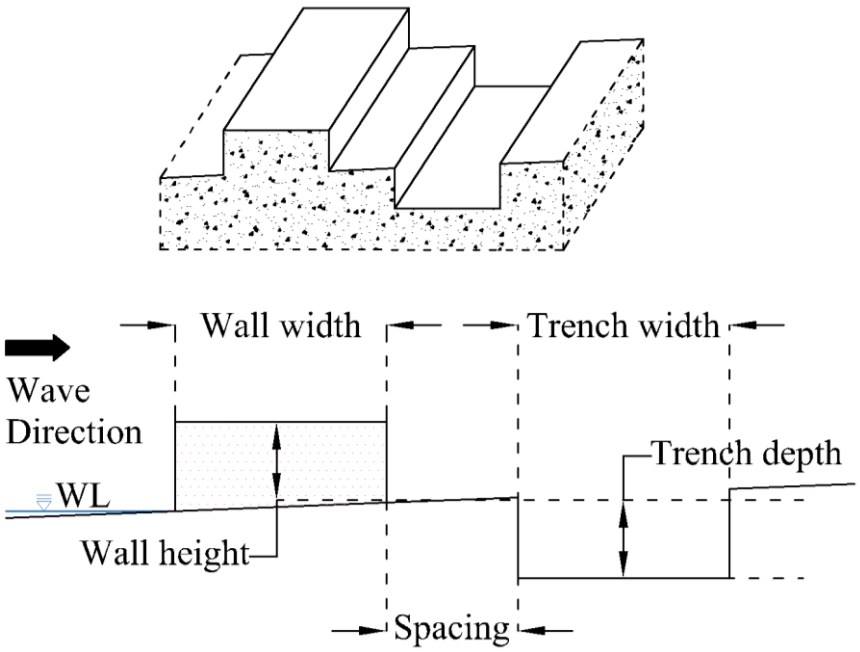

Figure 4.2. Geometry of the combined wall and trench system

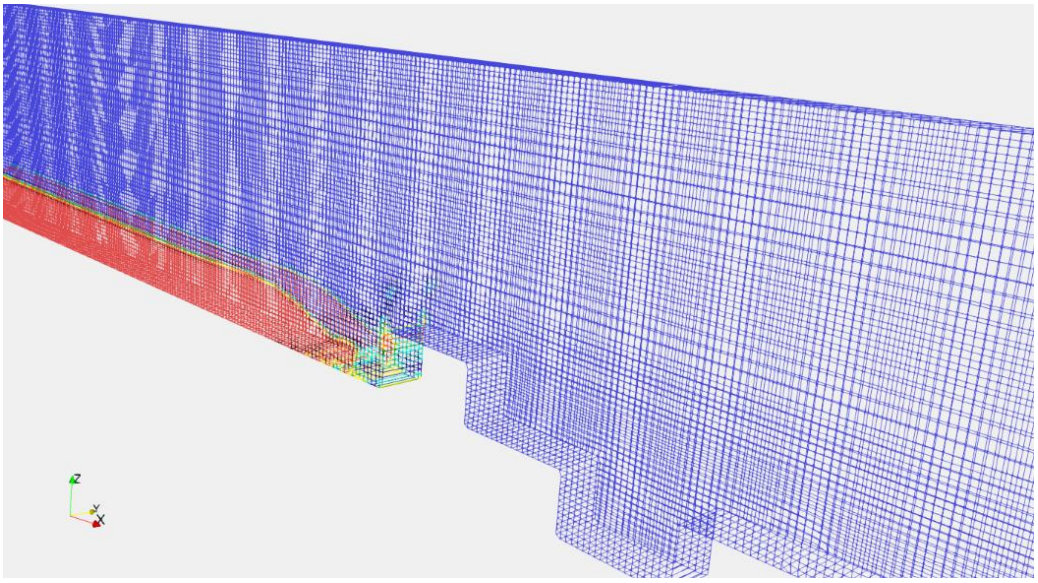

Figure 4.3. Tsunami propagation within the computational domain

Table 4.2. Description of simulation cases with details of onshore structures (in real scale)

Case no.	Description	Wall height (m)	Wall width (m)	Trench depth (m)	Trench width (m)	Spacing (m)
1	Without Structures	-	-	-	-	-
2	Single wall	5	10	-	-	-
3	Wall-trench	5	10	5	10	5
4	Wall-trench	5	10	5	10	10
5	Wall-trench	5	10	5	10	15
6	Wall-trench	5	10	5	5	10
7	Wall-trench	5	10	5	10	10
8	Wall-trench	5	10	5	15	10
9	Wall-trench	5	5	5	10	10
10	Wall-trench	5	10	5	10	10
11	Wall-trench	5	15	5	10	10
12	Wall-trench	5	10	2.5	10	10
13	Wall-trench	5	10	5	10	10
14	Wall-trench	5	10	7.5	10	10

Table 4.3. Description of simulation cases with details of onshore structures (in model scale)

Case no.	Description	Wall height (mm)	Wall width (mm)	Trench depth (mm)	Trench width (mm)	Spacing (mm)
1	Without Structures	-	-	-	-	-
2	Single wall	62.5	125	-	-	-
3	Wall-trench	62.5	125	62.5	125	62.5
4	Wall-trench	62.5	125	62.5	125	125
5	Wall-trench	62.5	125	62.5	125	187.5
6	Wall-trench	62.5	125	62.5	62.5	125

7	Wall-trench	62.5	125	62.5	125	125
8	Wall-trench	62.5	125	62.5	187.5	125
9	Wall-trench	62.5	62.5	62.5	125	125
10	Wall-trench	62.5	125	62.5	125	125
11	Wall-trench	62.5	187.5	62.5	125	125
12	Wall-trench	62.5	125	31.25	125	125
13	Wall-trench	62.5	125	62.5	125	125
14	Wall-trench	62.5	125	93.75	125	125

4.3.4 Assessment of the Wall and Trench Combination with Single Seawall

Thereafter, tsunami interaction with the combined wall and trench system was compared with tsunami interaction ahead of a single sea wall system. A typical embarkment type sea wall was considered when comparing with the wall and trench system. Figure 4.4 show the layout of the single wall and the wall and trench system that were compared with each other. The height of the wall was the only variable parameter in the comparison. Table 4.4 gives the simulation cases and the geometries of each structure combination.

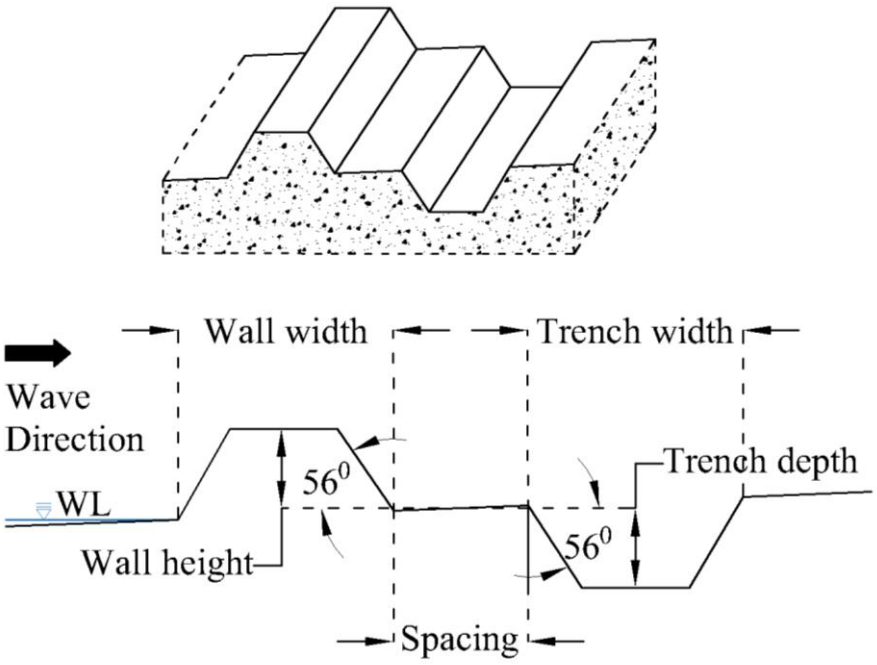

Figure 4.4. Geometry of the combined wall and trench system which is applied in Section 4.3.4

Table 4.4. Description of simulation cases with details of onshore structures

Model Scale						
Case no.	Description	Wall height (mm)	Wall width (mm)	Trench depth (mm)	Trench width (mm)	Spacing (mm)
15	Single wall	37.5	125	-	-	-
16	Single wall	50	125	-	-	-
17	Single wall	62.5	125	-	-	-
18	Single wall	75	125	-	-	-
19	Wall-trench	37.5	125	62.5	125	62.5
20	Wall-trench	50	125	62.5	125	62.5
21	Wall-trench	62.5	125	62.5	125	62.5
22	Wall-trench	75	125	62.5	125	62.5

Prototype						
Case no.	Description	Wall height (m)	Wall width (m)	Trench depth (m)	Trench width (m)	Spacing (m)
15	Single wall	3	10	-	-	-
16	Single wall	4	10	-	-	-
17	Single wall	5	10	-	-	-
18	Single wall	6	10	-	-	-
19	Wall-trench	3	10	5	10	5
20	Wall-trench	4	10	5	10	5
21	Wall-trench	5	10	5	10	5
22	Wall-trench	6	10	5	10	5

4.3.5 Behavior of the Structure Ahead of Different Tsunami Conditions

So far, same tsunami condition (13cm) was used for all of the simulation cases. However, when looking at the results of simulation cases with variable spacing between the wall and the trench, it was clear that the combined wall and trench structure combination behave quite differently ahead of different tsunami levels when the spacing between the wall and the trench changes. Therefore, it was decided to investigate those observations by applying the structure systems with variable spacings into different tsunami conditions. Table 4.5 and Table 4.6 gives the description of the simulation cases of this section.

Table 4.5. Description of simulation cases with details of onshore structures (in model scale)

Case no.	Tsunami condition (cm)	Description	Wall height (mm)	Wall width (mm)	Trench depth (mm)	Trench width (mm)	Spacing (mm)
23	11	Wall-trench	62.5	125	62.5	125	0
24	13						
25	15						
26	17						
27	11	Wall-trench	62.5	125	62.5	125	25
28	13						
29	15						
30	17						
31	11	Wall-trench	62.5	125	62.5	125	50
32	13						
33	15						
34	17						
35	11	Wall-trench	62.5	125	62.5	125	62.5
36	13						
37	15						
38	17						
39	11	Wall-trench	62.5	125	62.5	125	75
40	13						
41	15						
42	17						
43	11	Wall-trench	62.5	125	62.5	125	100
44	13						
45	15						
46	17						
47	11	Wall-trench	62.5	125	62.5	125	125
48	13						

49	15						
50	17						
51	11	Wall-trench	62.5	125	62.5	125	187.5
52	13						
53	15						
54	17						

Table 4.6. Description of simulation cases with details of onshore structures (in real scale)

Case no.	Tsunami condition (cm)	Description	Wall height (m)	Wall width (m)	Trench depth (m)	Trench width (m)	Spacing (m)
23	11	Wall-trench	5	10	5	10	0
24	13						
25	15						
26	17						
27	11	Wall-trench	5	10	5	10	2
28	13						
29	15						
30	17						
31	11	Wall-trench	5	10	5	10	4
32	13						
33	15						
34	17						
35	11	Wall-trench	5	10	5	10	5
36	13						
37	15						
38	17						
39	11	Wall-trench	5	10	5	10	6
40	13						

41	15						
42	17						
43	11	Wall-trench	5	10	5	10	8
44	13						
45	15						
46	17						
47	11	Wall-trench	5	10	5	10	10
48	13						
49	15						
50	17						
51	11	Wall-trench	5	10	5	10	15
52	13						
53	15						
54	17						

4.3.6 Investigation of Horizontal Pressure Forces Acting on the Structure

As the next step, several simulation cases were carried out to calculate the horizontal pressure forces that are acting on the onshore structure system when the tsunami interacts. The forces are calculated by integrating the calculated pressure over the sectional area of the structure (Chapter 2, Section 2.5.17). Moreover, forces in simulation with the single wall was calculated directly while the forces in simulation with wall and trench system had to be calculated by treating the wall and the trench as separate structures. The simulation cases for this section are given in Table 4.6.

Table 4.7. Description of simulation cases with details of onshore structures

Model Scale						
Case no.	Description	Wall height (mm)	Wall width (mm)	Trench depth (mm)	Trench width (mm)	Spacing (mm)
55	Single wall	62.5	125	-	-	-
56	Wall and trench	62.5	125	62.5	125	62.5
Prototype						
Case no.	Description	Wall height (m)	Wall width (m)	Trench depth (m)	Trench width (m)	Spacing (m)
55	Single wall	5	10	-	-	-
56	Wall and trench	5	10	5	10	5

4.3.7 Assessment of the directional position of the trench

Lastly, the combined wall and trench structure system is evaluated by changing the directional position of the trench. Few trial simulations were run to find out the best spacing between the wall and the trench which gives the best reduction to the water levels and to the current speeds. Thereafter, the results of those two simulations were compared with each other. The details of simulation cases that are carried out under this section is given in Table 4.8.

Table 4.8. Description of simulation cases with details of onshore structures

Model Scale						
Case no.	Description	Wall height (mm)	Wall width (mm)	Trench depth (mm)	Trench width (mm)	Spacing (mm)
57	Wall in front of trench	62.5	125	62.5	125	62.5
58	Trench in front of the wall	62.5	125	62.5	125	0
Prototype						
Case no.	Description	Wall height (m)	Wall width (m)	Trench depth (m)	Trench width (m)	Spacing (m)
57	Wall in front of trench	5	10	5	10	5
58	Trench in front of the wall	5	10	5	10	0

4.4. RESULTS AND DISCUSSION

4.4.1 Comparison of Wave Transformation

Figures 4.5.a, 4.5.b and 4.5.c illustrate the comparison between measured and simulated water level variations at each gauge location. Elevation was measured from the most bottom of the flume (Bottom left in Figure 4.1). From the below figures, it can be proposed that the numerical model is capable of reproducing the water level variations, which are generated by the striking wave. High frequency oscillations of the free surface were also reproduced well before and after wave breaking. As it was observed in the experiments, wave breaks somewhere

between location A and B. However, higher deviation is observed once the wave reached onshore. When comparing the simulated water level variations with the results of Chapter 3 (Section 3.4.1), it can be clearly seen that the multiphase model (OpenFoam – interFoam solver) is capable of simulating the tsunami transformation with better accuracy by the shallow water Boussinesq model (Delft3D).

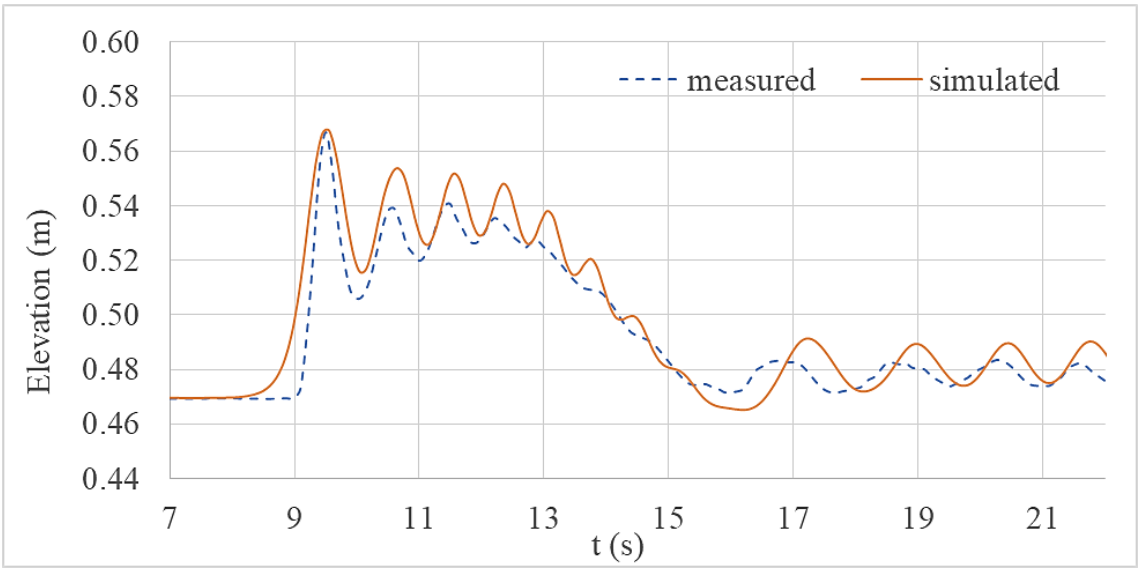

Figure 4.5.a. Comparison of water level variations at location A

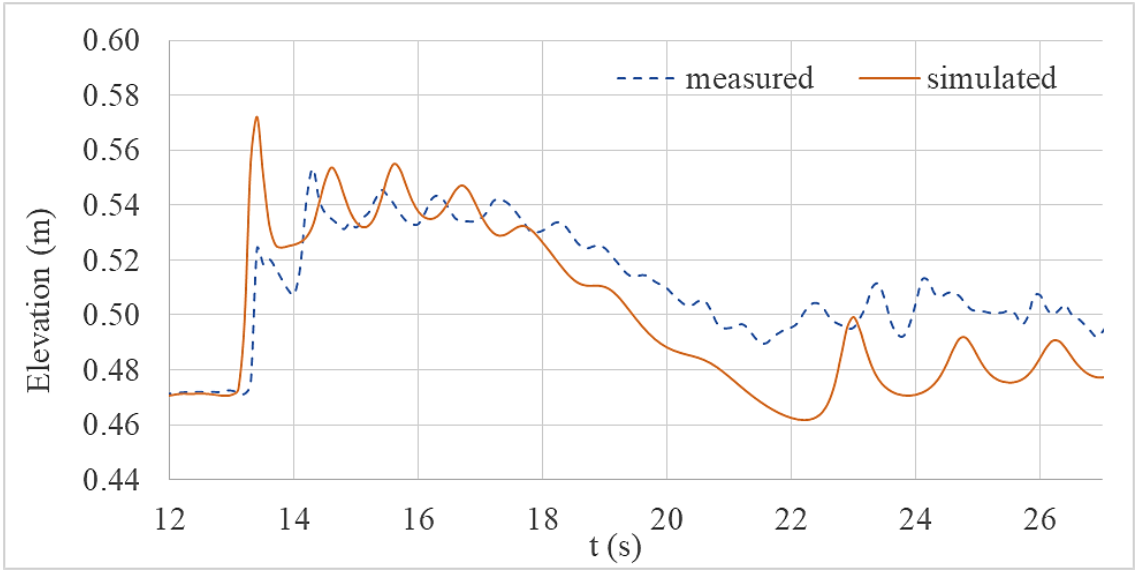

Figure 4.5.b. Comparison of water level variations at location B

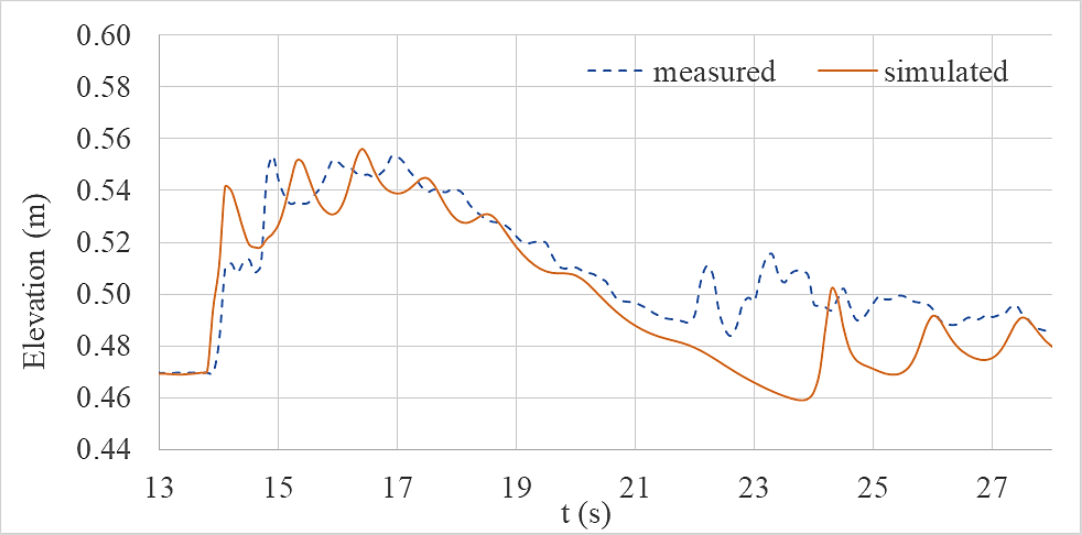

Figure 4.5.c. Comparison of water level variations at location C

Figures 4.6.a and 4.6.b show the comparison of measured and simulated current velocity variations at B and C gauge locations. Due to limited resources and some practical difficulties, the authors measured current velocity variations only at B and C locations. By examining both figures, it is clear that the shape of the current velocity variations were also reproduced comparatively well by the numerical model. Though there is a deviation at the end of the wave bore, the maximum current velocities were accurately predicted by numerical simulations.

When comparing the simulated current velocity variations with the results of Chapter 3 (Section 3.4.1), it can be clearly seen that the multiphase model (OpenFoam – interFoam solver) is capable of simulating the tsunami transformation with better accuracy than the shallow water Boussinesq model (Delft3D). However, it should be noted that the measured current velocity variations presented under Chapter 3 (Section 3.4.1) are found to be less accurate than the current velocities measured in the experiments that are presented here.

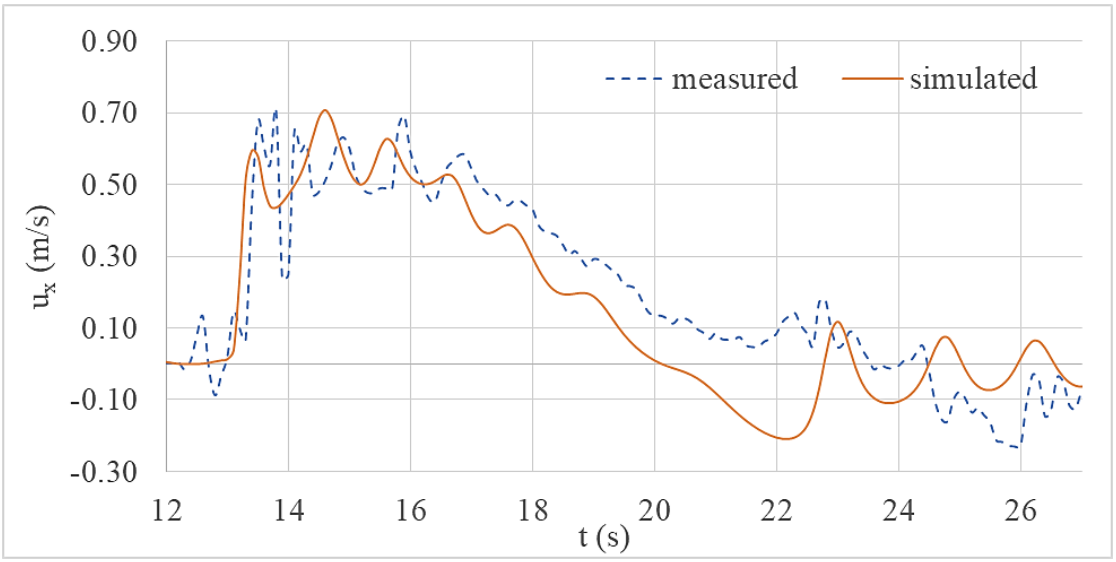

Figure 4.6.a. Comparison of current velocity (x-component) at location B

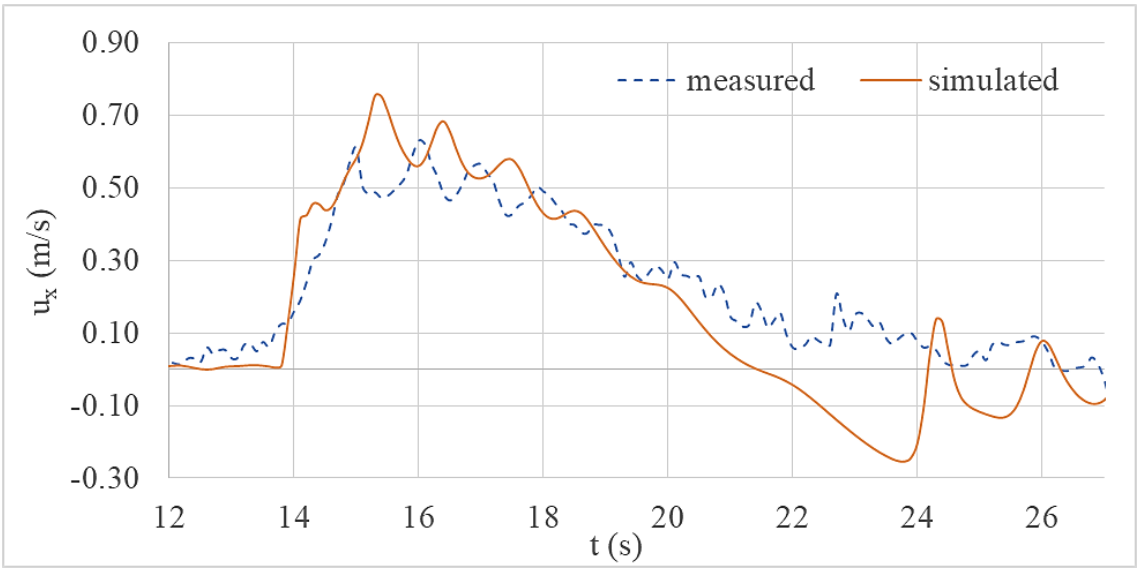

Figure 4.6.b. Comparison of current velocity (x-component) at location C

4.4.2 Assessment of Each Onshore Structure

The water level variations and current velocity variations at gauge locations are given in the following figures. Figures 4.7.a and 4.7.b represent the variations of above parameters at location D (lee side of the structure) for Cases 1 to 5.

Case 1 is simulated without onshore structures. Case 2 is the simulation with a single vertical seawall. Case 3 is a simulation with a combined wall and trench system with a spacing of 5m. In Cases 4 and 5, the spacing between the wall and the trench was increased as 10m and 15m respectively (Tables 4.1 and 4.2) while keeping constant values for other geometrical parameters.

Figure 4.7.a. Comparison of water level variations at location D

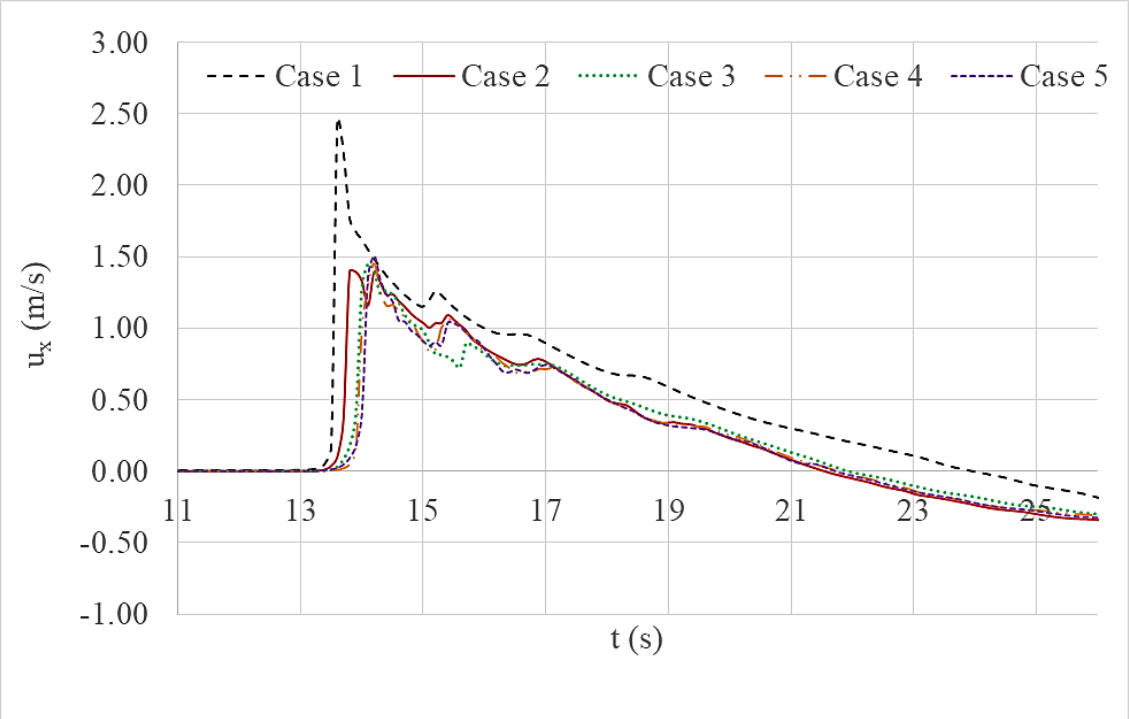

Figure 4.7.b. Comparison of current velocity (x-component) variations at location D

Figure 4.7.a clearly shows a reduction of maximum water level variation after applying onshore structures. The wall and trench system with 5m spacing suppressed the upcoming wave better than other structure combinations. This is due to the fact that overtopping wave directly collapse into lee side trench. This phenomenon will be discussed in detail under the results of Section 4.4.5. Both of the other wall and trench systems also reduced the free surface variation better than the single seawall system.

Current velocity variations (Figure 4.7.b) of wall and trench cases does not show a significant reduction compared to the single wall system. However, arrival time of the wave was increased in wall and trench cases.

Figures 4.8.a and 4.8.b give a comparison of water level variations and current velocity variations respectively at location D for Cases 1, 2, 6, 7 and 8. The width of the trench was increased gradually in Cases 6, 7 and 8 to assess the impact while maintaining other geometric parameters of the structure system as the same.

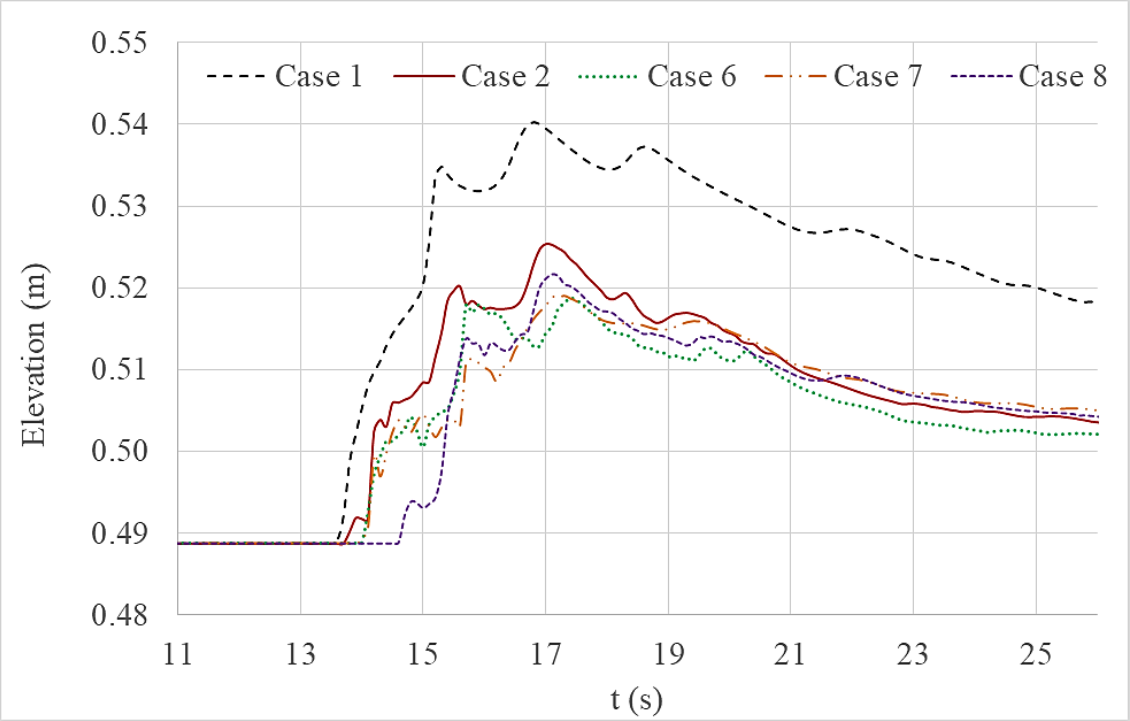

Figure 4.8.a. Comparison of water level variations at location D

Similar to Figure 4.7.a, Figure 4.8.a indicates a reduction of maximum water level variation after applying onshore structures. The wall and trench system with the widest trench suppressed the upcoming wave better than other structure combinations. Both of the other wall and trench systems also reduced the free surface variation better than the single seawall system.

Current velocity variations (Figure 4.8.b) of wall and trench cases also reflect suppressed values. Also, arrival time of the wave was increased in all wall and trench cases compared to the single seawall simulation. The case with the widest trench gives most effective suppression.

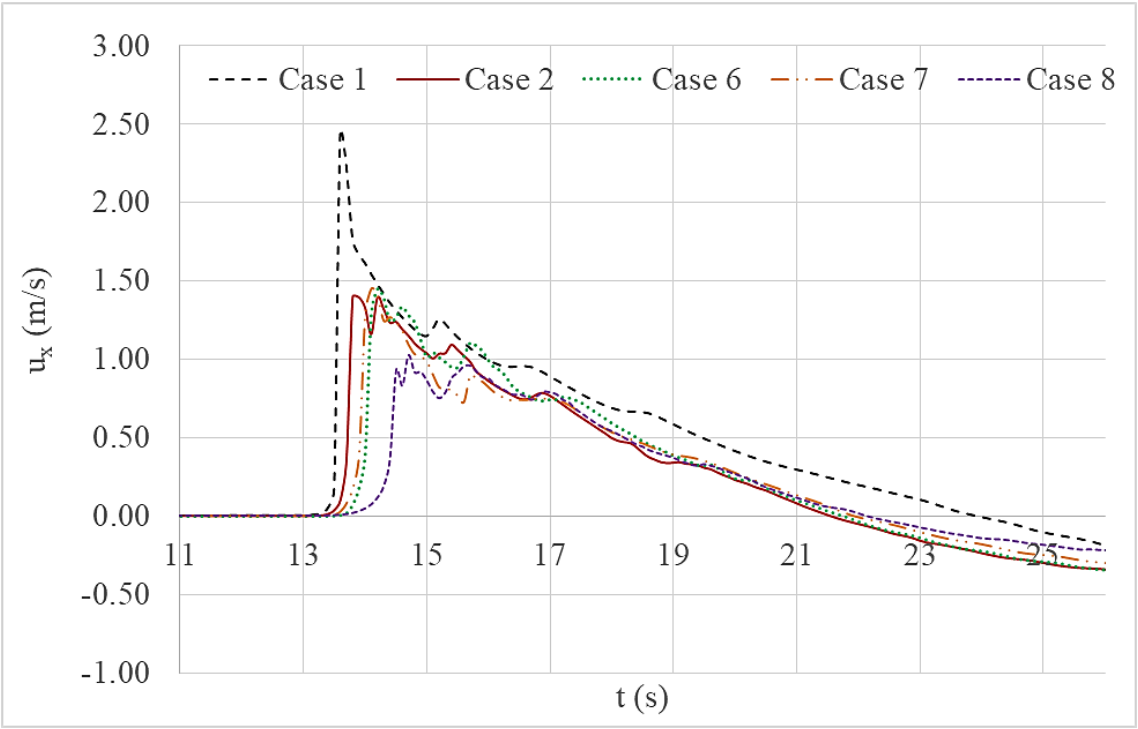

Figure 4.8.b. Comparison of current velocity (x-component) variations at location D

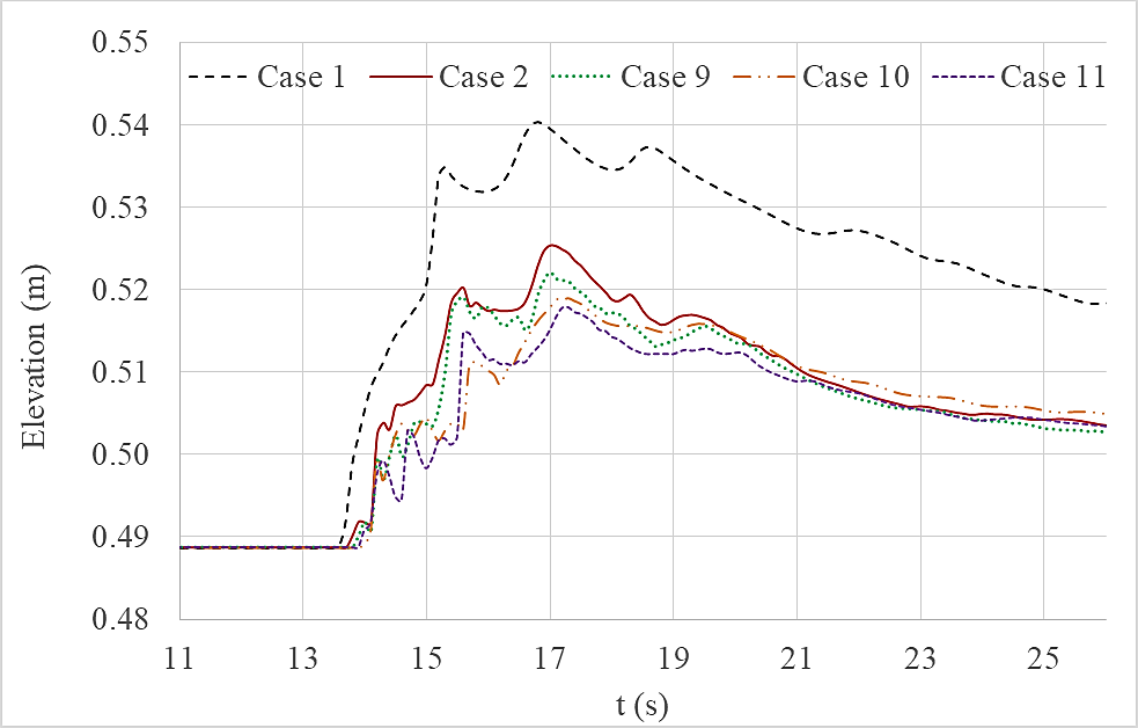

Figure 4.9.a. Comparison of water level variations at D

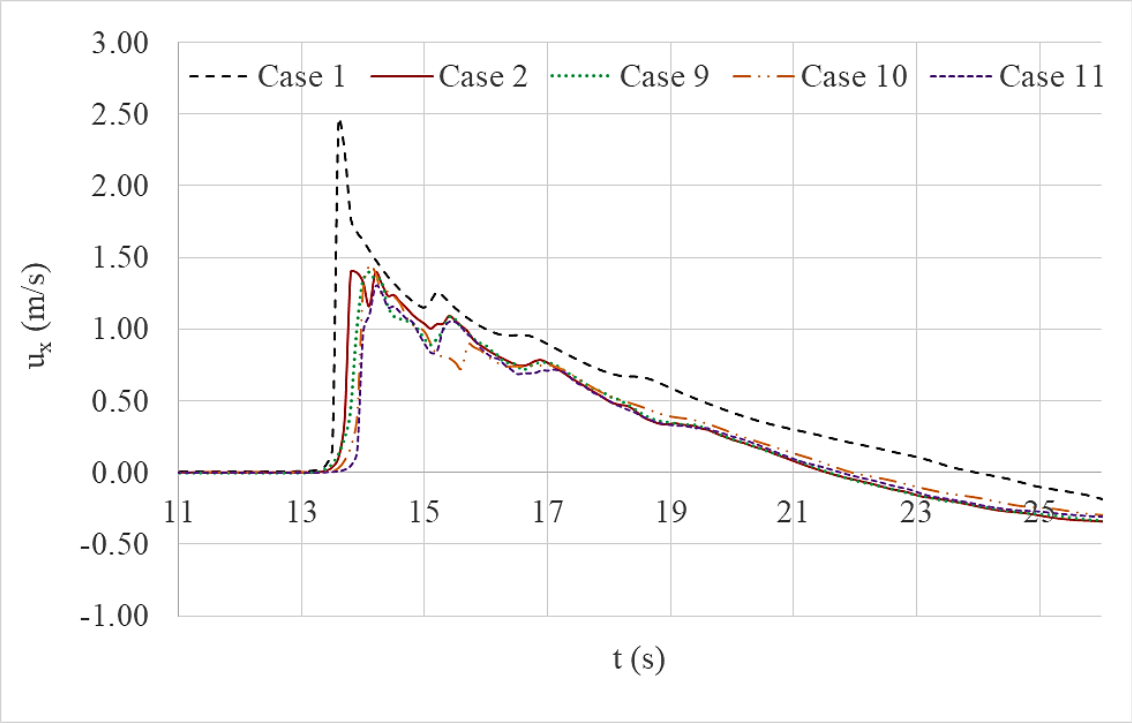

Figure 4.9.b. Comparison of current velocity (x-component) variations at location D

Figures 4.9.a and 3.9.b give a comparison of water level variations and current velocity variations respectively at location D for Cases 1, 2, 9, 10 and 11. The width of the wall was increased gradually in Cases 9, 10 and 11 to assess the impact while maintaining constant parameters for other geometric features.

Similar to Figure 4.8.a, Figure 4.9.a shows a reduction of maximum water level variation after applying onshore structures. The wall and trench system with the widest wall suppressed the upcoming wave better than other structure combinations. Both of the other wall and trench systems also reduced the free surface variation better than the single seawall system.

Though current velocity variations (Figure 4.9.b) of wall and trench cases does not show a significant reduction compared to single seawall case, tsunami arrival times were increased in all wall and trench cases. The Case with the widest wall looks the most effective structure from the viewpoint of free surface elevation and wave arrival time.

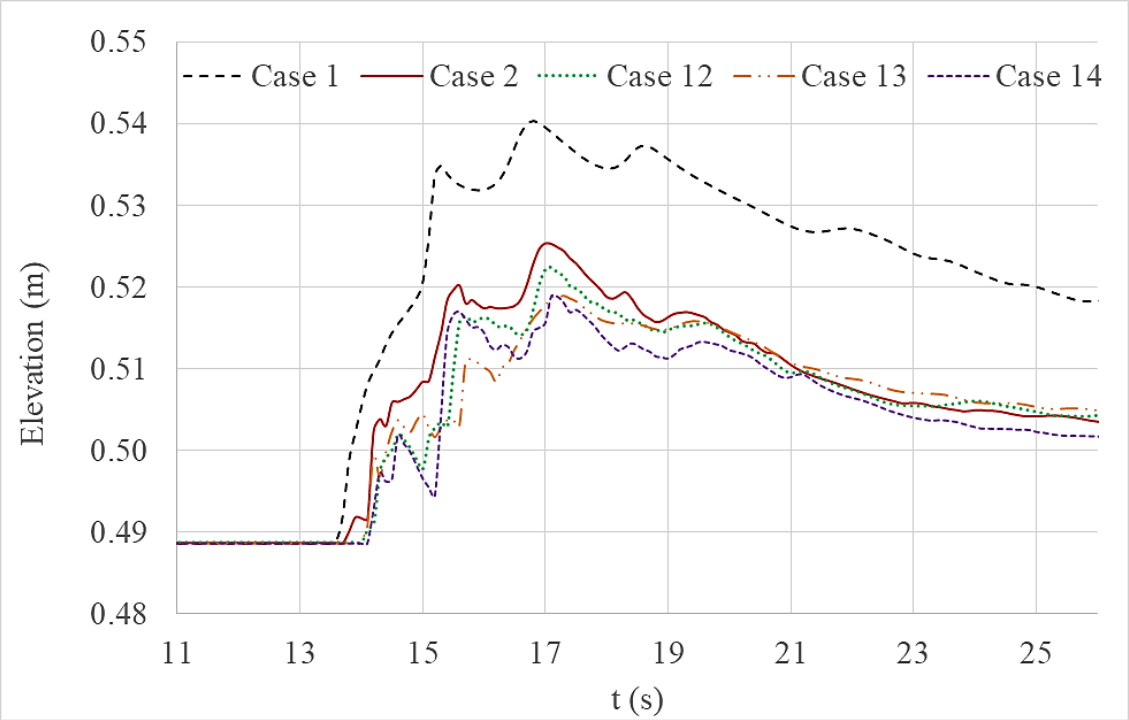

Figure 4.10.a. Comparison of water level variations at location D

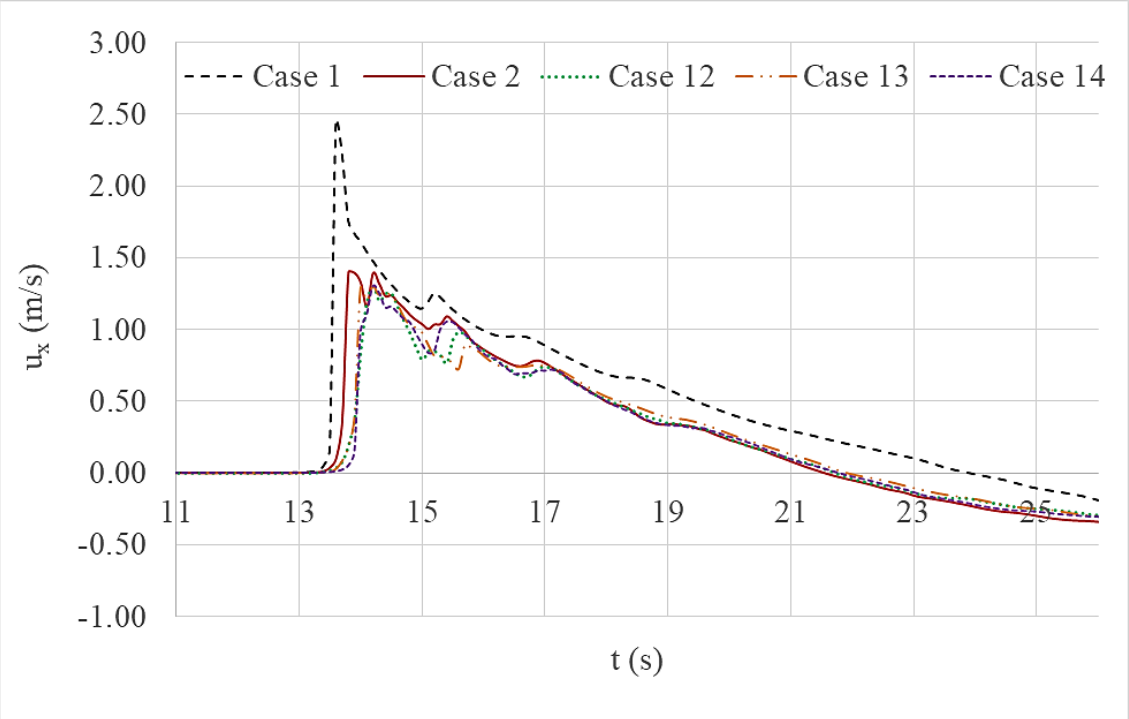

Figure 4.10.b. Comparison of current velocity (x-component) variations at location D

Figures 4.10.a and 4.10.b give a comparison of water level variations and current velocity variations respectively at location D for Cases 1, 2, 12, 13 and 14. The depth of the trench was increased gradually in Cases 12, 13 and 14 to assess the impact while maintaining constant parameters for other geometric features.

Similar to other comparisons, Figure 4.10.a shows a reduction of maximum water level variation after applying onshore structures. The wall and trench system with the deepest trench suppressed the upcoming wave better than other structure combinations. Both of the other wall and trench systems also reduced the free surface variation better than the single seawall system.

Current velocity variations (Figure 4.10.b) of wall and trench cases also show suppressed values. Moreover, arrival time of the wave was increased in all wall and trench cases compared to the single seawall simulation. The case with the deepest trench gives most effective suppression.

Thereafter, tsunami inundation at the 1:100 beach slope was investigated for each simulation case.

4.4.3 Tsunami Inundation at the beach slope

Inundations for a given time (240 seconds of simulation time) were plotted and presented in Figures 4.11 to 4.14. The y axis of the figures is in α which is the dimensionless factor defining water and air in simulations. Water is represented when $\alpha = 1$ and air is represented when $\alpha = 0$. Thus, the interface between 1 and 0 at the beach slope can be identified as the point where the water wave reached at a given time. α values between 0 and 1 indicates the air-water mixture at the fluid transition interface.

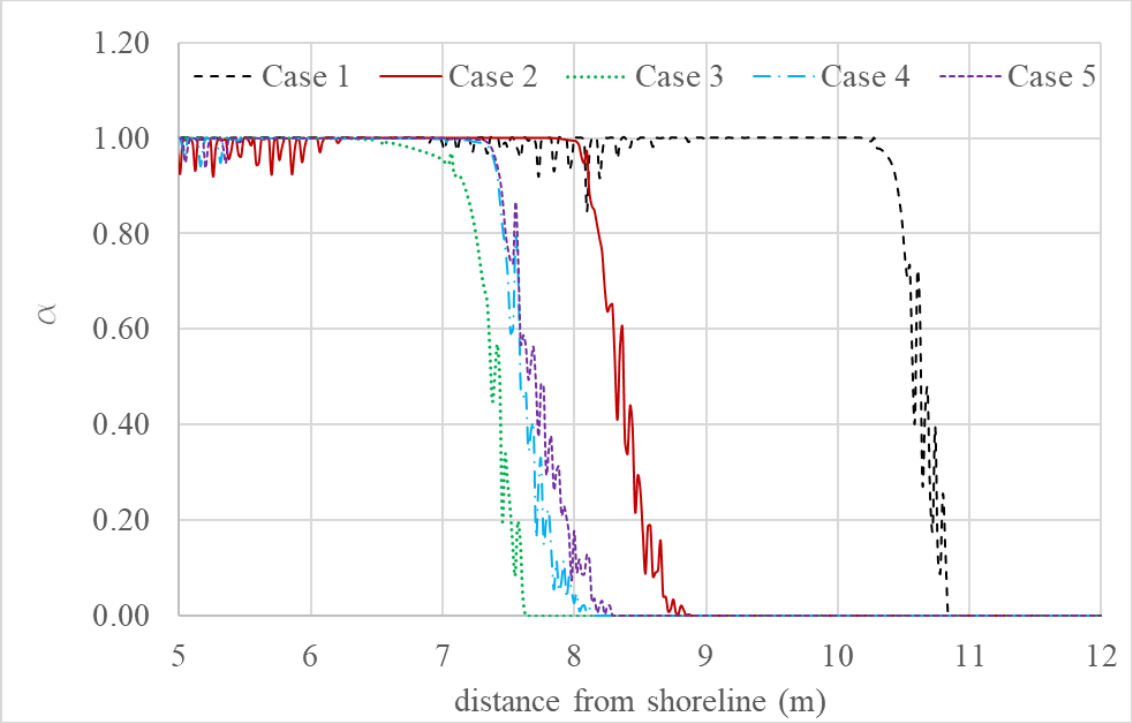

Figure 4.11. Comparison of wave run-up for each simulation case with different spacing between wall and trench.

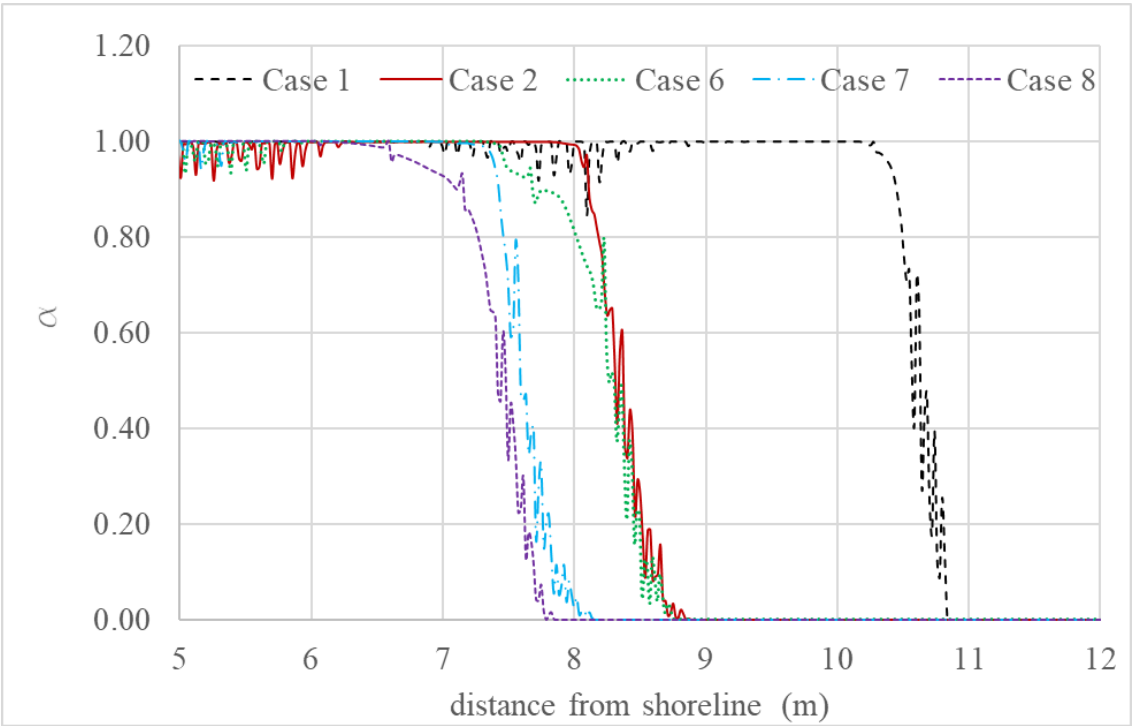

Figure 4.12. Comparison of wave run-up for each simulation case with different trench widths.

Figure 4.11 was plotted to compare simulations with wall and trench systems that have different spacings between the wall and the trench (Cases 1 to 5). It gives the maximum wave inundation along the x-axis for each simulation case.

By looking at the run-up reduction, it is clear that the wall and trench system with a 5m spacing produced the most effective suppression of the upcoming wave. Clearly, all cases with wall and trench systems resulted better inundation reduction compared to the case of single seawall.

Figure 4.12 was plotted to compare simulations with wall and trench systems that have different trench widths. The run-up reduction proves that the wall and trench system with a wider trench width can positively suppress an upcoming wave compared to the systems with narrower trench widths. Further, all cases with wall and trench systems resulted better inundation reduction compared to the case of single seawall.

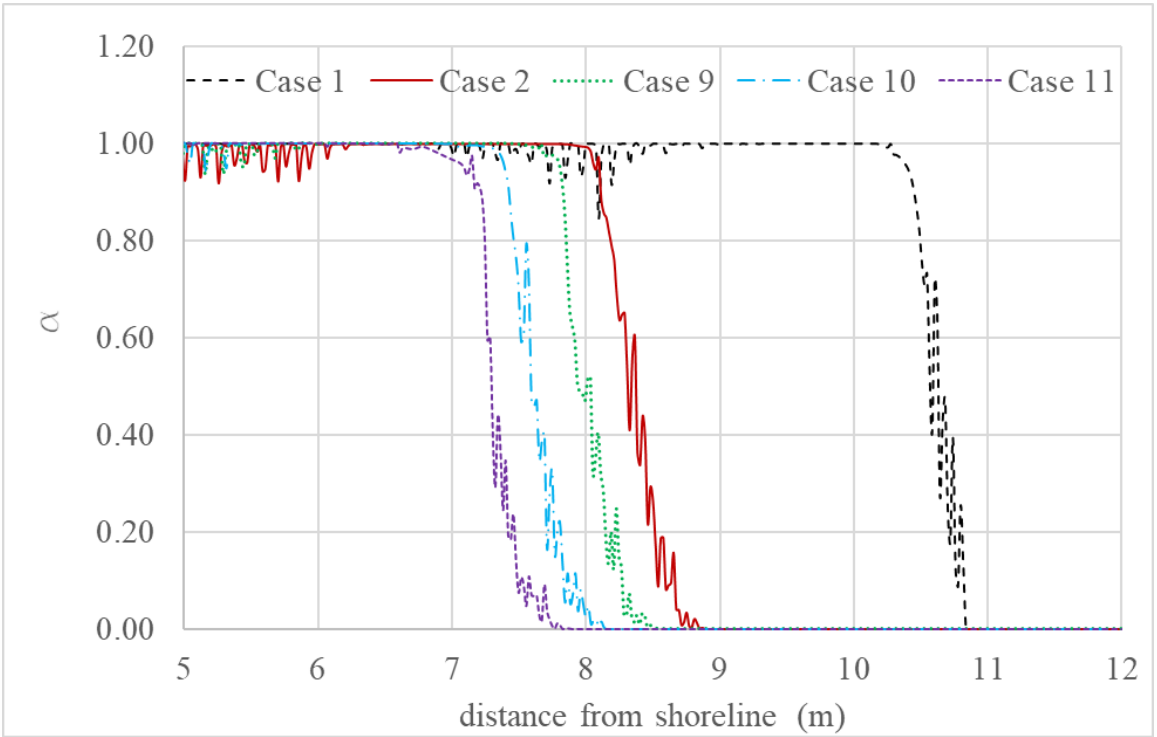

Figure 4.13. Comparison of wave run-up heights for each simulation case with different wall widths.

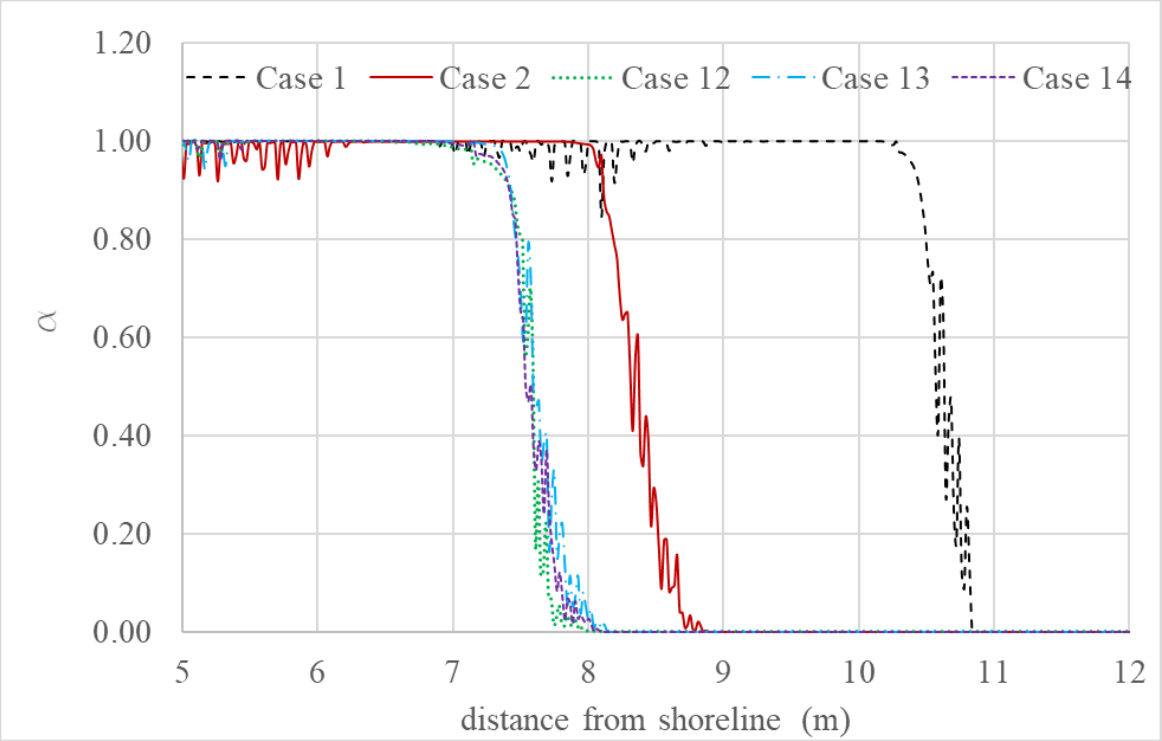

Figure 4.14. Comparison of wave run-up for each simulation case with different trench depths.

Figure 4.13. was prepared from simulations with wall and trench systems that have variable wall width. The run-up reduction reflects that the wall and trench systems with a wider wall widths can positively suppress an upcoming wave compared to the systems with narrower wall widths. Further, all cases with wall and trench systems resulted better inundation reduction compared to the case of single seawall. Figure 4.14 gives the same inundation comparison for simulations with wall and trench systems that have variable trench depth. Though there is no significant suppression happens when deepening the trench, all cases with wall and trench systems resulted better inundation reduction compared to the case of single seawall.

4.4.4 Comparison of the Wall and Trench Combination with a Single Seawall

This section presents the results of the simulations that were described under Section 4.3.4. The calculated maximum water levels from the simulation cases 15 to 22, were plotted against each other to evaluate the effectiveness of wall and trench systems compared to single seawall structures (Figure 4.15). Similarly, maximum current velocities of the same simulation

cases were also plotted and compared (Figure 4.16). Through these comparisons one can get an idea about how much the height of an existing seawall can be reduced if the wall is coupled with an associated trench.

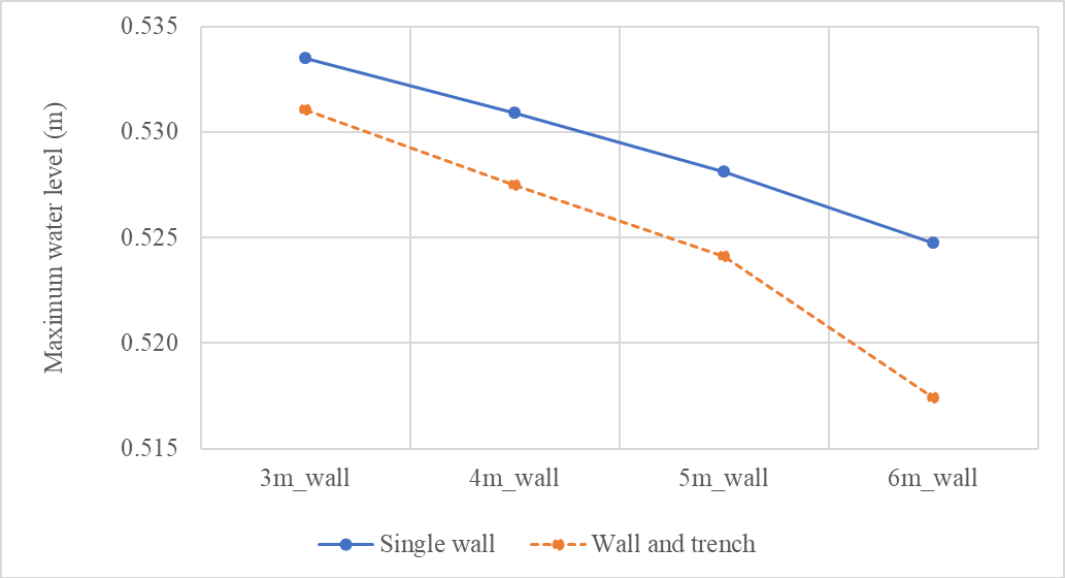

Figure 4.15. Comparison of maximum water levels observed at location D.

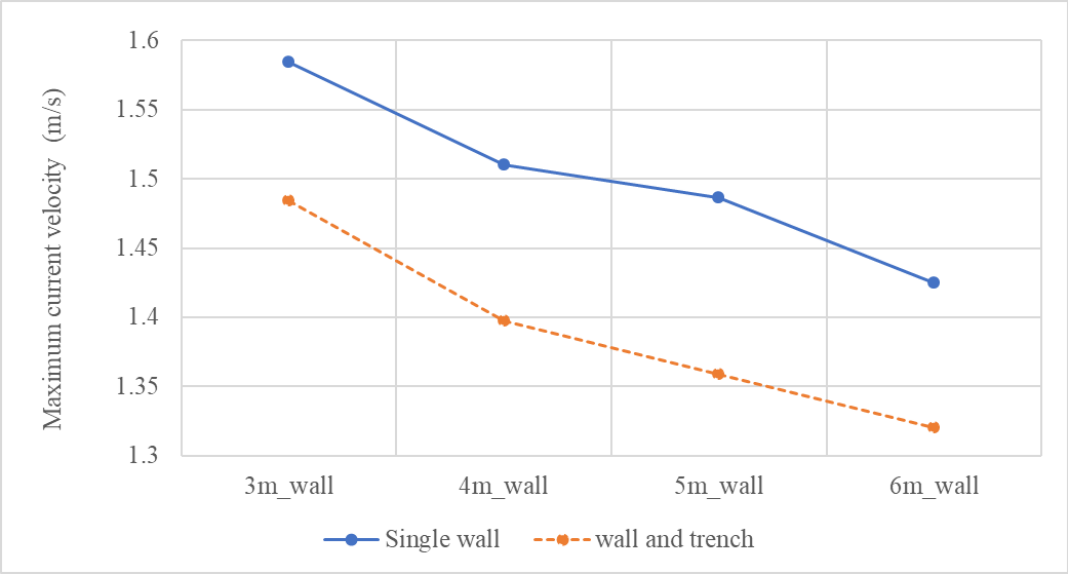

Figure 4.16. Comparison of maximum current velocity in x direction, observed at location D.

By comparing the two graph lines in Figures 4.15 and 4.16, it can be suggested that by combining an existing or planned seawall with an associate trench, the height of the seawall

could be reduced significantly (about 20%) to have the same protection from a striking tsunami. However, this suggestion only true if the wave overtops the structure.

4.4.5 Behavior of the Structure Ahead of Different Tsunami Conditions

As explained under Section 4.3.5, an identical tsunami condition (water level difference at the reservoir and the wave tank) which is generated by a dam break of a 13cm water level difference was applied to assess the onshore structures so far. However, it was noted that the behavior of the wall and trench system was also impacted by the tsunami wave height. This fact can be clearly observed by looking at the results of Section 4.4.2 (Figures 4.7.a and 4.7.b). Although the increment of the spacing between the wall and trench system gave comparatively reduced water level variations and current velocities, maximum reduction was observed for the structure which had 5m spacing (in real scale). The most reduced water level and current velocity variations were generated due to the overtopping wave directly crashing into the lee side trench. The wave did not crash directly into the trench when the spacing between the wall and the trench is increased or decreased. To examine this phenomenon, simulation cases (Case 23~54) that were described under Section 4.3.5 were carried out and the calculated maximum water level variations and current velocity variations at location D were plotted. Figures 4.17 and 4.18 give the comparison of these parameters. Water level variations for each tsunami condition at Location C are plotted in Figure 4.17.

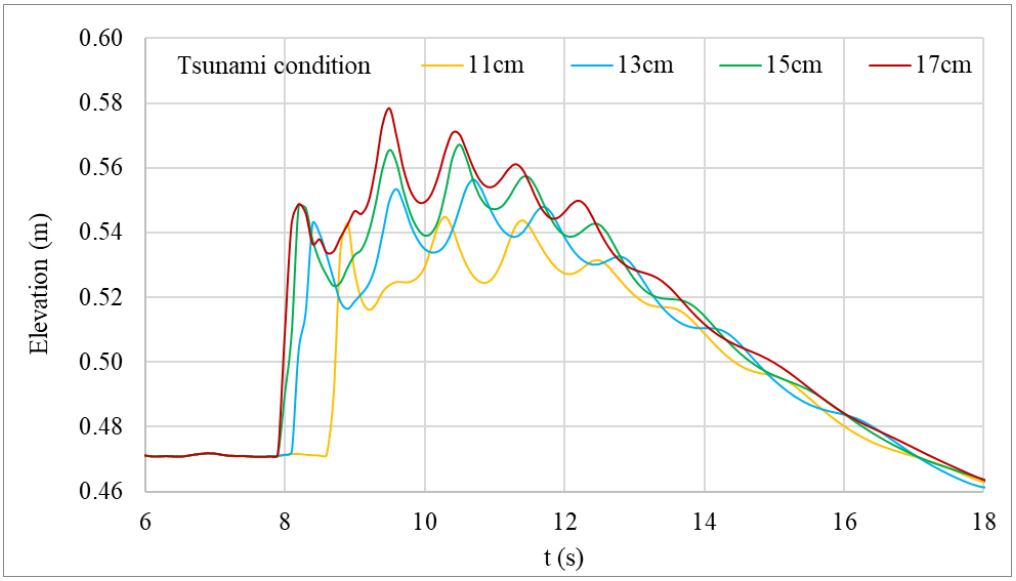

Figure 4.17. Water level variations at location C for different tsunami conditions

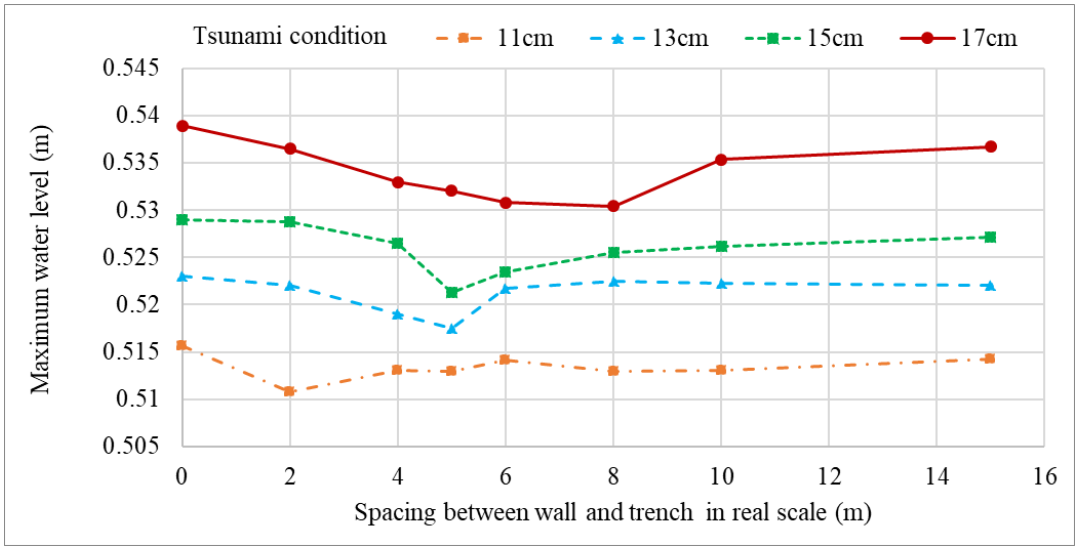

Figure 4.18. Comparison of maximum water levels observed at location D for different tsunami conditions.

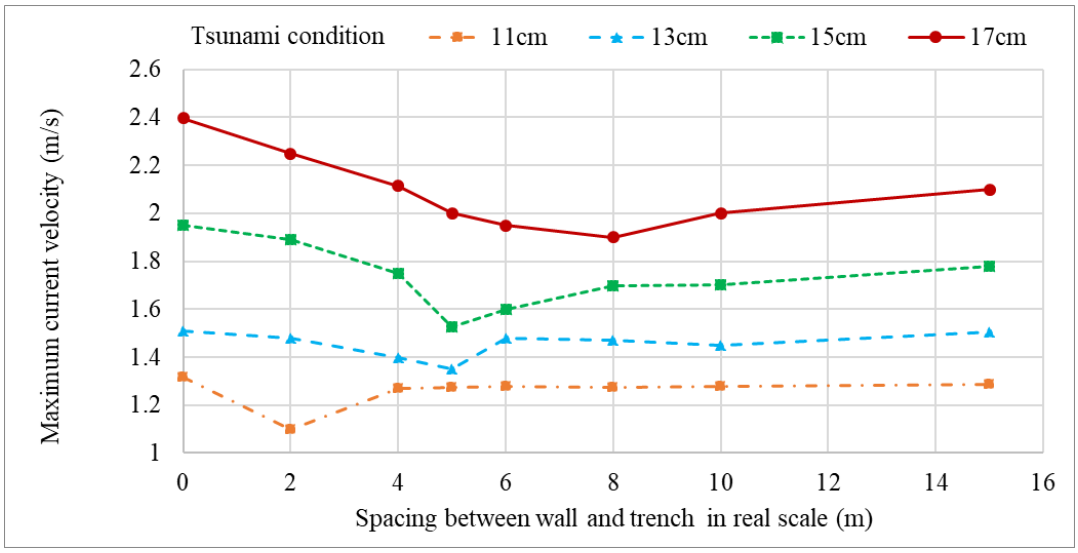

Figure 4.19. Comparison of maximum current velocity in x direction, observed at location D for different tsunami conditions.

By looking at Figures 4.18 and 4.19, the impact of the spacing between the wall and the trench of the onshore structure system can be clarified well. When a tsunami with a comparatively low wave height (11cm case) strikes, the overtopping wave front does not travel too far before it collapses to the lee side of the wall. Thus, 2m spacing between the wall and the trench is enough to capture the collapsing wave by trench. When the wave height of the tsunami increases, the travelling distance of the overtopping wave front is also increased and therefore, the spacing between the wall and the trench should also be increased to capture the collapsing wave to generate more turbulence to depress the wave energy. The generation turbulence when the wave crashes directly into the trench can be clearly understood by Figures 4.20.a to 4.20.c which shows velocity vector distribution. In Figure 4.20.a, the wave collapses after passing the trench for some extent, and in Figure 4.20.b, wave collapses in to the flat spacing between the wall and the trench. Therefore, the turbulence generated in both simulation Case 24 and Case 52 are much less than that of Case 36, in which the wave directly crashes in to the lee side trench and generates high velocity vortex with in the trench.

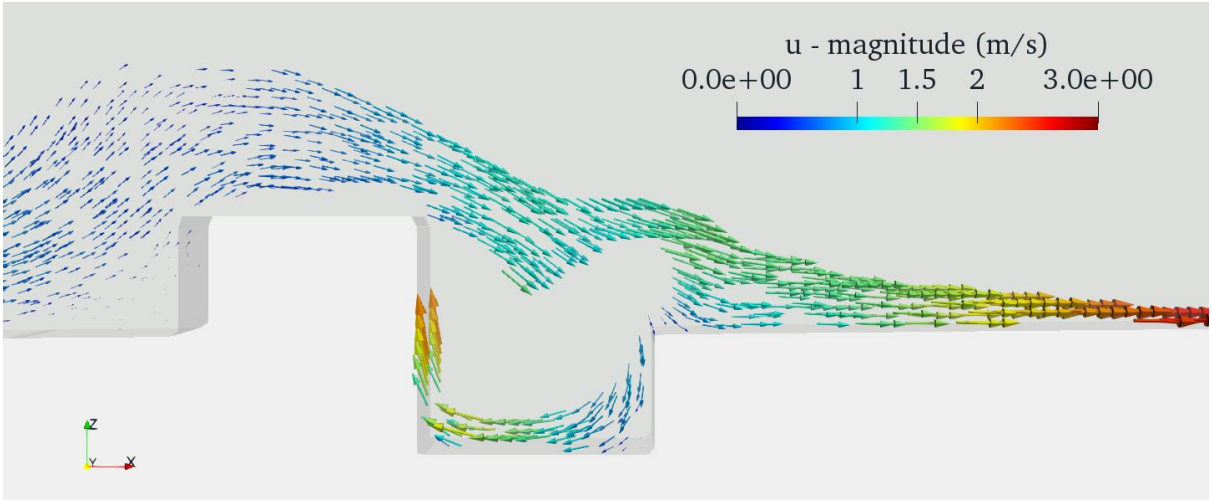

Figure 4.20.a. Velocity vector distribution of simulation Case 24. (0 spacing, 13cm tsunami condition at t = 13.5s)

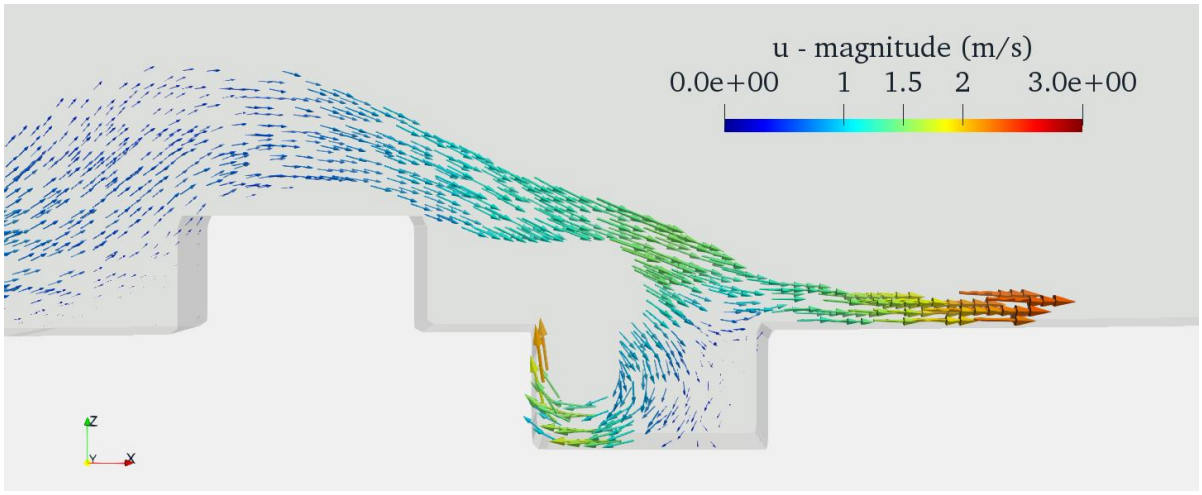

Figure 4.20.b. Velocity vector distribution of simulation Case 36. (6.25cm spacing, 13cm tsunami condition at *t* = 13.5s)

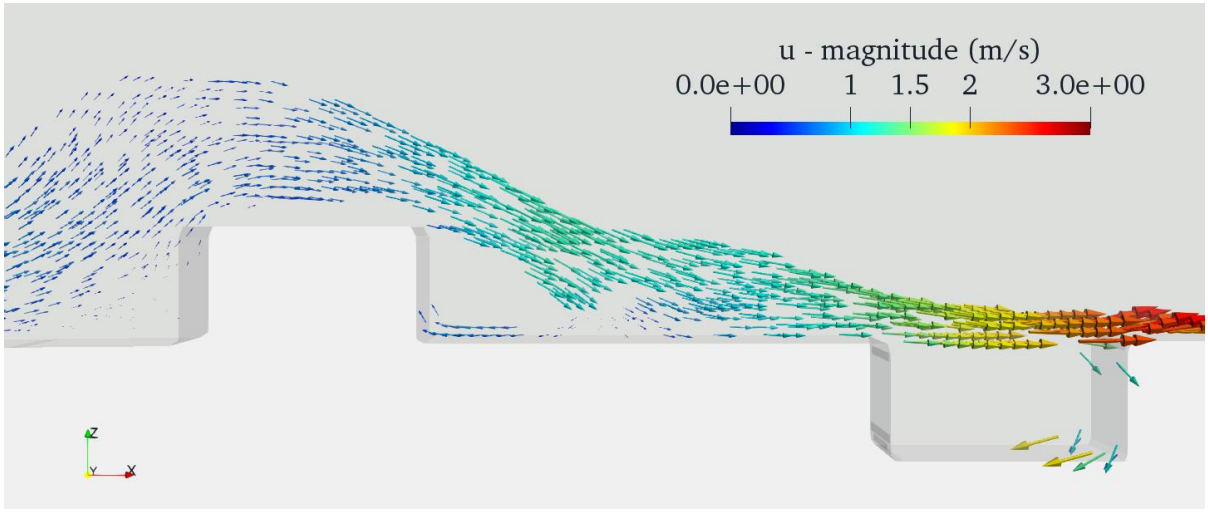

Figure 4.20.c. Velocity vector distribution of simulation Case 52 (18.75cm spacing, 13cm tsunami condition at *t* = 13.5s)

4.4.6 Characteristics of Turbulence

Figures 4.21~4.23 present the characteristics of the turbulent flow around the wall and trench structure. Turbulent kinetic energy (k), turbulent dissipation rate (ε) and turbulent viscosity (ν_t) are plotted respectively for the simulation Case 35 at t = 13.5s. The formation of turbulent vortex at the trench can be clearly identified by looking at the increase of turbulent

energy distribution in Figure 4.21. However, it should be noted that the turbulent characteristic were not only calculated for water, but also for air and air-water mixture. Therefore, Figures 4.21~4.23 cannot distinguish each turbulent characteristic of air and water individually. This problem is clearly visible in the Figure 2.23. Nevertheless, energy dissipation by the generation of turbulent vortex at the trench can be identified clearly.

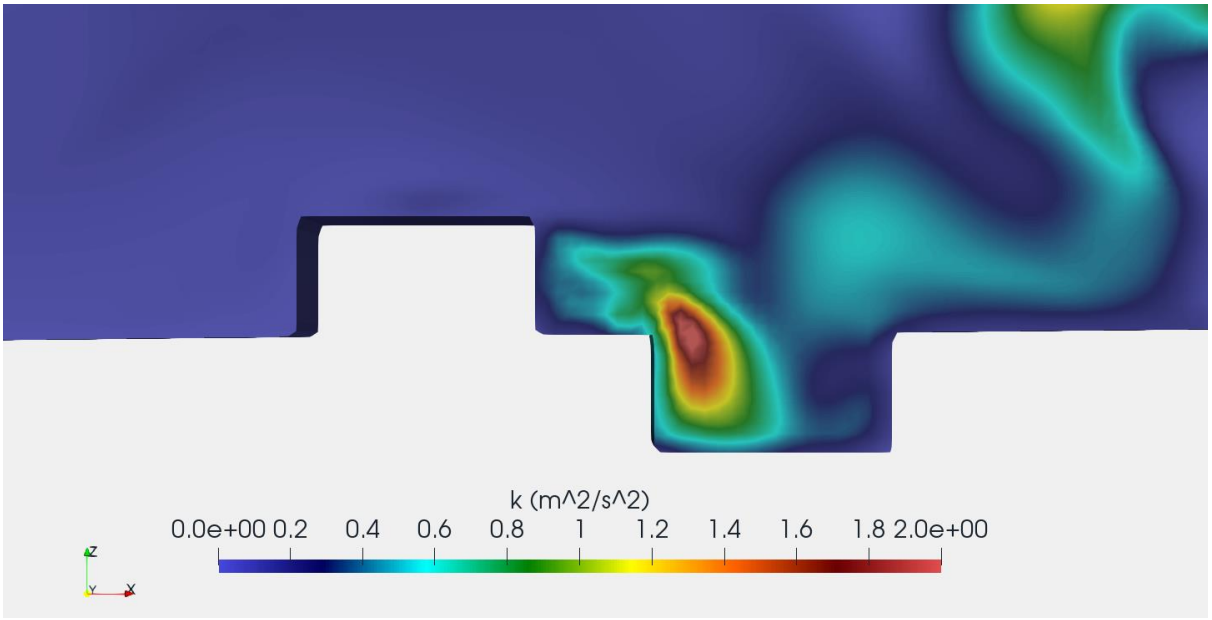

Figure 4.21. Turbulence energy (k) distribution at t = 13.5 s of simulation Case 35

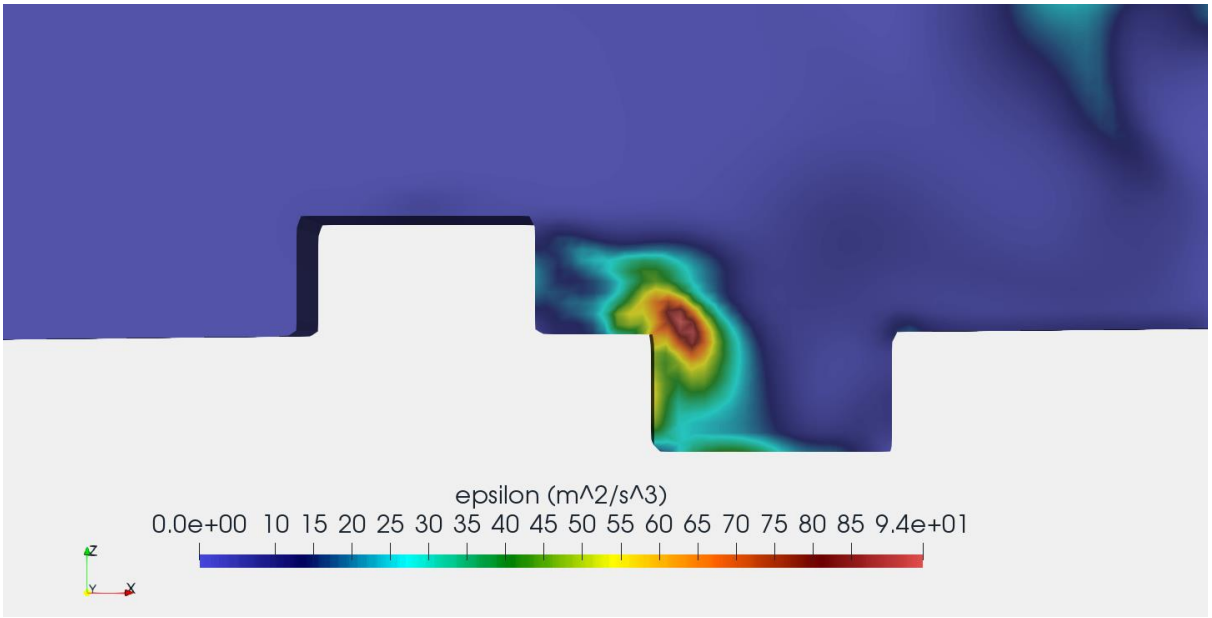

Figure 4.22. Turbulent dissipation rate (ε) distribution at t = 13.5 s of simulation Case 35

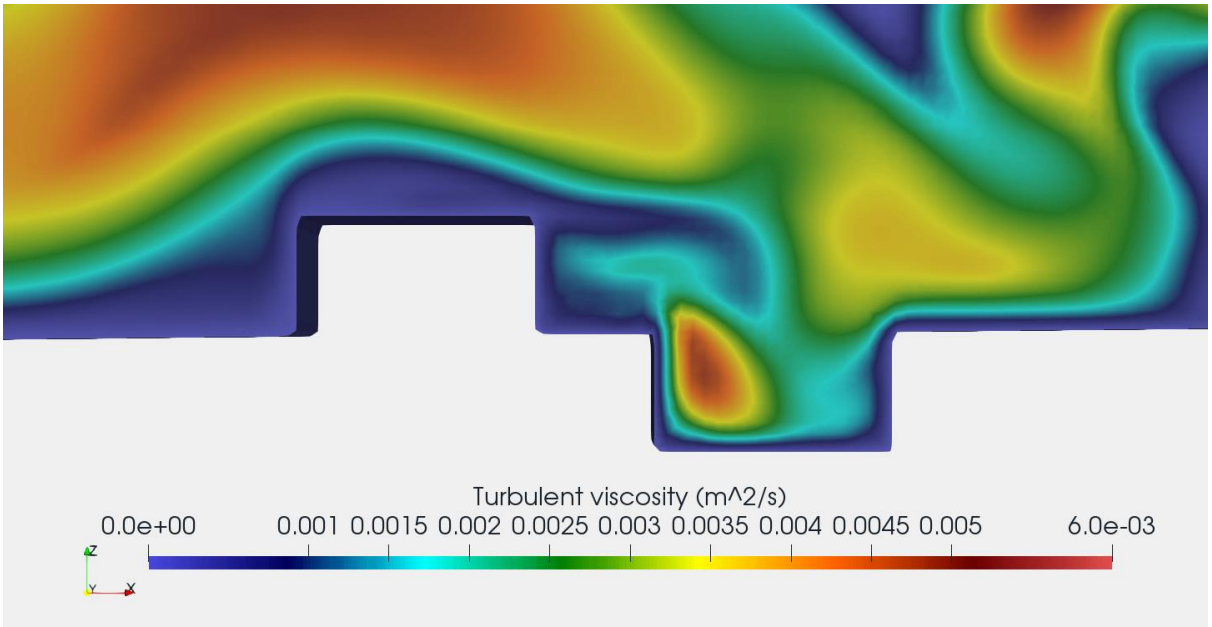

Figure 4.23. Turbulent viscosity (ν_t) distribution at t = 13.5 s of simulation Case 35

4.4.7 Investigation of Horizontal Pressure Forces Acting on the Structure

Figure 4.20 presents the comparison of distribution of horizontal pressure forces (in x direction) for the simulation cases (Case 55 and56) which were described under Section 4.3.6.

As it is explained earlier, the pressure forces acting on the structures were calculated extensively by integrating the simulated pressure values over the area of the structure. For the single sea wall case, forces acting on the wall were calculated directly and for the wall and trench combination, forces on the wall and the trench were calculated separately.

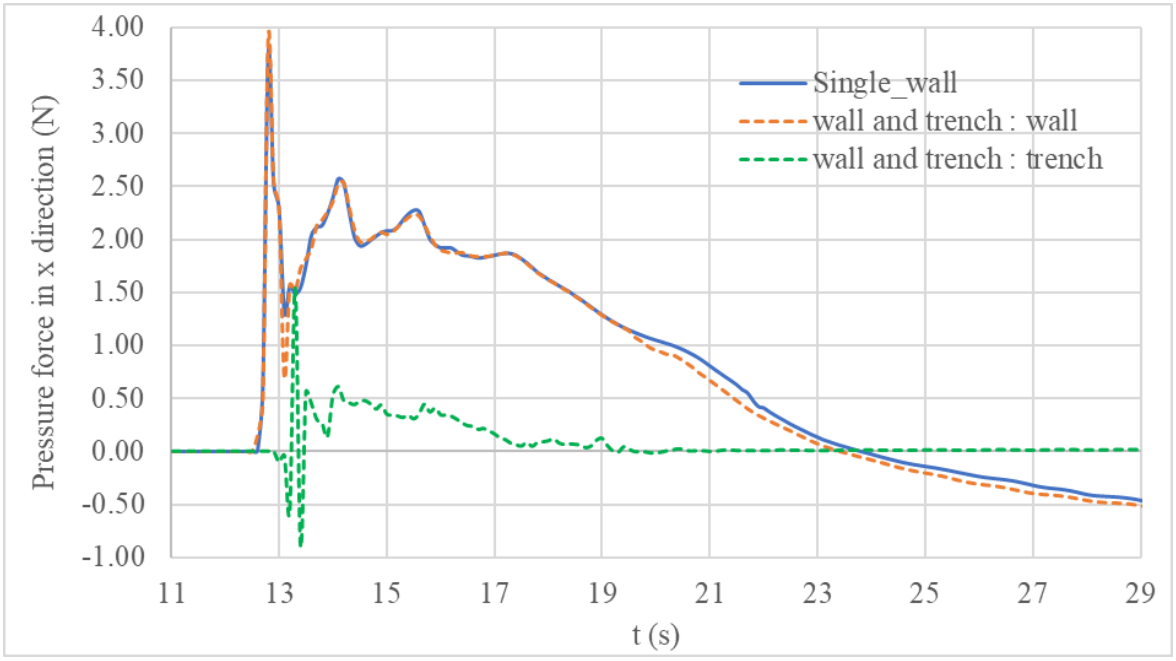

Figure 4.24. Horizontal pressure forces (in *x* direction) acting on each structure

Horizontal pressure forces acting on the wall of the wall and trench system does not show any significant change form the forces acting on the single seawall. However, quite lower forces resulted on the wall of the wall and trench system just after the wave front collapses at the lee side. This could be due to the generated turbulence resulted by the trench. Moreover, the trench itself handled a significant force at the lee side as shown in the green line of the graph.

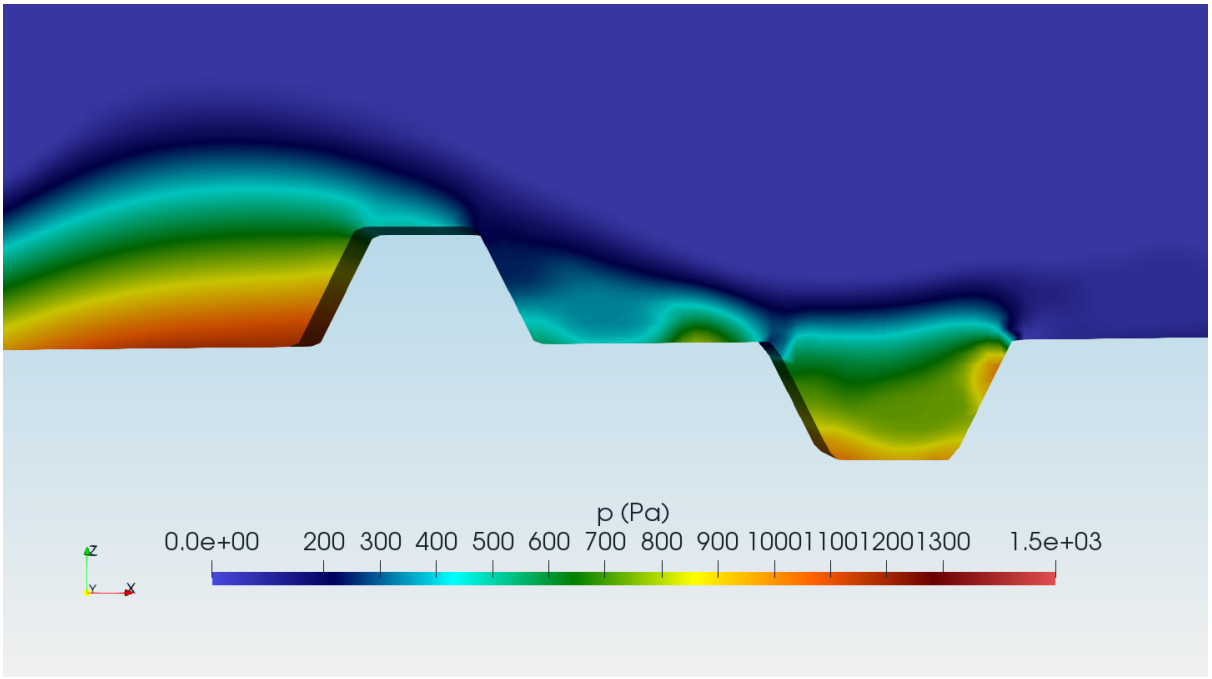

Figure 4.25. Pressure acting on the structure for the simulation Case 56 (by neglecting hydro static pressure)

Figure 4.25. shows the distribution of pressure acting on the structure. As it is seen, large amount of pressure is acting on the front face of the wall. When the wave crashes into the trench, pressure acts on the trench and can be clearly identified by looking at the Figure 4.25.

4.4.8 Assessment of the direction of the trench

Lastly, the impact of changing the direction of the trench is presented here. Figures 4.21.a and 4.21.b present the comparison of water level variations and current velocity variations at location D for each simulation cases (Case 57 and 58) which were described under Section 4.3.7.

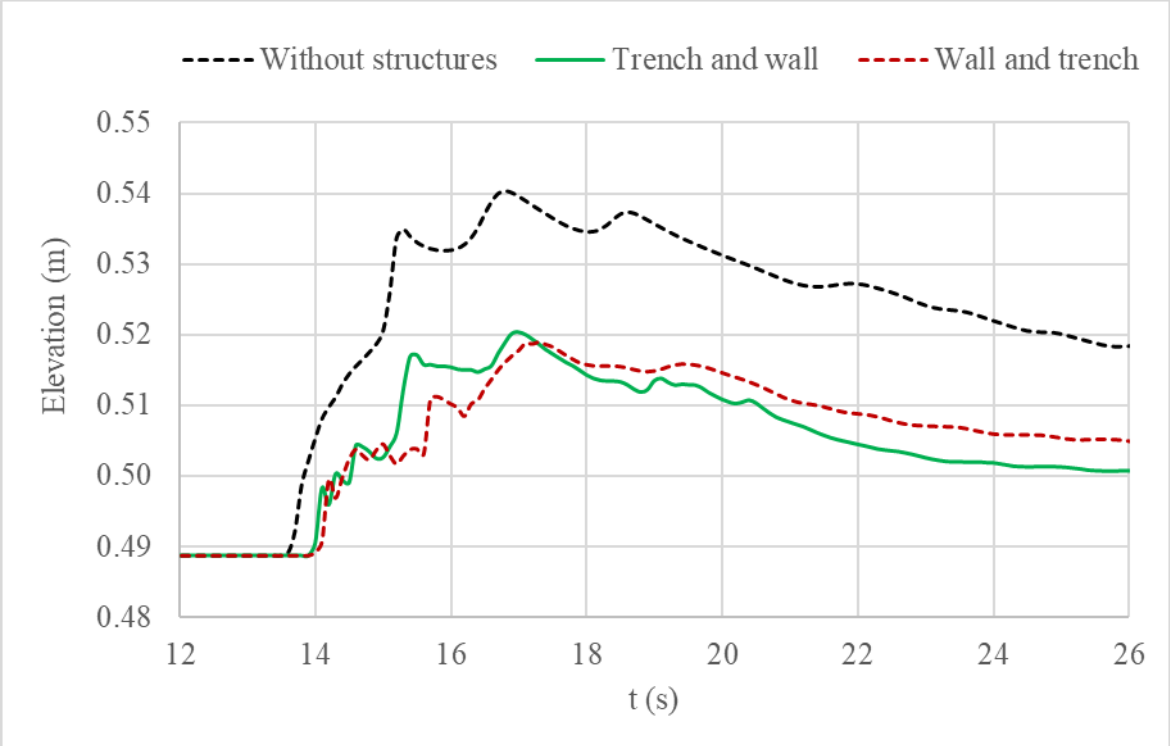

Figure 4.26.a. Comparison of water level variations at location D

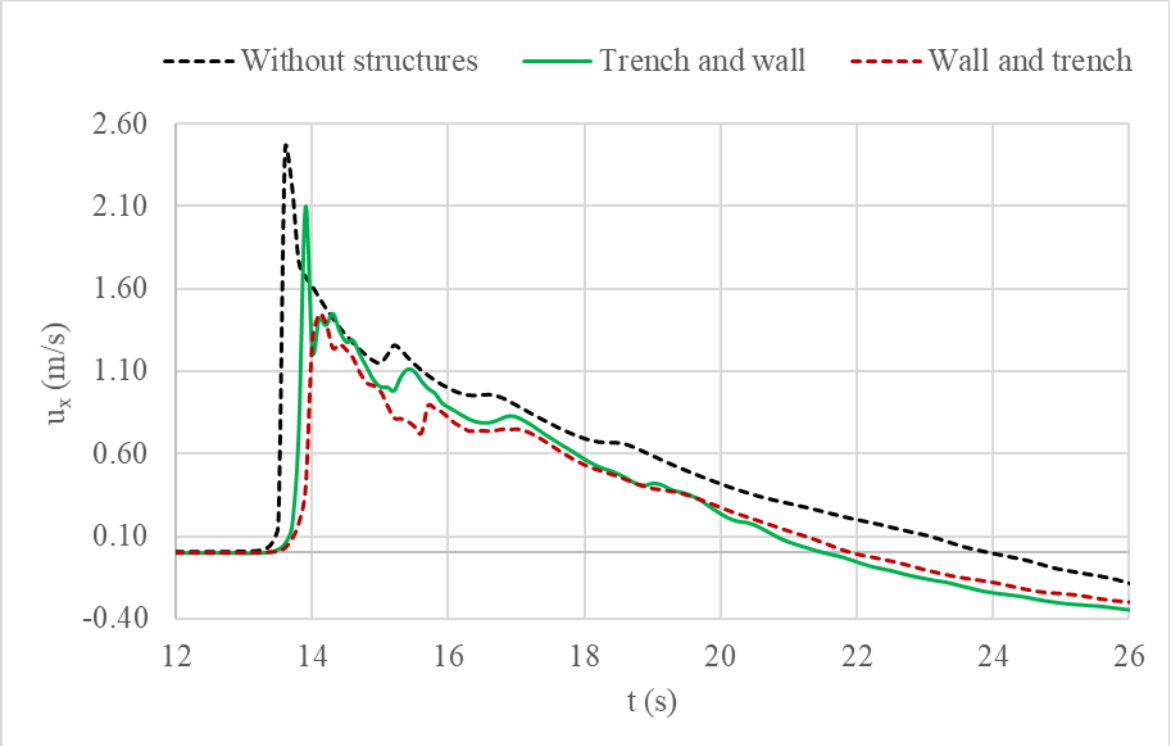

Figure 4.26.b. Comparison of current velocity (x-component) variations at location D

By looking at the above two graphs it can be suggested that, the combined wall and trench system suppressed the striking wave in a good way when the trench located at the lee side of the wall although there is not much significant difference comparing with the wall and trench system which have the trench located in front of the wall.

4.5. SUMMARY

A wall and trench combination which placed at the shore line is assessed in this chapter to find out its usability as a tsunami defense measure. The geometrical parameters of the structure system, such as wall width, wall height, trench width, trench height and the spacing between wall and trench were evaluated by numerical simulations by OpenFOAM InterFoam solver. Multiphase flow has been considered. Experimental results were used to calibrate the numerical model mainly for water level variations. The impact of the structure system resulted in reduced water level variations and current velocities at the land side. The reduction is found to be significant. It could be suggested that the structure system can mitigate an upcoming tsunami wave better than a single seawall. Conclusions of the results of these numerical and experimental tests are explained in detail under Chapter 5, Section 5.2.

CHAPTER 5

Chapter 5

CONCLUSIONS

OUTLINE

This chapter is allocated for discussing the conclusions of previous chapters. It consists of two main sections. Firstly, the conclusions of the first stage of the study is discussed based on the results that were given in Chapter 3. After that, the conclusions of the second part of the study is discussed based on the results that are given in Chapter 4.

5.1 CONCLUSIONS OF CHAPTER 3

Chapter 3 has examined the effect of submerged wall and trench systems ahead of a tsunami-like wave generated by a dam break event.

Firstly, an experiment was carried out in a 2D wave flume to capture water level variations and current velocities at several locations.

Secondly, the development of a numerical model was configured to the same dimensions used for the experimental setup. The model was calibrated acceptably for water level variations and marginally for current velocities. The shape of the velocity profiles were not reproduced accurately. However, the maximum current velocities deviated within 10% of the measured results. The numerical code used solves the shallow water equation in a depth-averaged domain. Thus, there are several limitations to the model. For example, the eddy formation in the vertical direction and the turbulence created after the wave breaking is not accounted for. In addition, the numerical model cannot solve the interaction between air and water surface accurately as the air properties are not accounted for either. Therefore, a multi-phase type model is required to solve the Navier-Stokes equations with minimum assumptions were used in the second stage of the study.

Submerged structures were then introduced into the numerical model. The impact of a single wall, double wall and wall-trench system was examined and compared for a tsunami-like wave striking land. All the structures resulted in suppressing the wave height at the lee side compared to a model without any defensive structures. This led to lower inundation lengths

and lower run-up heights on a 1:100 slope. The double submerged walls generated the most effective suppression of the tsunami-like wave. However, the wall and trench system produced a better suppression to the wave height at the lee side compared to a single submerged wall. It should be further noted that the introduction of submerged structures resulted in higher water levels at the seaside. This reaction should be investigated further, when designing such structures in three-dimensional space.

The wall and trench system was then assessed numerically, by changing the geometrical properties of the structure. A 0m spacing between the wall and trench system found to be more effective in suppressing the striking wave. The assessment found that the wider widths of the trench also had a positive effect for wave suppression. However, the gradient between the wave suppression and trench width was not very significant.

Wider walls resulted in higher reduction to the waveform. The gradient between wave suppression and wall width was quite significant when compared to the trench width assessment. Deeper trenches produced better depreciation of the waveform at the lee side. Thus, it can be concluded that a submerged wall and trench system near the shore can suppress an incoming a tsunami-like wave in an effective way.

However, submerged structures can only suppress the striking a tsunami-like wave for a certain extent and cannot provided a complete defense system. However, the reduction of wave heights and current speeds may in fact be sufficient to avoid a deadly disaster. Furthermore, these effective submerged structures can also reduce the design heights of onshore wave walls and other hard measures.

Lastly, it should be highlighted that the performance of the wall and trench system presented in this thesis has not been validated by an experimental study. It would be beneficial for such a study to be conducted to improve upon the results presented in this thesis.

5.1 CONCLUSIONS OF CHAPTER 4

Chapter 4 has examined the behavior of a combined seawall and trench system at onshore ahead of a tsunami-like wave which is generated by a dam break event.

Firstly, a set of experiments were carried out in a 2D wave flume to capture water level variations and current velocities at several locations.

Secondly, a numerical model was set up in the OpenFOAM environment to replicate wave flume experiments. The numerical model was calibrated acceptably well for water level variations and for current velocities. Though there were few deviations observed when comparing experimental and numerical results, the maximum free surface elevations and maximum current velocities were accurately reproduced by the numerical model.

Thirdly, onshore structures were introduced into the numerical model. The impact of a single wall and the wall-trench system were assessed and compared for a tsunami-like wave. All the structures resulted in depreciated water level variations at the lee side compared to a model without any defensive structures. This led to lower inundation lengths and lower run-up heights on a 1:100 slope.

The typical wall and trench system resulted in lower water levels and lower current velocities at the lee side of the structure compared to a single wall. Also, the combined structure delayed the wave bore for some extent once the overtopping wave interacted with the trench.

The wall and trench system was then numerically assessed by changing the geometrical properties of the structure. A 5m spacing between the wall and trench system found to be more effective in suppressing the striking wave. In this case, the overtopping wave was crashed directly into the trench and produced higher turbulence in the trench. This behavior was further investigated by subjecting the structure system into different tsunami levels. Results indicated that the most effective reduction to the water levels and current velocities achieve when the wave crashes directly into the lee side trench. When the tsunami height was comparatively low, the critical spacing between the wall and the trench was also found out to be lower. Once the spacing between wall and trench increases than the critical spacing, the wave suppression has come into a threshold which still resulted in lower water level variations and current velocities at the land side compared to those with a single seawall system.

The assessment found that the trench width also had a positive impact on wave suppression. Wider trenches resulted the better suppression to the wave. Similarly, wider walls lowered the water level variations and current velocities of the wave in a positive way. Further, deeper trenches produced better depreciation of the waveform. Furthermore, by referring to the

inundation comparisons, the reader can have a better idea and justification on above discussed points.

When comparing the water level reductions and current velocity reductions resulted by incorporating a trench to an existing embankment type single seawall, it was noted that the height of an existing or a planned seawall can be reduced about 20% - 30% and can achieve the same protection that would be expected by the single seawall.

By investigating the pressure force acting on the wall of single seawall system and on the wall of wall and trench system, no significant difference observed. However, a significant pressure force acted on the lee side trench of the wall and trench system dissipating a portion of the energy of the overflowing wave. This would be the main governing factor resulting in lower wave runup and lower current velocities compared to those in single seawall system.

The behavior of the wall and trench system was also investigated by changing the positioning of the trench. However, no significant change was observed for water level reductions or current velocity reductions even though the trench positioned in front of the wall or at the back of the wall.

As the results of Chapter 4 suggests, it can be concluded that a combined wall and trench system at onshore can effectively reduce an incoming a tsunami-like wave. The reduction is comparatively better than the reduction happened when an overtopping wave passes through a conventional single seawall system.

As the wall and trench system resulted in reduced wave run up heights and reduced current velocities at the land side and as it increased the tsunami arrival time compared to a single seawall system, it would be beneficial to consider these types of structure in future planning and implementing tsunami defense measures. However, the proposed structures can still suppress the striking a tsunami-like wave for a certain extent and cannot provided a complete defense. And importantly, it should be highlighted that the performance of the wall and trench system presented in this chapter has not been validated by an experimental study. Such a study would be beneficial for improving the results presented in this chapter.

Nevertheless, it should be noted that the wall and trench system that is evaluated in the study was only assed by considering the structure parameters. The main focus was to find out the most significant geometrical parameters of the structure system from the view point of

tsunami reduction. However, as it is known, the run-up height and run-up length of a striking tsunami is largely governed by the duration of overtopping, volume of water, energy dissipation, and storage volume (longitudinal-section shape). Although, this study was not focused on those factors when assessing the structure system and no quantitative analysis has been done for above mentioned governing phenomena, a brief understanding can be identified from the results that was presented under Chapter 04 (Section 4.4.5).

Lastly, it should be noted that the results presented in Chapter 04 are not validated by physical experiments. Although the numerical model was calibrated by experimental data, the tsunami induced current velocities and inundation reductions were not measured in the experiments. Therefore, it is necessary to validate the model by measuring the wave characteristics around the structure in order to prove the validity of the result that were generated by the numerical simulations. Future studies are necessary and should be carried out in the future for this purpose.

REFERENCES

Apotsos, A., Buckley, M., *et al.* (2011) 'Nearshore Tsunami Inundation Model Validation: Toward Sediment Transport Applications', *Pure and Applied Geophysics*, 168(11), pp. 2097–2119. doi: 10.1007/s00024-011-0291-5.

Apotsos, A., Gelfenbaum, G., *et al.* (2011) 'Tsunami inundation and sediment transport in a sediment-limited embayment on American Samoa', *Earth-Science Reviews*. Elsevier B.V., 107(1–2), pp. 1–11. doi: 10.1016/j.earscirev.2010.11.001.

Berberović, E. *et al.* (2009) 'Drop impact onto a liquid layer of finite thickness: Dynamics of the cavity evolution', *Physical Review E - Statistical, Nonlinear, and Soft Matter Physics*, 79(3). doi: 10.1103/PhysRevE.79.036306.

Bona, J. L., Chen, M. and Saut, J. C. (2002) *Boussinesq equations and other systems for small-amplitude long waves in nonlinear dispersive media. I: Derivation and linear theory*, *Journal of Nonlinear Science*. doi: 10.1007/s00332-002-0466-4.

Brackbill, J. U., Kothe, D. B. and Zemach, C. (1992) 'A continuum method for modeling surface tension', *Journal of Computational Physics*, 100(2), pp. 335–354. doi: 10.1016/0021-9991(92)90240-Y.

Briggs, M. J. *et al.* (1995) 'Laboratory experiments of tsunami runup on a circular island', *Pure and Applied Geophysics PAGEOPH*, 144(3–4), pp. 569–593. doi: 10.1007/BF00874384.

Calabrese, M., Vicinanza, D. and Buccino, M. (2008) '2D Wave setup behind submerged breakwaters', *Ocean Engineering*, 35(10), pp. 1015–1028. doi: 10.1016/j.oceaneng.2008.03.005.

Carrier, G. F. and Greenspan, H. P. (1958) 'Water waves of finite amplitude', *Journal of Fluid Mechanics*, 4(1), pp. 97–109.

Chang, H. K. and Liou, J. C. (2007) 'Long wave reflection from submerged trapezoidal breakwaters', *Ocean Engineering*, 34(1), pp. 185–191. doi: 10.1016/j.oceaneng.2005.11.017.

Chugunov, V., Fomin, S. and Shankar, R. (2014) 'Influence of underwater barriers on the distribution of tsunami waves', *Journal of Geophysical Research: Oceans*, 119(11), pp. 7568–7591. doi: 10.1002/2014JC010296.

Daily News (2019). Available at: https://www.dailynews.lk/2019/12/26/local/206717/sri-lanka-marks-15th-tsunami-anniversary-today.

Dao, N. X., Adithyawan, M. B. and Tanaka, H. (2013) 'Sensitivity analysis of shore-parallel canal for tsunami wave energy reduction', *Journal of Japan Society of Civil Engineers, Ser. B3 (Ocean Engineering)*, 69(2), p. I_401-I_406. doi: 10.2208/jscejoe.69.i_401.

Deltares (2018) '3D/2D modelling suite for integral water solutions: Wave', p. 214.

Dutykh, D. (2008) *Mathematical modelling of tsunami waves*. École normale supérieure de Cachan, ENS Cachan.

Engquist and Majda (2010) 'Absorbing Boundary Conditions for the Numerical Simulation of Waves', *Mathematics of Computation*, 31(139), pp. 629–651.

Engsig-Karup, A. P. *et al.* (2006) 'Nodal DG-FEM solution of high-order Boussinesq-type equations', *Journal of Engineering Mathematics*, 56(3), pp. 351–370. doi: 10.1007/s10665-006-9064-z.

Esteban, M. *et al.* (2017) 'Overtopping of coastal structures by tsunami waves', *Geosciences (Switzerland)*, 7(4), pp. 1–17. doi: 10.3390/geosciences7040121.

Fridman, A. M. *et al.* (2010) 'Tsunami wave suppression using submarine barriers', *Uspekhi Fizicheskih Nauk*, 180(8), p. 843. doi: 10.3367/ufnr.0180.201008d.0843.

Gadelho, J. F. M., Lavrov, A. and Soares, C. G. (2013) 'Modelling the effect of obstacles on the 2D wave propagation with OpenFOAM', *Developments in Maritime Transportation and Exploitation of Sea Resources*, (January), pp. 1057–1066. doi: 10.1201/b15813-133.

Goring, B. D. G. and Raichlen, F. (1992) ‘Propagation o f longwaves onto shelf’, *Journal of Waterway, Port, Coastal and Ocean Engineering*, 118(1), pp. 43–61.
Grilli, S. T. *et al.* (2007) ‘Source constraints and model simulation of the December 26, 2004, Indian Ocean tsunami’, *Journal of Waterway, Port, Coastal and Ocean Engineering*, 133(6), pp. 414–428. doi: 10.1061/(ASCE)0733-950X(2007)133:6(414).
Ha, T. *et al.* (2014) ‘Numerical study on tsunami hazard mitigation using a submerged breakwater’, *Scientific World Journal*, 2014. doi: 10.1155/2014/863202.
Hirsch, C. (1991) *Numerical Computation of Internal and External Flows: Fundamentals of numerical discretization*. Wiley. Available at: http://books.google.co.in/books?id=pswYAQAAIAAJ (Accessed: 12 June 2020).
Hirt, C. . and Nichols, B. . (2018) ‘Chaotic Self-Tuning PID Controller Based on Fuzzy Wavelet Neural Network Model’, *Iranian Journal of Science and Technology - Transactions of Electrical Engineering*, 42(3), pp. 357–366. doi: 10.1007/s40998-018-0069-1.
Hsiao, S. C. and Lin, T. C. (2010) ‘Tsunami-like solitary waves impinging and overtopping an impermeable seawall: Experiment and RANS modeling’, *Coastal Engineering*. Elsevier B.V., 57(1), pp. 1–18. doi: 10.1016/j.coastaleng.2009.08.004.
Huang, C. J., Chang, H. H. and Hwung, H. H. (2003) ‘Structural permeability effects on the interaction of a solitary wave and a submerged breakwater’, *Coastal Engineering*, 49(1–2), pp. 1–24. doi: 10.1016/S0378-3839(03)00034-6.
Huang, C. J. and Dong, C. M. (2001) ‘On the interaction of a solitary wave and a submerged dike’, *Coastal Engineering*, 43(3–4), pp. 265–286. doi: 10.1016/S0378-3839(01)00017-5.
Hur, D. S., Kawashima, N. and Iwata, K. (2003) ‘Experimental study of the breaking limit of multi-directional random waves passing over an impermeable submerged breakwater’, *Ocean Engineering*, 30(15), pp. 1923–1940. doi: 10.1016/S0029-8018(03)00046-5.
Irtem, E., Seyfioglu, E. and Kabdasli, S. (2011) ‘Experimental investigation on the effects of submerged breakwaters on tsunami run-up height’, *Journal of Coastal Research*, (SPEC. ISSUE 64), pp. 516–520.
ITIC (2019) *ITIC, International Tsunami Information Center*. Available at: http://itic.iocunesco.org/index.php?option=com_content&view=article&id=1158&Itemid=2026.
Jasak, H. (1996) *Error analysis and estimation for finite volume method with applications to fluid flow*. Imperial College of Science, Technology and Medicine.
Jasak, H. and Weller, H. . (2002) ‘Interface tracking capabilities of the inter-gamma

differencing scheme', *Mechanical Engineering*, (2), pp. 1–9. Available at: http://powerlab.fsb.hr/ped/kturbo/OpenFOAM/papers/InterfaceTrackingReport1995.pdf (Accessed: 12 June 2020).
Kimura, S. (2016) 'When a seawall is visible: infrastructure and obstruction in post-tsunami reconstruction in Japan', *Science as Culture*, 25(1), pp. 23–43. doi: 10.1080/09505431.2015.1081501.
Kobayashi, B. N. and Wurjanto, A. (1989) 'beach . The related problem of wave transmission by overtopping', 115(2), pp. 235–251.
Leendertse, J. J. (1967) 'Aspects of a Computational Model for Long- Period Water–Wave Propagation', *Rand Corporation*, p. 165.
Leendertse, J. J. and Gritton, E. C. (1971) 'A water quality simulation model for well mixed estuaries and coastal seas: Vol. II, Computation Procedures', p. 63.
Leendertse, J. and Liu, S. (1975) *a Three-Dimensional Model for Estuaries and Coastal Seas: Volume 11, Aspects of Computation.*
Lopes, P. M. B. (2013) *Free-surface flow interface and air-entrainment modelling using OpenFOAM (Thesis Project in Hydraulic, Water Resources and Environment Doctoral Program in Civil Engineering)*. University of Coimbra.
Los Angeles Times (2019). Available at: https://www.dailynews.lk/2019/12/26/local/206717/sri-lanka-marks-15th-tsunami-anniversary-today.
Madsen, P. A., Bingham, H. B. and Schäffer, H. A. (2003) 'Boussinesq-type formulations for fully nonlinear and extremely dispersive water waves: Derivation and analysis', *Proceedings of the Royal Society A: Mathematical, Physical and Engineering Sciences*, 459(2033), pp. 1075–1104. doi: 10.1098/rspa.2002.1067.
NASA (2019). Available at: https://www.nasa.gov/topics/earth/features/japanquake/sun_mar_13_2011.html.
OpenFOAM (2020) *OpenFOAM User's Guid*.
Patankar, S. V (1980) *Numerical Heat Transfer and Fluid Flow*. Hemisphere Publishing Corporation.
Plas, van der (2007) *A STUDY INTO THE FEASIBILITY OF TSUNAMI PROTECTION STRUCTURES*. Delft University of Technology.
Raby, A. *et al.* (2015) 'Implications of the 2011 Great East Japan Tsunami on sea defence design', *International Journal of Disaster Risk Reduction*. Elsevier Ltd, 14, pp. 332–346. doi:

10.1016/j.ijdrr.2015.08.009.
Rahman, M. M., Schaab, C. and Nakaza, E. (2017) 'Experimental and numerical modeling of tsunami mitigation by canals', *Journal of Waterway, Port, Coastal and Ocean Engineering*, 143(1), pp. 1–11. doi: 10.1061/(ASCE)WW.1943-5460.0000355.
Rambabu, A. C. and Mani, J. S. (2005) 'Numerical prediction of performance of submerged breakwaters', *Ocean Engineering*, 32(10), pp. 1235–1246. doi: 10.1016/j.oceaneng.2004.10.023.
Rao, R. *et al.* (2005) 'Buckingham Canal saved people in Andhra Pradesh (India) from the tsunami of 26 December 2004', *Current Science*, 89(1), pp. 12–13.
Rusche, H. (2003) 'Computational Dispersed Two-Phase Dynamics Flows of At Phase Fractions', (December 2002).
Shen, Y. M., Ng, C. O. and Zheng, Y. H. (2004) 'Simulation of wave propagation over a submerged bar using the VOF method with a two-equation k-ε turbulence modeling', *Ocean Engineering*, 31(1), pp. 87–95. doi: 10.1016/S0029-8018(03)00111-2.
Silva, A. and Araki, S. (2018) 'Tsunami interaction with bay beaches and associated headlands - A numerical case study based on 2004 and 2011 tsunami disasters', *Proceedings of the International Offshore and Polar Engineering Conference*, 2018-June, pp. 1517–1524.
Silva, A. and Araki, S. (2020) 'Combined Wall and Trench Systems at Onshore to Suppress Tsunami Impact on Coast', in *Proceedings of the International Offshore and Polar Engineering Conference*. ISOPE, 2019.
Stelling, G. and Leendertse, J. (1992) 'Approximation of convective processes by cyclic AOI methods', in *cedb.asce.org*, pp. 771–782. Available at: https://cedb.asce.org/CEDBsearch/record.jsp?dockey=0076939 (Accessed: 12 June 2020).
Stoker, J. (1957) *Water waves: The mathematical theory with applications*. Wiley Classics Library. Available at: https://books.google.com/books?hl=en&lr=&id=9CSOiCmZXKAC&oi=fnd&pg=PR23&ots=e-CBhB6rPF&sig=31nF0NWa8FrUakauzW2FggXThcg (Accessed: 12 June 2020).
Synolakis, C. E. (1987) 'The runup of solitary waves', *Journal of Fluid Mechanics*, 185(May), pp. 523–545. doi: 10.1017/S002211208700329X.
Synolakis, C. E. *et al.* (2012) 'Field survey of the coastal impact of the March 11 , 2011 great East Japan tsunami', in *European Geosciences Union (EGU) General Assembly 2012*, p. 1.
Synolakis, C. E. and Bernard, E. N. (2006) 'Tsunami science before and beyond Boxing Day 2004', *Philosophical Transactions of the Royal Society A: Mathematical, Physical and*

Engineering Sciences, 364(1845), pp. 2231–2265. doi: 10.1098/rsta.2006.1824.
Tang, H. and Wrobel, L. C. (2005) 'Modelling the interfacial flow of two immiscible liquids in mixing processes', *International Journal of Engineering Science*, 43(15–16), pp. 1234–1256. doi: 10.1016/j.ijengsci.2005.03.011.
Tokida, K. and Tanimoto, R. (2012) 'Lessons and views on hardware countermeasures with earth banks against tsunami E=estimated in 2011 Great East Japan Earthquake', *Proceedings of the International Symposium on Engineering Lessons Learned from the 2011 Great East Japan Earthquake*, pp. 463–474.
Tonkin, S. *et al.* (2003) 'Tsunami scour around a cylinder', *Journal of Fluid Mechanics*, 496(496), pp. 165–192. doi: 10.1017/S0022112003006402.
Tsai, C. P., Chen, H. Bin and Lee, F. C. (2006) 'Wave transformation over submerged permeable breakwater on porous bottom', *Ocean Engineering*, 33(11–12), pp. 1623–1643. doi: 10.1016/j.oceaneng.2005.09.006.
Ubbink, O. (1997) *Numerical prediction of two fluid systems with sharp interfaces*. University of London.
Verboom, G. K. and Slob, A. (1984) 'Weakly-reflective boundary conditions for two-dimensional shallow water flow problems', *Advances in Water Resources*, 7(4), pp. 192–197. doi: 10.1016/0309-1708(84)90018-6.
Versteeg, H. . and Malalasekera, W. (2005) *An Introduction to Parallel Computational Fluid Dynamics*, *IEEE Concurrency*. doi: 10.1109/mcc.1998.736434.
Wijesundara, A. and Ranagalage, M. (2004) 'Identification of Tsunami Risk Area Using Geographical Information Systems & Remote Sensing (a Case Study of Weligama Coastal Belt Area , Sri Lanka)', *Integrated Journal of Engineeting Research and Technology*, 1(2348), pp. 161–170.
Yakhot, V. *et al.* (1992) 'Development of turbulence models for shear flows by a double expansion technique', *Physics of Fluids A*, 4(7), pp. 1510–1520. doi: 10.1063/1.858424.
Young, Y. L. *et al.* (2009) 'Liquefaction potential of coastal slopes induced by solitary waves', *Acta Geotechnica*, 4(1), pp. 17–34. doi: 10.1007/s11440-009-0083-6.